MEASUREMENT OF SPATIAL COLOCALIZATION OF OBJECTS IN N-CHANNEL CONFOCAL IMAGES

by

MATTHEW ROBERT LOSANNO

(Under the Direction of Suchendra Bhandarkar)

ABSTRACT

A method has been developed to measure multi-parametric colocalization of color- or channel-specific light intensities in 3D space using a sequence of planar confocal microscopic images. A region growing algorithm has been implemented that analyzes the 3D image stack produced by a confocal microscope and identifies regions of interest. This algorithm selects threshold values from control images and analyzes the histogram information from each image to intelligently select and categorize object pixels from background pixels. A new technique for measuring the ratio of colocalization has also been proposed in conjunction with the region growing algorithm that results in an intuitive and easily understandable metric for characterization of the spatial colocalization throughout the whole x-y-z image set. This research successfully extends the currently available colocalization metrics by modifying the original equations to work on multi-parametric inputs. The consistency of the results on a range of input channel values is demonstrated via Monte Carlo simulation. A new spatial colocalization metric has also been proposed and implemented which results in a colocalization ratio that includes object information from all images in the colocalization experiment.

INDEX WORDS: Colocalization, Confocal microscopy, 3D spatial analysis, 2D spatial analysis, Region growing, Region-of-interest (ROI)

MEASUREMENT OF SPATIAL COLOCALIZATION OF OBJECTS IN N-COLOR CONFOCAL IMAGES

by

MATTHEW ROBERT LOSANNO

B.S., Franklin Pierce University, 2007

A Thesis Submitted to the Graduate Faculty of The University of Georgia in Partial Fulfillment of the Requirements for the Degree

MASTER OF SCIENCE

ATHENS, GEORGIA

2013

MEASUREMENT OF SPATIAL COLOCALIZATION OF OBJECTS IN N-CHANNEL CONFOCAL IMAGES

By

MATTHEW ROBERT LOSANNO

Major Professor: Suchendra Bhandarkar

Committee: Walter D. Potter

Khaled Rasheed

Electronic Version Approved:

Maureen Grasso
Dean of the Graduate School
The University of Georgia
August 2013

TABLE OF CONTENTS

Page

LIST OF TABLES vi

LIST OF FIGURES ix

LIST OF EQUATIONS xii

CHAPTER

1 INTRODUCTION 1

1.1 Purpose of the Study 1

2 BACKGROUND AND SIGNIFICANCE 5

2.1 What is Colocalization? 5

2.2 What is Confocal Microscopy? 6

2.3 Measurement of Pixel-based Colocalization in Confocal Microscopy 9

2.4 Pixel-Based Image Analysis Basics 10

2.5 Hill Climbing Algorithm Basics 11

2.6 Exhaustive Search Algorithm Basics 12

2.7 Overview of Common Metrics Used to Describe Colocalization 13

2.8 Colocalization Analysis State-of-the-Art 18

2.9 Limitations of Current Approaches 25

2.10 Addressing the Limitations 27

3 IMPLEMENTATION 29

3.1 Solving the Channel Limitations 29

3.2 Benchmark Images....34
3.3 Testing Model....35
3.4 Implementing a 3D Spatial Analysis Technique....38
3.5 Automatic Thresholding through Bimodal Histogram Analysis via Population-Based Hill Climbing....42
3.6 Automatic Thresholding through Bimodal Histogram Analysis via Limited Exhaustive Search....45
3.7 Monte Carlo Simulation Tests....48
4 RESULTS....50
4.1 Modified Equation Results....50
4.2 Testing Model Results....56
4.3 Multi Channel Analysis Using the Spatial Colocalization Coefficient (L_s)....57
4.4 3D Spatial Analysis of the Objects by the Region Growing Algorithm....59
4.5Automatic Thresholding through Bimodal Histogram Analysis via Population-Based Hill Climbing....65
4.6 Monte Carlo Simulation Results....79
5 DISCUSSION....104
5.1 Pearson's Correlation Coefficient (Rp)....104
5.2 Overlap Coefficient (r)....106
5.3 Manders' Colocalization Coefficient (M)....107
5.4 Testing Model on Benchmark Images....108
5.5 Region Growing Versus Edge Detection....108
5.6 Spatial Colocalization Coefficient (L_s)....109

5.7 Comparing Results from a Confocal Test Image Case 110
5.8Automatic Thresholding through Bimodal Histogram Analysis via Population-Based Hill Climbing 111
5.9 Automatic Thresholding through Bimodal Histogram Analysis via Limited Exhaustive Search 113
5.10 Monte Carlo Simulation 113
5.11 Problems and Limitations 116
5.12 Future Development 116
5.13 Summary 117

REFERENCES 119

LIST OF TABLES

Page

Table 1: Two Channel (Axis) Example..... 30

Table 2: Three Channel (Axis) Example..... 31

Table 3: PCC Implementation Test One..... 51

Table 4: PCC Data from PCC Implementation Test One 51

Table 5 PCC Implementation Test Two 52

Table 6 PCC Data from PCC Implementation Test Two 52

Table 7 PCC Implementation Test Three 53

Table 8 PCC Data from PCC Implementation Test Three 53

Table 9: Manders' Results..... 56

Table 10: Modified Equation Results 56

Table 11: Two Channel Results with the Spatial Colocalization (L_s) algorithm.....58

Table 12: Three Channel Results..... 59

Table 13: 3D Spatial Analysis Test on Stack AAA – AAA..... 60

Table 14: 3D Spatial Analysis Test on Stack AAA – AAB Data 62

Table 15: 3D Spatial Analysis Test on Stack AAA – BAB Data 64

Table 16: Population Occurrence of the Population-Based Hill Climbing Algorithm on Figure 13 67

Table 17: Selected Threshold from Table 16 67

Table 18: Population Occurrence of the Population-Based Hill Climbing Algorithm on Figure 15 71

Table 19: Selected Threshold from Table 18 71

Table 20: Population Occurrence of the Population-Based Hill Climbing Algorithm on Figure 18 73

Table 21: Selected Thresholds from Table 20 74

Table 22: Population Occurrence of the Population-Based Hill Climbing Algorithm on Figure 20 76

Table 23: Selected Threshold from Table 22 76

Table 24: Confocal Test Case 1 Results 77

Table 25: Confocal Test Case 2 Results 78

Table 26: Confocal Test Case 3 Results 79

Table 27: Monte Carlo Simulation PCC 5 Slices 80

Table 28: Monte Carlo Simulation PCC 10 Slices 82

Table 29: Monte Carlo Simulation PCC 15 Slices 84

Table 28: Monte Carlo Simulation OC 5 Slices 86

Table 31: Monte Carlo Simulation OC 10 Slices 88

Table 32: Monte Carlo Simulation OC 15 Slices 90

Table 33: Monte Carlo Simulation MCC 5 Slices 92

Table 34: Monte Carlo Simulation MCC 10 Slices 94

Table 35: Monte Carlo Simulation MCC 15 Slices 96

Table 36: Monte Carlo Simulation L_s 5 Slices 98

Table 37: Monte Carlo Simulation L_s 10 Slices 100

Table 38: Monte Carlo Simulation L_s 15 Slices 102

Table 39: Anti-Correlation Analysis 105

LIST OF FIGURES

Page

Figure 1: Confocal Microscope Diagram 8

Figure 2: Pearson's Correlation Coefficient Two Channel Example..... 30

Figure 3: Modified Pearson's Correlation Coefficient Example..... 32

Figure 4: The Modified Overlap Coefficient 33

Figure 5: Modified Manders' Colocalization Coefficient Example 34

Figure 6: Benchmark images..... 37

Figure 7: Pseudo code for the Bimodal Histogram Analysis via Population-Based Hill Climbing..... 45

Figure 8: Pseudo code for the Bimodal Histogram Analysis via Limited Exhaustive Search. 47

Figure 9: Stack AAA-AAA 61

Figure 10: Stack AAA-AAB 63

Figure 11: Stack AAA-BAB 65

Figure 12: Image A 66

Figure 13: Histogram of Figure 12 67

Figure 14: Real Image One 69

Figure 15: Histogram of Figure 14 70

Figure 16: Scaled Histogram of Figure 14 70

Figure 17: Real Image Two 72

Figure 18: Histogram of Figure 17 73

Figure 19: Real Image Three 75

Figure 20: Histogram of Figure 19 76

Figure 21: Confocal Test Case 1 Images 77

Figure 22: Confocal Test Case 2 Images 78

Figure 23: Confocal Test Case 3 Images 79

Figure 24: Monte Carlo Simulation PCC 5 Slices 81

Figure 25: Monte Carlo Simulation PCC 10 Slices 83

Figure 26: Monte Carlo Simulation PCC 15 Slices 85

Figure 27: Monte Carlo Simulation OC 5 Slices 87

Figure 28: Monte Carlo Simulation OC10 Slices 89

Figure 29: Monte Carlo Simulation OC15 Slices 91

Figure 30: Monte Carlo Simulation MCC 5 Slices.....93

Figure 31: Monte Carlo Simulation MCC 10 Slices.....95

Figure 32: Monte Carlo Simulation MCC 15 Slices.....97

Figure 33: Monte Carlo Simulation L_s 5 Slices.....99

Figure 34: Monte Carlo Simulation L_s 10 Slices.....101

Figure 35: Monte Carlo Simulation L_s 15 Slices.....103

LIST OF EQUATIONS

Page

Equation 1: Pearson's Correlation Coefficient 13

Equation 2: Original Pearson's Correlation Coefficient 14

Equation 3: Overlap Coefficient 16

Equation 4: Manders' Colocalization Coefficient 17

Equation 5: Modified Pearson's Correlation Coefficient Equation 32

Equation 6: Modified Overlap Coefficient 32

Equation 7: Modified Manders' Colocalization Coefficient 33

Equation 8: Spatial Colocalization Coefficient 42

CHAPTER 1

INTRODUCTION

1.1 Purpose of the Study

Historically, spatial colocalization analyses of confocal images have often relied on comparisons between two measured or derived channels of color or light intensity. Furthermore, the resultant colocalization metrics have always been derived from two-dimensional space, as the images produced are compressed representations of the thickness of the examined slice. However, these individual X-Y planar images from these slices originate from a three-dimensional object. While microscope hardware can collect high-resolution multi-parametric spatial (3D) or time elapsed (4D) data, biologically meaningful analyses have been restricted largely due to the limitations of available analysis software. Recent work has been expanding colocalization analysis to include 2D two channel spatial analysis which is currently limited to the Pearson Correlation coefficient (Kuchcinski 2011).

Furthermore, there is often a need to examine more than two color intensities interacting in a specimen. In the case of confocal microscopy, each fluorescent label on a specimen usually produces a unique channel consisting of grayscale values which represent the range of fluorescent light intensity, ranging from black to saturation. These values are compared within pixels and between channels to generate colocalization metrics used to define the outcome of the experiment. It is possible with current approaches to compare three or more fluorescence

channels, but this process is cumbersome and involves the generation of a derived track that represents the colocalization between a first and second channel and comparing that to a third channel. This study aims to provide analysis methods that can not only analyze multiple (i.e., > 2) derived channels of light intensity, but to analyze X-Y planar images in such a way that they reconstruct the 3D spatial X-Y-Z image. These methods are accomplished by using a combination of computer vision and artificial intelligence techniques to reconstruct, filter, threshold, grow regions of interest, and then calculate the relevant colocalization coefficients.

Biological processes outside of a controlled laboratory environment are rarely restricted to two interactions. Organisms and their interactions with other organisms are very complex, and similarly complex to analyze. Colocalization is a method used to determine the amount of interaction between interacting organisms. When testing cures, studying viruses, growing bacteria, and numerous other activities, it is crucial to understand how quickly and completely the cure/virus/bacteria are overcoming an organism. A human cell attacked by a virus may only be affected in a specific region, knowing which region allows a researcher to pursue a cure or treatment. Colocalization can be used to identify cellular or sub cellular interactions that are crucial to advancing our knowledge of how biological systems interact (Barlow 2010). By restricting the studying of these interactions to only two limits the progress that can be made because the entire complexity is not able to be examined.

Multi-channel colocalization is especially important when it comes to understanding the human body. The human body and brain are remarkably complex: protein synthesis, chemical events, and genes are all examples of processes that can be examined with confocal microscopy and analyzed with colocalization. As researchers have found out, turning one gene off or on has

cascading effects that are currently beyond our prediction capability. Analyzing the events from gene manipulation will offer insight into how our bodies work and make way for advancements in every facet of medical research. Particularly with the study of genes interactions are not limited to two. Allowing multi-channel colocalization will enable researchers to study complex interactions in several organisms.

This a glossary of the terms used to describe colocalization and its metrics. Following the glossary is a description of common colocalization metrics.

GLOSSARY

Channel: A channel refers to a set of images produced for a specific fluorescence label.

Colocalization: Refers to observation of the spatial overlap between two (or more) different fluorescent labels, i.e. the interactions between specimens.

Dimension: The minimum number of points needed to specify a point within the object. Two dimensions need two coordinates, eg. X,Y.

Fluorescence labels: A dye attached to part of a specimen. When a high-energy laser is focused on this dye, it emits a different wavelength light.

Image Slice (slice): An image read in from the confocal microscope from one of the channels.

N-channel: Refers to the number of channels in a confocal examination. 'N' referring to the number of channels actually used. Is the same as n-color.

N-color: Refers to the number of different fluorescence labels used. Is the same as n-channel.

Specimen: The whole object being observed by the confocal microscope.

Voxel: A pixel with volume. Spatial pixel information. A voxel would be pixel information from adjacent slices of the same channel.

X-Dimension: The X plane of an object. On a plain piece of paper it would be the width.

Y-Dimension: The Y plane of an object. On a plain piece of paper it would be the length.

Z-Dimension: The Z plane of an object. On a plain piece of paper it would be the thickness of the sheet.

ChN- This refers to a specific Channel. Ch1 is Channel 1, Ch2 is Channel 2, Ch3 is Channel 3, …,ChN is Channel N.

ChNavg: Is the average pixel intensity value for the Channel image. The equations that use these values only work in 2 dimensions, therefore it is only the average for the Image Slice in question. Ch1avg is the Channel 1 pixel intensity average for the Image Slice being examined, Ch2avg is the Channel 2 pixel intensity average for the Image Slice being examined, …,ChNavg is the Channel N pixel intensity average for the Image Slice being examined.

CHAPTER 2

BACKGROUND AND SIGNIFICANCE

2.1 What is Colocalization?

Colocalization is a term used to describe the spatial location of two or more objects that are found in the same space. The degree of closeness or overlap of these objects can be qualified and/or quantified with various coefficients. This project addresses the degree of colocalization of two or more different fluorescent labels as measured by confocal microscopy. Confocal microscopes have the ability to take spatial images of a specimen. Spatial analysis of the resulting images from a confocal microscope is also addressed. This project focuses on 8-bit image analysis; this means that there are at most 256 different levels of intensity for each channel.

Through pixel based colocalization analysis, it is possible to describe the variance of two or more images. Two general approaches to measure pixel based colocalization analysis, given two grayscale images, are a measure of overlap and averaging. The overlap approach compares intensity levels for each pixel from one image with the corresponding pixel intensity in another image. If the pixel values are relatively close then those pixels are considered colocalized. If the pixel intensities are not similar (non-overlapping) then the colocalization is either considered weak or non-existent (Bolte 2006). The averaging approach computes the average pixel intensity of each image. Then the pixel intensities are compared to the average pixel intensity for that

image. If the pixel intensities are close to the average for each image then the colocalization is stronger. The further the pixel values are from the average the weaker the colocalization (Bolte 2006).

2.2 What is Confocal Microscopy?

Confocal microscopy is an optical imaging technique most commonly used to construct visually crisp, "in focus" images of reflected fluorescent or transmitted light from a specimen. It differs from conventional microscopy in that the examined specimen is not flooded evenly in light from the light source, exciting all parts at the same time. Instead, confocal microscopy relies on the placement of a physical pinhole at a convergence area in the optical path to block out-of-focus reflected light. This point illumination only allows in-focus light to make it to the final image. By eliminating out-of-focus light, unfocused background area is reduced, thus, increasing resolution and contrast of the image. The resultant images are 2D (X-Y) representations of a "slice" of the sample and have a true thickness related to the pinhole diameter. While the (X-Y) planar images consist of an array of bitmapped pixels with a virtual thickness of only one pixel, the actual space represented by each 2D pixel does indeed have a real Z-dimensional component. The real-space (X-Y-Z) volume that the virtual pixel represents is also referred to as a voxel. The three-dimensional nature of a specimen can be represented by a sequential series of images that are captured by moving the specimen though the focal point of the microscope and collecting multiple planar images.

Confocal microscopy is an optical imaging technique used to construct 2-D scans or three-dimensional (3D) images by sequentially changing the focal point within the specimen and

eliminating out-of-focus light. The 3D image is not an actual 3D image, rather it is a collection of 2D images that when examined in the specified order represents the 3D object. The basic foundation of confocal microscopy lies in fluorescence labeling. Fluorescence is caused by the absorption of light particles of one wavelength and the emission of light particles at another wavelength. These emitted wavelengths are measured in confocal and fluorescence imaging. The fluorescence labels, when hit with a beam of light, emit a specific wavelength. The wavelength is unique to that fluorescence. The specimens being studied are able to be stained with certain fluorescence labels. These fluorescence labels allow the researcher to stain specific areas of their specimens so specific interactions can be studied.

The microscope uses a dichromatic mirror to only reflect light shorter than a certain wavelength. The light that is allowed to pass through must be longer than that minimum. That light that is able to pass through the mirror hits lenses designed to focus the point of light at a specific point. (Patwardhan and Manders 1996). A confocal microscope uses a laser to excite the fluorescence labels that the specimens are dyed with. This light from the laser (Figure 1: 'laser') reflects off the dichromatic mirror (Figure 1: 'rotating mirrors'). Then the light hits two mirrors, these mirrors are mounted on motors to be able to change the focal point (which allows for a 3D spatial image to be captured). The light reflected off of these mirrors hits the specimen (Figure 1: 'fluorescent specimen').

The fluorescence label, that is used to stain specific areas of the specimen, emits a different wavelength light that passes through the same mirrors that the laser just passed through. The returning light also passes through the mirror and is focused into the pinhole (Figure 1: 'screen with pinhole'). Light that is not focused into the pinhole does not get measured by the detector. The detector is a photomultiplier tube (Figure 1: 'PMT').

A photomultiplier tube is a detector of radiant energy. It works in the ultraviolet, visible, and near infrared spectra. The photomultiplier tube takes the current from the light emission and multiplies the current. This current is passed to a computer and a pixel value is calculated (Metamorph). Basically, the photomultiplier tube takes light energy and converts it to a current; the current is then measured and associated with pixel intensity. The detector is attached to a computer that builds the image as the lenses move over the entire sample. Only a very small section of the sample, one pixel, is imaged at a time.

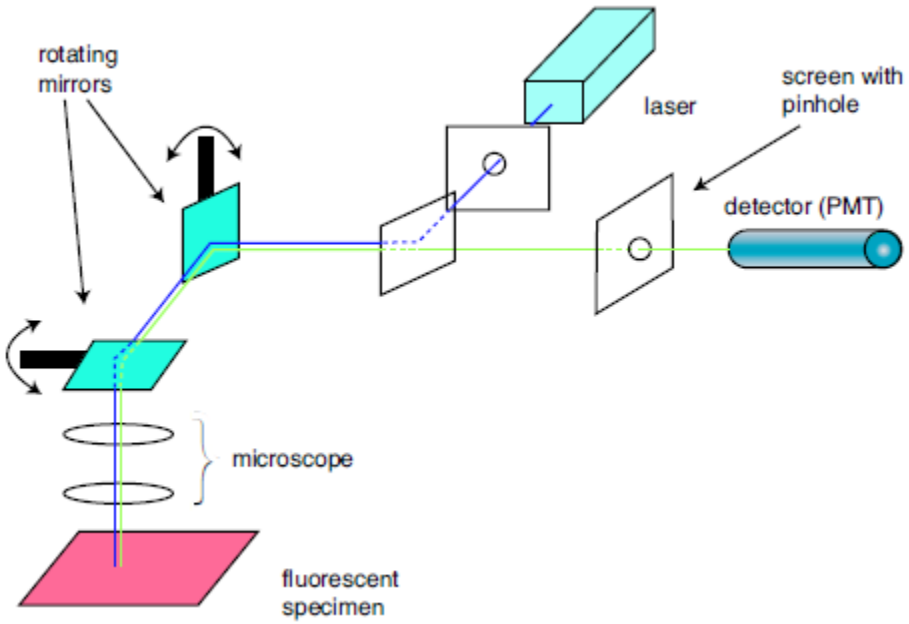

Figure 1: Confocal Microscope Diagram. This is a complete diagram of the internal workings of a confocal microscope. The horizontal 'Aperture' at the bottom is the pinhole the returning light must pass through in order to hit the 'Light detector' that will transform the light energy into a digital format for the computer to build the image. The focal plane is the location the dichromatic lens is focusing the light from the laser. (Patwardhan and Manders 1996).

The confocal lens moves over the fluorescent specimen sequentially, in the X-Y plane. Once the first layer of the specimen has been imaged, the focal point is changed along the Z axis.

The focal point change is accomplished by focusing the light from the laser at a different distance. This distance change will now cause a different area of the specimen to be imaged. This process is continued until the whole specimen has been imaged.

The 3D spatial data (i.e., along the Z axis) is collected by changing the focal point of the microscope. As with a camera, when the focal point is set for a certain distance (say 1m), objects 1m away will appear clear. Objects 10m away will be out of focus; the same is true on a confocal microscope. By taking images at 1m – 10m (changing the focal point to get the clearest image) a clear 3D spatial image could be constructed. The confocal microscope is designed to block the out-of-focus light (Figure 1: 'screen with pinhole') so that each image contains minimal spatial information in each image slice.

2.3 Measurement of Pixel-based Colocalization in Confocal Microscopy

The process of actually converting the light intensity to pixel-based values is the first step in creating each 2D image. Point-scanned light from an appropriate laser is used to excite fluorochromes on a specimen and the emitted light is captured with a photomultiplier tube (PMT). The light is converted to an electrical signal proportional to the light intensity and bitmapped to create the 2D image of pixel-based values. As the light intensity goes up, the pixel produced becomes more saturated towards a maximum pixel value (255 in 8 bit images).Absence of measureable light intensity will yield a pixel value of zero. A more in-depth description of how a confocal microscope collects data is described in the appendix. For the purpose of assessing comparative colocalization, once the images are reconstructed the final process involves the analysis of the pixel values. The presence/absence and/or degree of light intensity as

represented by pixel values are compared for the fluorochromes of interest (channels). Several metrics, represented by different equations, are commonly used to assess comparative colocalization of pixels across multiple channels.

2.4 Pixel-Based Image Analysis Basics

To understand how the equations in this thesis work, a basic understanding of pixel-based image analysis is required. Standard grayscale images that are used in this research are 8-bit images. This means that the stored data for each pixel contains 8 bits of binary information representing a value from 0 to 255. Therefore, any pixel in the images that are being examined will only have intensity values between 0 and 255. An 8-bit grayscale image is essentially a grid of intensity values between 0 and 255. Black (dark) pixels represent intensity values equal to or around 0, whereas white pixels represent intensity values equal to or around 255. The shades of gray seen in these images represent intensity values somewhere in-between 0 and 255.

There are several imaging packages that can be used to read image data. Using one of these packages, the pixel intensity can be referenced by the X,Y pixel location for the data that needs to be obtained. If the image is examined as in a grid of pixel intensities, X refers to the row number, and Y refers to the column number of that grid. Using the pixel intensity information, other metrics can be calculated that are useful in measuring colocalization. The equations used in this research interpret the pixel intensity at the X,Y location in the image to generate colocalization coefficients.

2.5 Hill Climbing Algorithm Basics

A hill climbing algorithm, as used in this research, examines a data set and attempts to find any maxima that may be present. For instance, the data set that the hill climbing algorithm examines is a histogram. This histogram consists of 255 values on the x-axis; this represents all the possible pixel values in an 8-bit image. The y-axis is the frequency of the pixel intensities found throughout the image. The hill climbing algorithm finds the most frequently occurring pixel intensities in the image. If an image consisted of only black pixels (intensity 0) and white pixels (intensity 255) then there would be two maxima in the histogram (0 and 255).

Consider an image that has every pixel intensity value from 0 to 255 in different frequencies, as many images contain. The histogram for this image would have tens or even hundreds of tiny peaks, known as local maxima. If the goal is to find one or two of the most frequented (tallest peak if looking at the histogram) maxima, then the entire histogram needs to be examined. Selecting the two largest maxima in the histogram is not completely straightforward. If the two most frequented pixels were selected, they may be right next to each other. Since we are trying to find the highest point of the peak, one step down cannot be considered a separate peak. This is actually very likely to happen. This issue is resolved by using a population-based hill climbing algorithm. A limited exhaustive search algorithm was also examined to find the two largest maxima in the histogram, but was determined to not be as effective, as will be shown.

The population-based hill climbing algorithm has, for example, one hundred people. These people are on a mountain range trying to find the two highest peaks. If they all start at one end, they will likely get to the first peak and think it is the highest not knowing that 200 miles

away is a much higher peak. Therefore, all the people get spread out over the entire mountain range. Each person tries to find the highest peak nearest them. Once everyone has climbed the highest peak they can find, the number of people at each peak is counted. Whichever one, or two, mountains have the largest number of people on the top, are the highest peaks in the mountain range.

This is exactly how a hill climbing algorithm is used on a histogram of pixel intensities. People, termed individuals, are placed uniformly throughout the entire data sets range. Each of these individuals tries to find the highest peak nearest them. They are limited to how far they can see and move if the goal is to find more than one global maximum, otherwise they would all converge on the same mountain top. In this paper we use a population-based hill climbing algorithm to calculate the pixel intensity boundaries of the object and background pixels to segregate the image.

2.6 Exhaustive Search Algorithm Basics

As with the population-based hill climbing algorithm, the goal of an exhaustive search algorithm is to find the largest maxima in the data set. An exhaustive search algorithm examines every peak in the data set. Following with the hill-climbing example it would be as if one person climbed every peak in the mountain range and then picked which were the two highest peaks. This method for determining the pixel intensity boundaries of an object and background pixels to segregate the image was not used due to a decreased effectiveness when compared to the population-based hill climbing algorithm. The details of the shortcomings of using the limited

exhaustive search algorithm versus the population-based hill climbing algorithm will be reviewed. Results for both algorithms will be shown for a given data set.

2.7 Overview of Common Metrics Used to Describe Colocalization

Pearson's Correlation Coefficient (PCC). Pearson's Correlation Coefficient (Equation 1) is based on a statistical method of analysis. The coefficient of this algorithm is meant to show the variance between image one and image two with respect to each images' average. Pearson's Correlation Coefficient (Equation 1) is a modeling technique used to describe a relationship between two or more variables. This implementation of Equation 1 is found in Manders' et al (1993). This equation has been modified from the original equation (Equation 2) for image analysis.

$$Rp = \frac{\sum_{Y=0}^{Ymax} \sum_{X=0}^{Xmax} ((Ch1_{(x,y)} - Ch1_{avg}) * (Ch2_{(x,y)} - Ch2_{avg}))}{\sqrt{\sum_{Y=0}^{Ymax} \sum_{X=0}^{Xmax} (Ch1_{(x,y)} - Ch1_{avg})^2 * \sum_{Y=0}^{Ymax} \sum_{X=0}^{Xmax} (Ch2_{(x,y)} - Ch2_{avg})^2}}$$

Equation 1: Pearson's Correlation Coefficient. The ∑ is the summation symbol, everything contained in its argument is summed. Each of these summations are for the image width (x) and height (y). For pixel y=0 means the top of the image, x=0 means the left edge. So when both x and y=0 the equation is examining the top-left pixel in the image. The subscript next to Ch is the channel number being examined, since the equation works with multiple derived channels, in this case two, it is examining channel one and channel two. Ch(x,y) is the pixel intensity value at that (x, y) location. Ch1avg equals the average intensity of all the pixels from the image in Ch1. The numerator sums the product of the pixel intensity minus the intensity average between all channels being examined. The denominator sums the difference between the channel average and pixel intensity squared, before multiplying across all the channels being compared. This value is then taken to a square root.

$$r = \frac{\sum_{i=1}^{n}(Xi - \bar{X})\,(Yi - \bar{Y})}{\sqrt{\sum_{i=1}^{n}(Xi - \bar{X})^2}\sqrt{\sum_{i=1}^{n}(Yi - \bar{Y})^2}}$$

Equation 2: Original Pearson's Correlation Coefficient. This equation defines the covariance of two variables divided by the product of their standard deviations. It is identical to the Pearson's Correlation Coefficient in Equation 1except that the notion of channels, specific for use in image colocalization analysis.

Pearson's Correlation Coefficient (Equation 1) works by comparing each pixel intensity to the average of the pixel values for that image. By comparing a pixel to the image average, a measure of how well that pixel represents the entire image is gathered. If the pixel is a good representation of the image, the resulting ratio will be more affected by it. The numerator takes the summation of each pixel's difference from the image average by the product of each pixel's difference from the image average for the second image. There are six possible scenarios that can arise in the numerator when examining two images. The six possible scenarios are based on whether the pixel in the first image is more or less than the average and the same for the second image. Half of the six possible scenarios are redundant and thus there are only three unique scenarios that can arise. An example of the redundancy is that one equation is the reverse of another. These are the three scenarios that have different results:

1) Two Positives: This will give a positive result and cause the coefficient to move in the direction of complete colocalization. This is the same as Negative * Negative, as this will result in a positive value and hence positive correlation.
2) A Positive and a Negative: This will give a negative result and bring the coefficient towards negative correlation (since Pearson's Correlation Coefficient ranges from -1 to 1).
3) A Zero and (Positive or Negative): This will not change the value of the numerator because if the pixel value is zero that area is part of the background.

The denominator of the equation squares each pixel minus the average before it is multiplied by the other image values. By doing this, the denominator adds the variance from the average for the entire image. The numerator will change depending on which scenario the pixels in question fall into. The denominator adds up all the differences, while the numerator only increases when colocalization is evident. The ratio gives the coefficient and will range from +1 in the case of a perfect positive (increasing) linear relationship, to −1 in the case of a decreasing (negative) linear relationship. As it approaches zero there is less of a relationship. The closer the coefficient is to either −1 or 1, the stronger the correlation between the variables (Adler 2010).

The sum of the numerator of Equation 1increases as pixels between the channels are on the "same side" of the average. The pixel values can either be above or below the channel average. If all pixel values for that (x, y) location across every channel being examined are above or below (exclusively), then the numerator will increase. The further the two pixels are away from the average (on opposite sides) the more the sum of the numerator will decrease. Likewise, if both pixel values are above or below (exclusively) the average, the sum of the numerator will increase. This calculates a degree of similarity between the channels, only penalizing (because the numerator will decrease and hence the coefficient will decrease) when they are far apart, on opposite sides of the average.

Overlap Coefficient (OC). Another commonly used metric is known as the Overlap Coefficient (Equation 3) proposed by Manders et al. (1993). The coefficient produced by this equation describes how well the two images overlap, as if placed on top of each other. The Overlap Coefficient (Equation 3) differs from Pearson's Correlation Coefficient (Equation 1) in one major

way: The Overlap Coefficient (Equation 3) compares each X,Y pixel to the corresponding X,Y pixel in the other image, whereas in the Pearson's Correlation Coefficient (Equation 1) the pixels are reduced by the average of the image pixel values. This results in the Overlap Coefficient (Equation 3) ranging between 0 which denotes no colocalization and 1 which denotes complete colocalization. Pearson's Correlation Coefficient (Equation 1) will show negative correlation while the Overlap Coefficient (Equation 3) will only show the degree in which correlation exists. Pearson's coefficient can show a negative linear correlation, which would mean anti-correlation.

$$r = \frac{\sum_{Y=0}^{Y_{max}} \sum_{X=0}^{X_{max}} (Ch1_{(x,y)} * Ch2_{(x,y)})}{\sqrt{\sum_{Y=0}^{Y_{max}} \sum_{X=0}^{X_{max}} (Ch1_{(x,y)})^2 * \sum_{Y=0}^{Y_{max}} \sum_{X=0}^{X_{max}} (Ch2_{(x,y)})^2}}$$

Equation 3: Overlap Coefficient. The ∑ is the summation symbol; everything contained in its argument is summed. Each of these summations are for the image width (x) and height (y). For pixel y=0 means the top of the image, x=0 means the left edge. So when both x and y=0 the equation is examining the top-left pixel in the image. The subscript on the 'Ch' is the channel number being examined, since the equation works with multiple derived channels, in this case two, it is examining channel one and channel two. Ch(x, y) is the pixel intensity value at that (x, y) location. The numerator sums the product of the pixel intensities between all channels being examined. The denominator sums the channel intensity squared, before multiplying across all the channels being compared. This value is then taken to a square root.

Manders' Colocalization Coefficient (MCC). A third metric, the Colocalization Coefficient (Equation 4) was proposed by Mander's et al. (1993). The equation describing this measurement is very versatile and, unlike the previously mentioned approaches, allows for the comparison of any number of images. Furthermore, it provides insight into how one fluorescence label interacts with every other fluorescence label individually (Adler 2010). In this equation, the numerator sums the intensities of every pixel for the image being examined if the corresponding pixels in all the other images are above zero (Manders et al. 1993). Manders et al. (1993) state that this coefficient gives the amount of fluorescence of the co-localizing objects between components in

the image compared to the total fluorescence in that component. Even if the signal intensities differ greatly, the colocalization coefficient can still be determined.

$$M_1 = \frac{\sum_{Y=0}^{Y_{max}} \sum_{X=0}^{X_{max}} Ch1_{(x,y)} * Coloc_{i(x,y)}}{\sum_{Y=0}^{Y_{max}} \sum_{X=0}^{X_{max}} Ch1_{(x,y)}}$$

$$\text{Where Coloci}(x, y) = \begin{cases} 1, \text{if Ch1}_{(x,y)} > 0 \; for \; all \; j \neq i \\ 0, \text{Otherwise} \end{cases}$$

Equation 4: Manders' Colocalization Coefficient. Mn is the Manders' coefficient for the channel n being examined. The $\sum$ is the summation symbol, everything contained in its argument is summed. Each of these summations are for the image width (x) and height (y). For pixel y=0 means the top of the image, x=0 means the left edge. So when x, y=0 the equation is examining the top-left pixel in the image. $Ch_1(x,y)$ is the pixel intensity value for pixel x, y for the channel that is being examined. $Coloc_i$ is the intensity for that x, y pixel, but it is only used if it is considered colocalized. The numerator sums all the pixel intensity values if the pixel is considered colocalized. The denominator sums every pixel intensity value in the image regardless of being colocalized or not.

This coefficient has many advantages over the previous equations. For one, this method can easily be used on any number of channels by only allowing the numerator to be colocalized if all other channels are above zero. In this way, it is apparent if the fluorescence label is interacting with another specific fluorescence label or not, and the objects from that image are colocalized with all other fluorescence labels. Pearson's Correlation Coefficient (Equation 1) and the Overlap Coefficient (Equation 3) provide a global measure of colocalization across the channels being examined. While Manders' Colocalization Coefficient gives the amount of colocalization for each image channel when compared against every image channel in the dataset. Manders' Colocalization Coefficient (Equation 4) returns one value for each channel in the dataset.

One potential drawback to this equation is that the Manders' metric assumes that if the other channels are above zero, it is colocalized. While most background pixels are of pixel intensity zero, there are many background pixels that are above zero. This would result in

inflated coefficient values. This equation would perform better if the threshold was based on an analysis of the background instead of assuming the background is zero, or if the background was normalized to zero. The accuracy of the results would depend on the implementation of the equation. Since not all background pixels have the intensity of zero, many of these background pixels are considered object pixels. By not including background pixels the resulting ratio is based only on object pixels.

2.8 Colocalization Analysis State-of-the-Art

There are two main methods of colocalization analysis, Intensity Correlation Coefficient-based (ICCB) analysis and Object-based analysis. ICCB relies on the pixel intensity information of the images to calculate colocalization. Object-based analysis attempts to find objects in the images and only calculates colocalization for those objects. In both analysis techniques using the visual data from the overlap channel of the image is crucial. The overlap channel is the resulting data from performing ICCB or object-based analysis on the input image data set. This channel contains all the object pixels for the respective channel used to calculate the colocalization.

2.8.1 Intensity Correlation Coefficient-based (ICCB) Analysis

Intensity Correlation Coefficient-based (ICCB) analysis is the most frequently used and implemented. Due to the relative ease of implementation, most software packages contain ICCB analysis methods. Several of these methods can be implemented in about thirty lines of code each. These methods of analysis are now widely available in free software packages, and among

the most used are Pearson's Correlation Coefficient and Manders' Colocalization Coefficient (Dunn 2011).

Among the ICCB analysis methods are the three previously mentioned equations: Pearson's Correlation Coefficient (Equation 1), the Overlap Coefficient (Equation 3), and Manders' Colocalization Coefficient (Equation 4) (Zunchuk 2007). The major drawback to these methods is that no 3D spatial analysis is possible (Bolte 2006). However, a spatial Pearson' Correlation Coefficient has been implemented that is capable of analyzing two channels (Kuchcinski 2011). One of the main drawbacks of using the ICCB analysis methods is that high-throughput analysis is difficult. First, color images are created and a 2D histogram plot is generated. A visual inspection of the histogram is used to determine threshold levels. By automatically selecting the thresholds and analyzing the 8-bit grayscale images, high-throughput becomes possible (Kreft 2004). Since PCC and the OC are unable to produce results on more than two channel inputs, MCC was created to analyze any number of channels. However, MCC still has the limitation of absence of 3D spatial image analysis. For these reasons, object-based analysis methods have been introduced using computer vision techniques.

2.8.2 Object-based Image Analysis

Current confocal microscopy colocalization analysis techniques utilize image analysis to assist in detection of objects. Using the thickness of the image, some of these techniques are able to obtain 3D spatial analysis on a single image slice. Specifically there are three edge detection techniques used for object-based image analysis, the Canny edge detector, Laplacian of Gaussian edge detector, and the Sobel operator. The implementations of these object-based image analysis

techniques that are used are typically those implemented in the MatLab software package (Jaskolski et al. 2005). The output of the MatLab software package produces a matrix of intensity values of the processed image. This image can then be imported into a colocalization software analysis tool. It would be ideal to have the colocalization analysis methods integrated into MatLab, since many of the image processing techniques are already developed and widely used (Xu et al. 2007).

Some object-based analysis methods can be used to provide 3D spatial image analysis. The analysis is done on a single image slice using voxel information to get a 3D estimation of the cell structure. Voxel, (i.e., a pixel with volume), information is obtained using the thickness of the image slice. The main techniques that are currently used for colocalization image preprocessing is the Canny edge detector, the Laplacian of Gaussian, and the Sobel operator for edge detection. Many of these object-based analysis methods are being used for colocalization analysis (Kuchcinski 2011).

Using edge detection allows the objects to be transposed to a secondary image which can be analyzed. From this secondary image, data analysis can be performed on only the perceived objects. There are some drawbacks to the edge detection algorithms. Non-uniform structures can produce artificially detected concentric edges (Bolte and Cordelieres 2006). In edge detection-based techniques, 3D spatial analysis is performed on a single image slice using the thickness of the image. Edge pixels are delineated from object pixels by creating an edge map of each object, edge maps are created by determining the outline of the object. Edge detection is used to find edges of objects in images. There are three basic steps to edge detection.

i. Filtering: A filter is used to reduce the impact of noise on the edge detection algorithm. The filter blurs the image, making the noise less significant. The more an image is filtered the more edge strength, i.e., the confidence in whether the pixel is part of an edge or not, is lost.

ii. Enhancement: The enhancement process looks at neighboring pixels to determine if there is significant change in intensity in the area; this is a strong indication of an edge pixel.

iii. Detection: Search for pixels that are considered strong edges.

Canny Edge Detector

The Canny edge detector was developed to find optimal edges of objects in images. Its use in colocalization analysis is to find the objects and disregard the background and noise. The resulting image is then used as input for the colocalization algorithms. Preprocessing the images using any of these image processing techniques allows the researcher to obtain results based only on object image data, which the colocalization algorithms are not currently proficient at doing.

Steps:

I. Smooth the image with a Gaussian filter.

II. Compute the gradient magnitude and orientation using finite-difference approximations for the partial derivatives.

III. Apply non-maxima suppression to the gradient magnitude.

IV. Use the double thresholding algorithm to detect and link edges.

The first stage of the Canny edge detection algorithm uses a noise reduction technique called a Gaussian filter. This step is necessary because the Canny algorithm is susceptible to noise that may be present in the image. A Gaussian filter smoothes the image, which reduces the effect of noisy pixels. The second stage of the Canny edge detector uses the smoothed image resulting from the Gaussian filter to determine the gradients. The gradient is used to determine the orientation of the pixel to verify which way the edge in the image points.

The third stage of the Canny edge detector will return a binary image that contains a set of edge pixels. This process is called non-maxima suppression and it is used to thin the edges. Non-maxima suppression examines the ridges of the gradient magnitudes and suppresses the pixels that are not the peak values of that ridge. The last stage of the Canny edge detector uses a thresholding technique to classify which edge pixels are real and which are noise. The double thresholding algorithm is provided with two thresholds, one that genuine edges are thought to be above and another which false edges are below. The double thresholding algorithm will go through all the potential edge pixels and classify them as edge and non-edge pixels. (Jain 1995).

Laplacian of Gaussian Operator

The Laplacian of Gaussian operator combines Gaussian filtering with the Laplacian operator. The Laplacian operator uses the second derivative of the pixel intensity to determine whether a pixel is an edge pixel. Since the second derivative of the pixel intensity is very sensitive to noise, a filter must be used before the edges are enhanced. A Gaussian filter can be used to smooth the image. The Laplacian operator is then used to enhance the edges. If there is a peak in the first derivative of the pixel intensity and a zero in the second derivative of the pixel intensity, the pixel is considered to be part of an edge. (Jain 1995)

Sobel Operator

The Sobel operator is another widely used edge detection algorithm, which is much simpler than the Canny edge detector and the Laplacian of Gaussian. The Sobel operator estimates the magnitude of the gradient, where the gradient is calculated using a 3x3 neighborhood about the pixel [i, j]. The magnitude of the gradient describes how the pixel is oriented compared to its neighbors. If the magnitude is high it is likely that the pixel is an edge pixel. By examining each pixel in the image, and using each neighboring pixel to determine the magnitude, it is possible to generate a new image in which the edge pixels are white and the remainder of the image is black.

The Sobel operator is technically an enhancement technique and is therefore sometimes used by the Canny edge detector. While the results of the Sobel operator won't always produce comparable results to the more involved edge detectors, it is a quick implementation that performs well on low-noise images. Object-based image analysis techniques do not perform colocalization, they are used for preprocessing to select only objects that should be analyzed by colocalization methods. These techniques provide the preprocessing needed to yield more accurate results with the colocalization analysis equations. The colocalization equations do not filter out noise and artifacts as the object-based image analysis algorithms do.

2.8.3 Visualizing Confocal Images

When the raw data is sent from the confocal microscope, it is not in color. Each channel is represented by a grayscale image. To make a visual inspection possible, color-coded channels are used to make a signal overlap image. The idea is that if the two channels are displayed as red

and green, the overlap will display as yellow (Bolte and Cordelieres 2006). When analyzing the signal overlap image, the result of combining the grayscale images, high-throughput analysis is not possible (Kreft et al. 2004).

Currently, the high-throughput limitation is evident in most implementations of the ICCB and Object-based analysis techniques. Work done by Kreft et al. (2004) has used the raw data information to analyze confocal images using Pearson's Correlation Coefficient (Equation 1) to offer high-throughput analysis. This work is restricted to two channel experiments and 2D spatial analysis. The current object-based analysis methods are only implemented using the signal overlap method. The signal overlap method uses the pixel intensities of one channel and compares it to the pixel intensity of an image in another channel; Pearson's Correlation coefficient, the Overlap Coefficient, and Manders' Colocalization coefficient are all examples of implementations of signal overlap methods. This implementation reduces the possibility of high-throughput analysis and has more potential for error. "The presence of yellow spots is highly dependent on the relative signal intensity collected in both channels; the overlay image will only give are liable representation of colocalization in the precise case where both images exhibit similar grey level dynamics, i.e. when the histograms of each channel are similar" (Bolte and Cordelieres 2006).

Since the object-based analysis methods analyze the signal overlap image, the standard colocalization equations are unable to analyze the processed images. The signal overlap image is one image containing all of the channel image information, where each channel is represented by a different color channel. The objects and edges are labeled on the signal overlap image/channel, which is not capable of being analyzed by the standard colocalization analysis equations. Therefore, these object-based analysis methods should be performed on the raw grayscale

images instead of the signal overlap images. This could be resolved by reformulating the equations to analyze the signal overlap images. However, since the data from the confocal microscope is in grayscale format, it makes more sense to keep the image analysis on the raw data files and only use the signal overlap for visual inspection.

2.9 Limitations of Current Approaches

Historically, the various approaches to colocalization analysis have been restricted to single (x, y) planar images due to limitations of available analysis software. Furthermore, the analysis has also been limited to comparisons between two measured or derived channels of color or light intensity. Biological processes are almost always complex and involve many different interactions, and the ability to analyze the interplay of multiple interactions would allow for better understanding of these systems. Furthermore, to be able to accurately examine these images, a consistent method of removing background noise must be employed as well. The measurement of multiple interactions and measurement in 3D space are the two major limitations of the available software. Overcoming these limitations will provide researchers the tools they need to make more accurate conclusions about the experiments. Insights to overall colocalization may be found throughout the whole sample being studied, not just in a single representative slice, and it is often important to examine the entire specimen. Being able to consider colocalization in context of the entire 3D spatial object would allow for greater accuracy of measurement.

Many investigations would be well served with the ability to analyze interactions of multiple parameters, however current metrics allow for examination of only two fluorescence

channels (two images) at a time. The existing approaches to comparative colocalization analysis (Equation 1, Equation 3 and Equation 4) are well suited for analyzing two interactions. However when posed with three or more interactions, averaging techniques would need to be implemented to get accurate results for more than two fluorescence labels. Instead of implementing averaging techniques on the results of the equations, the equations can be modified to work on multiple interactions. By modifying the equations (Equation 1, Equation 3 and Equation 4) to work on any number of input channels, the results produced would be identical to using an averaging technique just without the added steps for every channel after the first two.

The background of the images needs to be consistently removed to standardize the selected thresholds; the background does not only consist of pixels of intensity value zero (black) which is assumed in Equation 4. Selecting a pixel intensity threshold of one would make most of the background noise appear to be object pixels, whereas selecting a background pixel intensity threshold that is near the pixel intensity maximum (ex: a threshold of 200 where the maximum pixel intensity possible is 255) would make most of the object pixels appear to be background noise. Therefore, the selected thresholds greatly impact the colocalization results, as the ratios are dependent upon co-localizing object pixels. Without proving that a proper threshold has been selected for each image and channel, the results cannot be universally accepted. If the threshold selection was automated by an intelligent search heuristic, that is accepted to produce accurate results without user intervention, then the selected thresholds would not need to be proven for every image and channel. Realistically, if all of the background noise were to be considered as colocalized pixels, the colocalization results of the experiment would be significantly higher in all metrics. Automatically selecting the thresholds using a heuristic method presents a simple solution to overcome variability in threshold selection.

While it is possible to collect data on the 3D spatial data set, these equations are not able to examine the whole data set and produce one result. All of these methods only work on (x, y) planar images and only when analyzing two fluorescence labels at a time (with the exception of Manders' coefficient (Equation 4)). Since these equations produce results on only one 2D image at a time, the series of 2D images produced by the confocal microscope can only be examined in 2D. This software analyzes the 2D image series produced by the confocal microscope to recreate the 3D image and analyze spatial colocalization in 3D.

2.10 Addressing the Limitations

The limitations of 3D spatial analysis and n-channel analysis are overcome by implementing modified equations that work with more fluorescence labels and a new algorithm that is capable of 3D spatial analysis. The original equations have been modified so that they can produce results on samples that have more than two channels. A computer vision algorithm, Region Growing with Double Thresholding, grows objects between the (x, y) planar images as well as between (x, y, z) spatial images. The population-based hill climbing algorithm supplies the computer vision algorithm with two thresholds needed to grow regions of interest and remove background noise. Finally, a benchmarking procedure and a Monte-Carlo simulation procedure have been executed to prove the validity and accuracy of all the modified and newly implemented equations.

The pre-existing equations have been modified so that they are capable of producing results for samples stained with more than two fluorescence labels. By modifying the equations to work on two or more (n-) parameters instead of only two parameters, the equations are able to

scale to any number of fluorescence labels. A computer vision algorithm is implemented to grow regions of interest. This algorithm is used to grow objects within the XY planar images, as well as between the X,Y,Z images spatially. The algorithm works by selecting object pixels that are known to be of interest and ignores the parts of the image that are not regions of interest. Due to the algorithm's ability to ignore non-object pixels, it also performs well at removing background noise and artifacts in the images. The computer vision algorithm requires two thresholds to be able to grow regions of interest and remove background noise. The population-based hill climbing algorithm finds the two most significant modes, in this case the two most frequent pixel intensity values found in the histogram, of the multi-modal histogram of each image and uses those values as object and background thresholds. The population-based hill climbing algorithm takes the search space, in this case the 1D plot produced by a histogram, and climbs the peaks of the histogram to determine the two most significant modes.

Every equation and algorithm that was developed or modified was benchmarked against a set of images designed to give specific results. These images make it easy to see the expected results and therefore it is easy to see whether or not the equations (Equation 1, Equation 3 and Equation 4) perform as expected. The modified equations are benchmarked before and after modifications, so that the changes can be noted. By using a Monte Carlo simulation, it is shown that these modified equations will work spatially on n-channels. It is demonstrated that the results of Equation 5 and Equation 6 on repeated random sampling of data provides consistent results. The Monte Carlo method is often used to accompany a theoretical derivation. In this instance it was not feasible to provide an inductive proof to show the consistency of the modified equations.

CHAPTER 3

IMPLEMENTATION

3.1 Solving the Channel Limitations

Equations for Pearson's Correlation Coefficient (Equation 1), the Overlap Coefficient (Equation 3), and Manders' Colocalization Coefficient (Equation 4) were modified to allow the examination of more than two channels. The process of modifying the equations is explained in detail below, showing a step by step process.

3.1.1 Pearson's Correlation Coefficient

Pearson's Correlation coefficient (Equation 1) works well when examining two channels, but has not been implemented to be used on more than two. The structure of Pearson's Correlation Coefficient allows for analysis on two channels but with modifications, it is capable of working on n-channels. Outlined below is the process of modifying Pearson's Correlation Coefficient to work on n-channels (where $n>2$).

Table 1: Two Channel (Axis) Example. This example has two channels that are being examined. Each channel only contains one image; each image has only two pixels. This example is extremely simplified so that the entire equation can be shown. The two images being compared are the same image. Since the images are identical, the averages are the same and the pixel values are all the same. The equation can now be shown in its entirety without being too cumbersome.

Channel 1		Channel 2	
Pixel 1	Pixel 2	Pixel 1	Pixel 2
100	0	100	0
Channel 1 Average = 50		Channel 2 Average = 50	

Table 1 is a very simplified test case. There are only two channels being compared (two images total, one in each channel). Each image has only two pixels, one light (100), and one dark (0). The example is kept simple so the average is easy to calculate, the equation is easy to work out.

$$Rp = \frac{((100-50)*(100-50))+((0-50)*(0-50))}{\sqrt{((100-50)^2+(0-50)^2)*((100-50)^2+(0-50)^2)}}$$

Figure 2: Pearson's Correlation Coefficient Two Channel Example. Data from Table 1 is instantiated into Equation 1.

In Figure 2, the test data from Table 1 is inserted into Pearson's Correlation Coefficient (Equation 1) .The whole summation is laid out in both the numerator and the denominator. In the numerator we have pixel 1 intensity of channel 1 (100) subtracted by channel 1 average (50), this is multiplied by pixel 1 intensity of channel 2 (100) subtracted by channel 2 average (50). The data from pixel 1 is then added to the same calculations but for pixel 2.

The denominator of Figure 2 is similar to the numerator, but the calculations are made per channel instead of per pixel. So the intensity minus the channel average for pixel 1 and pixel 2 of channel 1 is calculated first, then the same is done but for channel 2.

Table 2: Three Channel (Axis) Example. This example has three channels that are being examined. Each channel only contains one image; each image has only two pixels. This example is extremely simplified so that the entire equation can be shown. The three images being compared are the same image. Since the images are identical, the averages are the same and the pixel values are all the same. The equation can now be shown in its entirety without being too cumbersome.

Channel 1		Channel 2		Channel 3	
Pixel 1	Pixel 2	Pixel 1	Pixel 2	Pixel 1	Pixel 2
100	0	100	0	100	0
Channel 1 Average = 50		Channel 2 Average = 50		Channel 3 Average = 50	
$Rp^3 = 1.0$					
$Rn^3 = 1.0$					
M1 = 1.0		M2 = 1.0		M3 = 1.0	

Equation 5 takes Pearson's Correlation Coefficient (Equation 1) and expands it to work on (n)-channels as well as three-dimensional spatial image stacks. As this equation can work on n-channels, it will work on 2 channels or 20 channels, or as many as needed permitting available memory space (RAM). The equation remains the same in the numerator, except that more channel information is included, but the nature of the equation isn't modified. The denominator of Equation 5 has been modified by generalizing the Euclidean norm to include all channels. To perform the 3D spatial analysis the numerator and denominator are summed on the z-axis as well.

$$Rp^n = \frac{\sum_{Z=0}^{Z_{max}} \sum_{Y=0}^{Y_{max}} \sum_{X=0}^{X_{max}} ((Ch1_{(x,y)} - Ch1_{avg}) * (Ch2_{(x,y)} - Ch2_{avg}) * \dots * (ChN_{(x,y)} - ChN_{avg}))}{\sqrt[N]{\sum_{Z=0}^{Z_{max}} \sum_{Y=0}^{Y_{max}} \sum_{X=0}^{X_{max}} (|Ch1_{(x,y)} - Ch1_{avg}|)^N * \sum_{Z=0}^{Z_{max}} \sum_{Y=0}^{Y_{max}} \sum_{X=0}^{X_{max}} (|Ch2_{(x,y)} - Ch2_{avg}|)^N * \dots * \sum_{Z=0}^{Z_{max}} \sum_{Y=0}^{Y_{max}} \sum_{X=0}^{X_{max}} (|ChN_{(x,y)} - ChN_{avg}|)^N}}$$

where, if the numerator contains an even number of negative values in a term, the absolute value of the term is taken.

Equation 5: Modified Pearson's Correlation Coefficient Equation. This equation is Pearson's Correlation Coefficient from Equation 1, modified to work spatially on n-channels (n>2).

$$Rp^3 = \frac{((100-50) * (100-50) * (100-50)) + ((0-50) * (0-50) * (0-50))}{\sqrt[3]{(|(100-50)|^3 + |(0-50)|^3) * (|(100-50)|^3 + |(0-50)|^3) * (|(100-50)|^3 + |(0-50)|^3)}}$$

Figure 3: Modified Pearson's Correlation Coefficient Example. This is the modified Pearson's Correlation Coefficient Equation 5 with the data from Table 2. The numerator and denominator are equal since there are more than one negative values in the second pixel calculation in the numerator – thus resulting in taking the absolute value of (0-50) * (0-50) * (0-50).

3.1.2 Overlap Coefficient

As with Pearson's coefficient (Equation 1), the Overlap Coefficient needs to be modified in order to be able to handle more than two channels. The numerator needs to incorporate every channel being examined, and therefore the (x, y) pixel value needs to be multiplied into the other pixel values. The denominator needs to be expanded to a Euclidean norm of size n. To perform the 3D spatial analysis the numerator and denominator are summed on the z-axis as well.

$$r^n = \frac{\sum_{Z=0}^{Z_{max}} \sum_{Y=0}^{Y_{max}} \sum_{X=0}^{X_{max}} (Ch1_{(x,y)} * Ch2_{(x,y)} * \dots * ChN_{(x,y)})}{\sqrt[n]{\sum_{Z=0}^{Z_{max}} \sum_{Y=0}^{Y_{max}} \sum_{X=0}^{X_{max}} (Ch1_{(x,y)})^n * \sum_{Z=0}^{Z_{max}} \sum_{Y=0}^{Y_{max}} \sum_{X=0}^{X_{max}} (Ch2_{(x,y)})^n * \sum_{Z=0}^{Z_{max}} \sum_{Y=0}^{Y_{max}} \sum_{X=0}^{X_{max}} (ChN_{(x,y)})^n}}$$

Equation 6: Modified Overlap Coefficient. This equation is the Overlap Coefficient (Equation 3), modified to work on n-channels (2+) and for 3D spatial analysis.

$$r^3 = \frac{(100 * 100 * 100) + (0 * 0 * 0)}{\sqrt[3]{(100^3 + 0^3) * (100^3 + 0^3) * (100^3 + 0^3)}}$$

Figure 4: The Modified Overlap Coefficient. The Modified Overlap Coefficient (Equation 6) with the data inserted from Table 2. The numerator and denominator equal (100*100*100), illustrating complete colocalization.

The same tests that were used for Pearson's Correlation coefficient (Equation 5) are used to examine the Overlap Coefficient (Equation 6). The pixel data is from Table 1 and Table 2, but the channel average is not needed for these tests.

3.1.3 Colocalization Coefficient

Manders' Colocalization coefficient (Equation 4) does not need any modifications to work on n-channels (where n>2). Since this equation only calculates a colocalization coefficient for one channel, and only considers a pixel value colocalized if all other channels are above a threshold, the only change needs to be made in the software to allow for those additional comparisons. For Manders' Colocalization Coefficient to work spatially in 3D, it will need to be modified to be summed over the z-axis.

$$M_1 = \frac{\sum_{Z=0}^{Z_{max}} \sum_{Y=0}^{Y_{max}} \sum_{X=0}^{X_{max}} Ch1_{(x,y)} * Coloc_{i(x,y)}}{\sum_{Z=0}^{Z_{max}} \sum_{Y=0}^{Y_{max}} \sum_{X=0}^{X_{max}} Ch1_{(x,y)}}$$

$$\text{Where Coloci(x, y)} = \begin{cases} 1, \text{if Ch1}_{(x,y)} > 0 \; for \; all \; j \neq i \\ 0, \text{Otherwise} \end{cases}$$

Equation 7: Modified Manders' Colocalization Coefficient. This equation is the Manders' Colocalization Coefficient (Equation 4), modified to perform 3D spatial analysis.

$$M_1 = \frac{(100 * 1) + (0 * 0)}{(100)}$$

$$M_2 = \frac{(100 * 1) + (0 * 0)}{(100)}$$

$$M_3 = \frac{(100 * 1) + (0 * 0)}{(100)}$$

Figure 5: Modified Manders' Colocalization Coefficient Example. The Modified Manders' Colocalization Coefficient (Equation 7) with the data inserted from Table 2. For each return value,(M1, M2 and M3) the numerator and denominator equal 100, illustrating complete colocalization.

3.2 Benchmark Images

Test images are used to evaluate the equations. Each equation is tested on different configurations of benchmark images that are designed to give certain results. The benchmark images (Figure 6) were designed by Manders' et al. (1993) and have not been changed for this research. These images are suitable test images because they show specific degrees of colocalization that are visible to the naked eye. The objects in the test images are all squares, and in a grid layout, making it easy to see which blocks are colocalized (Figure 6).

These benchmark images (Figure 6) are used to show colocalization ratios. There are blocks of pixels, either black or white, so there is either full colocalization or zero colocalization for each pixel. Each block of pixels contains the same number of pixels, they are all the same size and shape. The only difference between each block is the (x, y) location.

There are a total of 36 blocks. Between the test images, these blocks appear in different areas of the image. From one image to the next, one or more blocks may be out of alignment with each other. If every block aligns there is full colocalization, if no blocks align there is zero colocalization.

When examining the benchmark images with the software component of this project, each image is put into a separate channel. The first image would be considered as channel one, the second image as channel two and so on.

Using different combinations of these images it is possible to design experiments that yield specific results. Whether or not these specific results are returned by the software component of this project is used to test whether or not the equations function properly.

3.3 Testing Model

Each of the expanded equations has been tested on each image to show that they return the same results as reported by Manders et al. (1993). Following validation for two channels, the tests were then expanded to examine three channels. The equations were then tested to show they provide results on 3D spatial stacks as well.

The tests were arranged so that every image from Figure 6 was tested against image A (from Figure 6). In the first test, comparing image A to image A, there should be full colocalization as the images are identical and all pixels match exactly in location and intensity.

When comparing image A to image B there are a total of 45 different objects with 27 of them co-localizing completely. While it looks as though 75% of the objects are colocalized, the results should be 60%. If you were examining this test with Manders' Colocalization Coefficient the results should be 0.75. This is because the equation only compares the objects in one image to co-localizing objects in the other, not all the objects of both images.

When comparing image A to image C, there are 54 different objects with only 18 of them co-localizing completely. The colocalization ratios should be one-third because 18 of the 54

objects are colocalized, but if all the objects aren't taken into account from the second image the colocalization ratio would be one-half.

Using this testing model it is shown that Pearson's Correlation Coefficient (Equation 1), the Overlap Coefficient (Equation 3), and Manders' Colocalization Coefficient (Equation 4) do not produce desired results because they do not take all of the information into account. It is then shown that the new method introduced by this project does use all of the information to give a more complete explanation of the experiment.

After the equations were tested on two channels, they were then tested on three channels. By adding image A as the third channel the results should not change as there are no additional objects and there is no additional overlap. Therefore each test that was done on two channels is repeated with a third channel containing image A.

Following the validation of the equations on three channels, the equations were then executed on 3D spatial image stacks. There are three synthetic image stacks that were used for testing the modified equations. These synthetic image stacks use combinations of the benchmark images from Figure 6. The stacks have two channels and three images in depth (i.e., along the Z axis), so there are two stacks with three images in each. The channel one image stack has only image A, whereas the channel two image stack is varied to show how the results change.

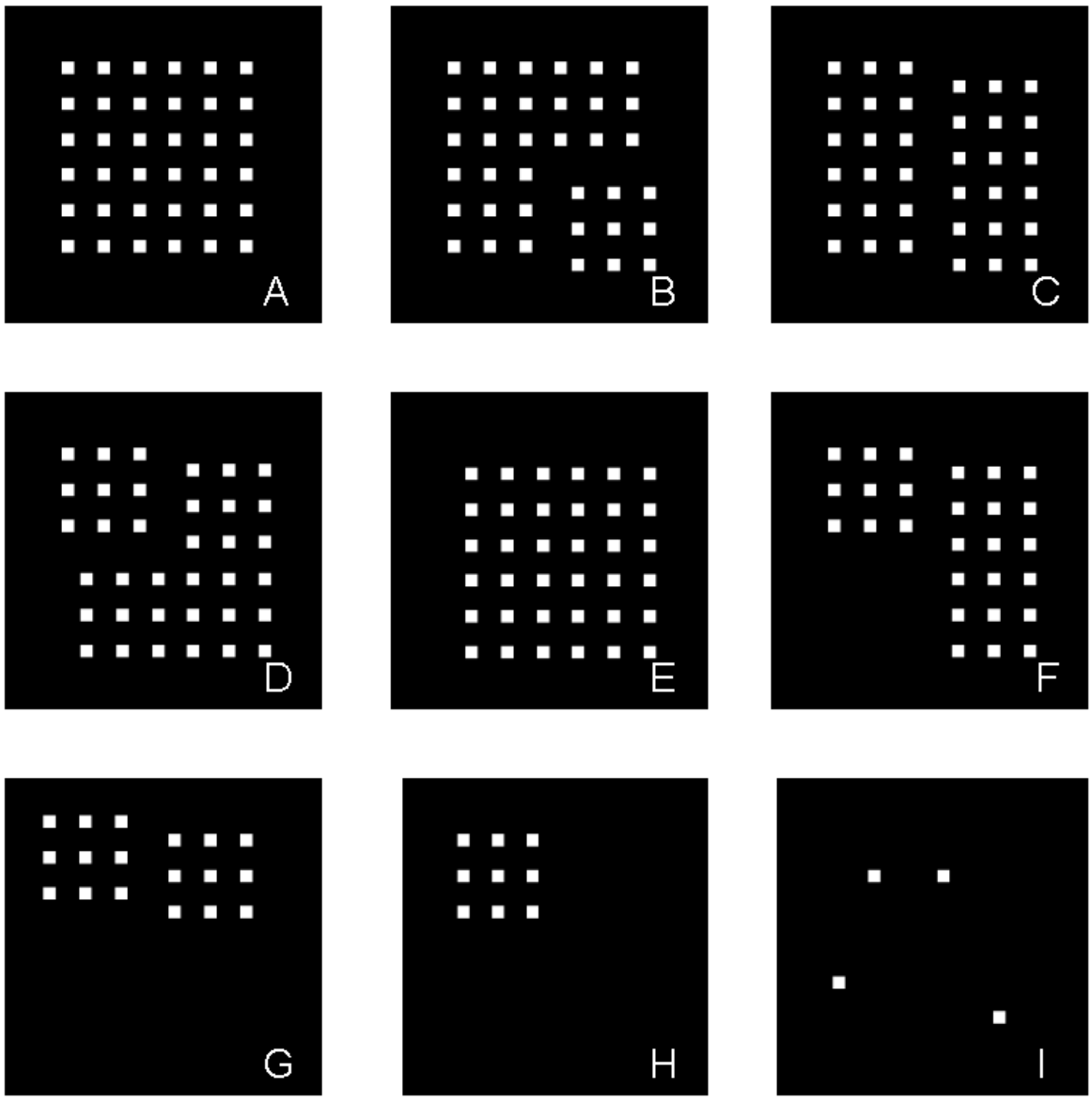

Figure 6: Benchmark images. The blocks in these images are all the same size, and they are set up in a grid layout. The letter on each image is not actually in the image, it is just used to reference the image in the text.

3.4 Implementing a 3D Spatial Analysis Technique

The 3D spatial analysis, the Spatial Colocalization Coefficient (Equation 8), technique was first implemented to work as an extension of 2D spatial analysis, like the original equations (Equation 1, Equation 3 and Equation 4), so that its results could be compared. This algorithm intelligently determines whether the 3D spatial analysis needs to be performed; it will perform both 3D spatial and 2D spatial analysis.

The Spatial Colocalization Coefficient (L_s) takes two thresholds as input parameters. One threshold is the pixel value for which all pixel intensity above it (with greater intensity) is considered an object pixel. The second threshold is the background threshold; every pixel below this threshold is considered to not be part of the objects (i.e., considered part of the background). These two thresholds are not the same. If there was only one threshold then all of the pixels would be either objects or background pixels. The objective of this algorithm is to categorize the pixels that are questionably significant. The background noise distribution may be skewed to the point that it is not clear whether it is background noise or not, this algorithm sorts through those questionable pixels to determine whether they are object or background pixels.

When performing a 2D spatial experiment the Spatial Colocalization Coefficient (L_s) compares the other pixels from the same image slice. When performing a 3D spatial experiment the Spatial Colocalization Coefficient (L_s) also compares pixels from the adjacent z-subsections. Only images that are above or below the image being examined are used to categorize the pixels; an image that is at the bottom of the 3D spatial object will not affect the image categorization at the top of the 3D spatial object. This means that any image adjacent to the image slice being examined will affect how those pixels are classified.

Each pixel from every image is examined. If a pixel is not above the object threshold, and not below the background threshold, it needs to be categorized. For these pixels the neighboring pixels need to be examined. If a neighboring pixel is an object pixel, it is classified as an object pixel. This is how the object regions are grown.

The 3D spatial analysis of the object is accomplished with a modification of the Region Growing with Double Thresholding algorithm. The Region Growing algorithm works spatially in 3D almost exactly as described for 2D spatial analysis with only one slight difference: image slices in a channel take into account the adjacent slices (slices above and below it). Basically the pixel must be an object pixel and have an adjacent object pixel on the (X, Y) plane as well as on the Z plane. It is not required to have a pixel both above and below, at least one is required. If there is not an object pixel adjacent (North, South, East, or West) or spatially above or below the pixel in question, it is considered an artifact and not part of the object. If any one of those adjacent pixels is considered an object pixel, then it too will be considered an object pixel.

To test the 3D spatial analysis method two channels were examined, each with three images. Three images were used for the 3D spatial analysis tests because more combinations of tests can be performed than on two images, and any more images would convolute the explanation of how the algorithm works. The first test only has image A (Figure 6). This should return 100% spatial colocalization. The second test has image A for all but one image, the second channel's bottom image is image B (Figure 6). The third test has the same images as test two, but with the second channels' top image being image B as well.

This algorithm will also be shown to work on three real test cases, along with the results of the other equations. By comparing the results from Pearson's Correlation Coefficient (Equation 1) the Overlap Coefficient (Equation 3), and Manders' Colocalization Coefficient

(Equation 4), to the results of the Colocalization Algorithm we will show that the Colocalization Algorithm results provide a unique perspective on colocalization analysis.

The Region Growing with Double Thresholding algorithm has 5 steps:

1) Two thresholds are selected (T1 and T2).

One of these thresholds should come from a negative control for that channel. A negative control is produced by imaging the samples before the treatment is applied to study the colocalization. A negative control gives the inherent background noise for the current settings of the confocal microscope. If a negative control is used and uploaded to the program then it will be used, otherwise the lower bound threshold will be calculated from the image being examined using the automatic thresholding technique. The lower bound threshold is the greatest pixel intensity value in 99^{th} percentile of the control. The upper bound threshold comes from the individual image and is the dominant mode of the histogram.

2) The image is then parsed into 3 regions, background pixels, object pixels, and questionable pixels so that the questionable pixels can be categorized as either object or background pixels.

Region 1 is every pixel that has a pixel value lower than T1. This is strictly the background pixels.

Region 2 contains all pixels that have pixel values between T1 and T2, inclusive.

Region 3 has all pixels that have a pixel value equal to or above T2. These pixels are object pixels and are used to grow the objects.

3) Each pixel in Region 2 is examined.

    If a region 2 (questionable) pixel is a neighbor of a pixel in Region 3 (object pixel), it is moved to Region 3 (with the other object pixels). Otherwise it is left in Region 2.

4) Step 3 is repeated until no pixels are reassigned.

5) Any pixels left in Region 2 should be moved to Region 1, as they are not connected to any object pixels and can be considered noise.

As with Pearson's Correlation Coefficient (Equation 1), the Overlap Coefficient (Equation 3), and Manders' Colocalization Coefficient (Equation 4), once the Colocalization Algorithm is performed the pixel intensities are now classified as either colocalized or non-colocalized (object or background, respectively). After the double thresholding algorithm classifies each pixel from every slice and every channel, it is possible to determine the total localization.

Once every pixel has been classified, a tally is taken. The numerator equals the sum of every (x, y) location in each slice across every channel that is considered colocalized. The denominator is the sum of every (x, y) location in each slice across every channel, if at least one pixel from any channel is considered to be colocalized.

$$L = \frac{\sum_{Z=0}^{Z_{max}} \sum_{Y=0}^{Y_{max}} \sum_{X=0}^{X_{max}} \sum_{C=0}^{Ch_{max}} (Coloc_{all\ (x,y,z)})}{\sum_{Z=0}^{Z_{max}} \sum_{Y=0}^{Y_{max}} \sum_{X=0}^{X_{max}} \sum_{C=0}^{Ch_{max}} (Coloc_{any\ (x,y,z)})}$$

$$Where\ Coloc_{all\ (x,y,z)} = \begin{cases} 1, if\ all\ Ch_{c(x,y,z)} are\ colocalized \\ 0, Otherwise \end{cases}$$

$$Where\ Coloc_{any\ (x,y,z)} = \begin{cases} 1, at\ least\ one\ Ch_{c(x,y,z)} is\ colocalized \\ 0, Otherwise \end{cases}$$

Equation 8: Spatial Colocalization Coefficient (L_s).

3.5 Automatic Thresholding through Bimodal Histogram Analysis via Population-Based Hill Climbing

To automate and standardize the threshold selection process, this algorithm has been implemented to provide input to the Double Thresholding with Region Growing algorithm. This algorithm finds a bimodal approximation of a multimodal histogram by determining two significant maxima that are reasonably well separated.

The upper bound threshold (T2) of the Double Thresholding with Region Growing algorithm is found using a local search heuristic on the image's histogram. By using a population-based local search or hill climbing, it is possible to find these bounds with limited effects to the overall processing speed of the data. This algorithm was tested on both benchmark images, as well as several test case images to show that proper threshold selection is possible through histogram analysis.

Population-based Hill Climbing:

The objective of the population-based hill climbing algorithm is to find the two most frequent pixel intensities in the histogram. A population is created that is one fifth the size of the histogram. The histogram has 256 possible intensities, so the population has a size of 51, each individual of the population is known as an individual. These 51 individuals are spaced evenly throughout the histogram. The population consists of pixel intensities; the value of the individual in the population is the frequency of the pixel intensity the individual represents. For example, individual 1 would have the histogram count of pixel intensity 1; individual 51 would represent the histogram count of pixel intensity 251. This way all individuals are spread out evenly throughout the histogram.

The next step in the histogram analysis is to examine the local area around each individual and compare histogram frequencies. The algorithm will run until there has been no change between iterations; this occurs when the global maxima have been found. To remove variability in the returned values of the automatic thresholding algorithm, there are no customizable parameters. The population size is automatically determined to be one fifth of the image bit depth so it will scale with images that have a larger color palette. The local neighborhood size is restricted to 15 to promote competition among maxima by preventing all individuals from moving immediately to the global maxima. This size local neighborhood allows a more gradual move towards global maxima while still allowing non-global maxima to be discovered.

Each individual is able to check other individuals within its local neighborhood. For these tests the distance was set to 15 because this value was large enough for all tests to find the global maxima while not going through needless iterations. The reason for allowing each individual to view many neighboring individuals is to give the individual the opportunity to climb down a hill

(out of a local maximum) and back up another (potentially a global maximum). If the individual was able to see only its adjacent neighbors, the population might not converge around global maxima. If the neighborhood size is set too low, it is likely that the individuals will get stuck in a local maximum. Local maxima are peaks in the histogram but do not represent one of the global maxima. A global maximum is a local maximum that is greater than all other local maxima. In this algorithm we want to find two global maxima to set as our thresholds for the Region Growing Double Thresholding algorithm, so the two highest local maxima are chosen.

After the algorithm has converged, and additional iterations will not change or improve the results, the population is examined. The total counts for each local maxima are found. These numbers are then compared; the two highest values are used as the upper and lower bound. The lower of these two intensity values can potentially be set to the lower bound (T1) for the Region Growing algorithm, if a negative control was not used. The higher intensity value will be used for the upper bound (T2) for the Region Growing algorithm. Using the population-based hill climbing algorithm a minimum separation of the returned thresholds is guaranteed without setting a minimum distance. Since each individual is able to see 15 neighbors to either side of its current location, the absolute minimum distance between any two maxima is greater than 15. There is some danger in putting a minimum distance between the two thresholds. If the image was very dim, mostly pixel intensities between 0 and 50, the upper bound might not be set. If the upper bound is not set, or it is left at a default of 255 and there are no pixel intensities at 255, there would be no object pixels. This would result in zero colocalization.

The distance an individual is allowed to move in any given turn affects the minimum distance between the two thresholds that are returned by the algorithm. In a situation where two peaks are potentially too close there are a few possible scenarios. One, there are only two peaks

and those two must be selected. Two, there is a third peak that is a further away; this peak will not compete with the other two and will very likely attract more individuals. Unless the two adjacent peaks are of the same height, they will compete for surrounding individuals.

Objective – Find two peaks with the highest pixel intensity frequency
Convergence Criteria – When no improvements are made between successive iterations

1- Generate Histogram *Histo*
2- Initialize Population P with Individuals I
3- Intialize Distance D

4- Find all local maxima
For All $i \in p$
  Find local maximum within range of +/- D neighbors
  $i_{location}$ = neighbor with highest frequency

5- Count inviduals at each peak

6- Take top two peaks with the most individuals
  Lowerbound threshold LB = peak with lower pixel intensity value
  Upperbound threshold UB = peak with higher pixel intensity value

Figure 7: Pseudo code for the Bimodal Histogram Analysis via Population-Based Hill Climbing.

3.6 Automatic Thresholding through Bimodal Histogram Analysis via a Limited Exhaustive Search

In addition to the population-based hill climbing algorithm a limited exhaustive search algorithm has been implemented to offer an alternative method for retrieving threshold values. The limited exhaustive search algorithm is less computationally expensive, resulting in faster processing of larger image sets. Typically an exhaustive search is much more computationally expensive than a population-based hill climbing or heuristic search. However, the limited exhaustive search

algorithm examines the entire histogram once and stores local maxima in sections, one-twentieth of the bit depth, of the histogram. The population-based hill climbing algorithm is being used to examine an entire data set while a hill climbing algorithm is typically used to examine a small section of the search space, and one individual usually climbs the hill. In the population-based hill climbing algorithm there are many individuals searching overlapping areas which results in the search space being traversed more than once. The population-based hill climbing algorithm returns a group of local maxima, ensuring that the returned thresholds are reasonably well separated.

The limited exhaustive search algorithm begins by segmenting the histogram into local neighborhoods. Each neighborhood is one-twentieth the range of pixel intensity values. Within each local neighborhood every pixel intensity frequency is examined. The largest pixel intensity frequency is selected as the local maximum for that local neighborhood. Each neighborhood is then compared to its adjacent neighborhoods. When the maximum in one local neighborhood has been found to be greater than those in adjacent neighborhoods in one-fifth of the range of pixel intensity values it is determined to be the maximum for that area. This is performed for the lower bound and the upper bound values, the lower bound beginning with pixel intensity value starting at zero and the upper bound with pixel intensity value equal to the bit depth.

This algorithm does not fit into the traditional exhaustive search algorithm specifications. Typically the exhaustive search algorithm would examine every pixel intensity frequency and select the largest value. Using a limited exhaustive search algorithm for threshold selection in images requires returning two values, not one. The approach has been modified to ensure that a lower bound and an upper bound are properly selected. Most images are skewed in pixel intensity frequency, either having a greater number of light or dark pixels. In either situation the

two largest pixel intensity frequencies are likely to be in the same area. Applying the limited exhaustive search algorithm in this manner results in threshold values more likely to represent the object or background regions.

Objective – Find two peaks with the highest pixel intensity frequency

1- Generate Histogram *Histo*
2- Generate groups of pixels (1/20th of the range of pixel intensities in size) for local maxima *Neighborhood*
3- Select greatest pixel intensity frequency *localMax* from each *Neighborhood*
4- Select lower bound threshold *LB*

For All *localMax* $\in$ *Histo*
Assign *LB* to *localMax* from the first *Neighborhood*
Compare *LB* to adjacent *localMax* values
If *LB* > *localMax* for consecutive *Neighborhoods*
totaling 20% of the range of pixel intensity values, return *LB*
If *localMax* > *LB*, *LB* = *localMax*

5- Select lower bound threshold *LB*

For All *localMax* $\in$ *Histo*
Assign *UB* to *localMax* from the last *Neighborhood*
Compare *UB* to adjacent *localMax* values
If *UB* > *localMax* for consecutive *Neighborhoods*
totaling 20% of the range of pixel intensity values, return *UB*
If *localMax* > *UB*, *UB* = *localMax*

6- Check *LB* < *UB*

If *LB* > *UB*
Temp = *LB*
LB = *UB*
UB = Temp

Figure 8: Pseudo code for the Bimodal Histogram Analysis via Limited Exhaustive Search.

3.7 Monte Carlo Simulation Tests

To verify the accuracy of the modified equations and the newly implemented equation, a Monte Carlo simulation was performed. A Monte Carlo simulation is a method of repeatedly testing an algorithm or equation with random data.

To perform a Monte Carlo simulation on the modified and newly implemented equations, random data needs to be generated. This random data is in the form of images, which make up an image stack. A varying number of input channels and input slices are used in a sequence of tests.

Each test will consist of a specific number of channels, a specific number of slices, and a number of times the test is performed. For example, one test will consist of 4 channels, with 10 slices in each channel. A colocalization computation of the base configuration is performed, then a random channel is added and the results recomputed. A duplicate channel is then added to the base configuration and the colocalization results recomputed.

The equations are run using the base configuration for an image stack; this configuration is used 50 times to generate the data. All of the data generated by this configuration is used to find the average change in value from the base configuration to the results from adding a randomly generated channel. The same procedure is repeated by adding a channel to the base configuration that already exists in the randomly generated image stack. This channel is referred to as a duplicate channel. Adding a random channel to the data set should on average decrease the colocalization since it is less likely there are overlapping objects. Adding a duplicate channel to the data set should result in more colocalization, since at least two channels are identical. When a duplicate channel is added to the image stack the resulting calculations should either increase, not change, or decrease less than when a random channel is added.

All possible configurations are simulated using a set of number of slices and a set of number of channels.

- Number of Slices = {5, 10, 15}
- Number of Channels = {2, 3, 4, 5, 6, 7, 8, 9}
- Adding a random channel
- Adding a duplicate channel

There are three different options for testing the number of slices and eight different options for testing the number of channels. Each test adds a random and a duplicate channel. For each modified equation 24 different configurations are generated, and the results averaged from 50 tests on each configuration. This is a total of 9600 tests completed on the modified colocalization metrics.

CHAPTER 4

RESULTS

4.1 Modified Equation Results

4.1.1 Pearson's Correlation Coefficient

In Figure 2, there are two channels, each only having one image. The following is a step by step analysis of the Pearson's Correlation Coefficient (PCC) using the sample data contained in Table 1. There are only two fluorescence labels and only one subsection of the experiment. To simplify the example, each image has only two pixels so that the equations can be shown. The numerator equals 2500 + 2500 = 5000. The denominator equals 5000 * 5000, and then the square root is taken. As expected, all the pixel intensities exactly overlap and the result is 5000/5000 = 1.0. This shows full colocalization, as it should because the images are identical. Equation 5 is the PCC (Equation 1), but modified to work on n-channels (n > 2).

In simple situations in which it is clear to visually see that the results should be 75%, 50%, or 25%, the results of this equation do not match those of Manders et al. This can be seen in the comparison charts on two and three channels (Table 11 and Table 12). On two channels it is clear that the result should be at 25% increments, and the other coefficients that are used give those expected results.

The results reported by Manders et al. (1993) and the results of this implementation differ (see Table 9 and Table 10). Using a simple test case it can be shown that the implementation used is producing accurate results. Using a 2-pixel by 2-pixel image, three examples can show that the returned results are accurate.

Table 3: PCC Implementation Test One. This table contains data for a 2-pixel by 2-pixel image. This data is used to show that the implementation of Pearson's Correlation Coefficient is producing accurate results.

Channel 1		Channel 2	
Pixel (0,0)	Pixel (0,1)	Pixel 1(0,0)	Pixel 2 (0,1)
255	255	0	255
Pixel (1,0)	Pixel (1,1)	Pixel (1,0)	Pixel (1,1)
0	0	0	0
Channel 1 Average 127.5		Channel 2 Average 63.75	

Table 4: PCC Data from PCC Implementation Test One. This is the returned data, calculating the output step by step through both the numerator and denominator. The left-most column dictates the pixel location in the 2x2 grid, (0,0) being the top left pixel, and (1,1) being the bottom-right pixel.

Pixel Location	Numerator		Denominator
0, 0	-8128.125	Channel 1	65025
0, 1	24384.375	Channel 2	48768.75
1, 0	8128.125		
1, 1	8128.125		
Total	32512.5		56313.30188
PCC Result	0.577350269		
Program Output	0.5773		

Table 5: PCC Implementation Test Two. This table contains data for a 2-pixel by 2-pixel image. This data is used to show that the implementation of Pearson's Correlation Coefficient is producing accurate results.

Channel 1		Channel 2	
Pixel (0,0)	Pixel (0,1)	Pixel (0,0)	Pixel (0,1)
255	255	255	255
Pixel (1,0)	Pixel (1,1)	Pixel (1,0)	Pixel (1,1)
0	0	0	0
Channel 1 Average 127.5		Channel 2 Average 127.5	

Table 6: PCC Data from PCC Implementation Test Two. This is the returned data, calculating the output step by step through both the numerator and denominator. The left-most column dictates the pixel location in the 2x2 grid, (0,0) being the top left pixel, and (1,1) being the bottom-right pixel.

Pixel Location	Numerator		Denominator
0, 0	16256.25	Channel 1	65025
0, 1	16256.25	Channel 2	65025
1, 0	16256.25		
1, 1	16256.25		
Total	65025		65025
PCC Result	1.0		
Program Output:	1.0		

Table 7: PCC Implementation Test Three. This table contains data for a 2-pixel by 2-pixel image. This data is used to show that the implementation of Pearson's Correlation Coefficient is producing accurate results.

Channel 1		Channel 2	
Pixel (0,0)	Pixel (0,1)	Pixel (0,0)	Pixel (0,1)
0	255	0	255
Pixel (1,0)	Pixel (1,1)	Pixel (1,0)	Pixel (1,1)
255	255	0	0
Channel 1 Average 191.25		Channel 2 Average 63.75	

Table 8: PCC Data from PCC Implementation Test Three. This is the returned data, calculating the output step by step through both the numerator and denominator. The left-most column dictates the pixel location in the 2x2 grid, (0,0) being the top left pixel, and (1,1) being the bottom-right pixel.

Pixel Location	Numerator		Denominator
0, 0	12192.1875	Channel 1	48768.75
0, 1	12192.1875	Channel 2	48768.75
1, 0	-4064.0625		
1, 1	-4064.0625		
Total	16256.25		48768.75
PCC Result	0.333333333		
Program Output:	0.3333		

In Table 3, Table 5 and Table 7 the test image pixels values are shown. Pixel (0,0) is the top-left pixel, pixel(0,1) is the top-right pixel, pixel(1,0) is the bottom-left pixel, and pixel (1,1) is the bottom-right pixel. The value below the pixel location is the pixel intensity, zero is the

lowest intensity and is black, 255 is the highest intensity and is white. The channel average is computed for each channel and is used in the evaluation of the PCC. The data from these tables is used to generate the numbers in Table 4, Table 6 and Table 8 respectively.

In Table 4, Table 6 and Table 8 the calculations are first made by pixel location for both the numerator and the denominator. For the numerator, the value at each pixel location equals the pixel intensity value for each pixel location minus the average for that channel. The numerator total is the sum of all the values returned for the numerator. The denominator generates two values, one for each channel. The sum of the denominator values is taken to the square root to generate the denominator total. The PCC Result is the numerator total divided by the denominator total. The 'Program Output' is the result generated by the software implementation. The 'PCC Result' is the hand computed results. Table 4, Table 6 and Table 8 compare the results generated by the software implementation and the hand computed results to show that while there is a discrepancy between the results reported by Manders et al. (1993) and the results of our software implementation, a manually computation is consistent with the results generated by our software implementation.

4.1.2 Overlap Coefficient

In Equation 6 the Overlap Coefficient (Equation 3) is modified to work on any number of channels. By substituting the two channel pixel data (Table 1) into the unmodified Overlap Coefficient equation (Equation 3) and into the modified Overlap Coefficient equation (Equation 6) and also substituting the three channel pixel data (Table 2) into the modified Overlap Coefficient equation (Equation 6), we show that the equation has been modified correctly.

Substituting the data from Table 1 into Equation 3 gives the numerator the values of 100*100+0*0, which is just 100*100 which equals 10,000. The numerator would have the values of $100^2 + 0^2 * 100^2 + 0^2$ which equals 10,000 * 10,000. After taking the square root the value is 10,000, which is the same as the numerator and giving the ratio a value of 1.0.

Substituting the data from Table 1 into Equation 6 will return the same results. 100*100+0*0 this equals 10,000. In the denominator, n will take on the value of two since there are only two channels being compared. Therefore the denominator is exactly the same, taking the square root of 10,000*10,000. The result is 1.0.

Substituting the data from Table 2 into Equation 6 will return the same results since all three channels (images) are identical. The numerator equals 100*100*100+0*0*0, which equals 1,000,000. The denominator will take on the values of $100^3+0^3 * 100^3+0^3 * 100^3+0^3$, which equals the cube root of 1,000,000 * 1,000,000 * 1,000,000, which equals 1,000,000. This gives the expected result of 1.0.

4.1.3 Colocalization Coefficient

Since the Colocalization Coefficient does not need to be modified the results only need to show that the equation is properly implemented. Table 9 shows the results from Manders et al. (1993), Table 10 are the results from our software implementation. The results are identical.

4.2 Testing Model Results

Using the testing model described in Section 3.3, the results of each equation are listed in Table 9 and Table 10.

Table 9: Manders' et al. Results (1993). These results are directly from Manders et al. (1993). Pearson's Correlation Coefficient (Equation 1)(Rp), Overlap Coefficient (r)(Equation 3), Manders' Colocalization Coefficient (Equation 4)(M1, M2…, Mn).

Number of Objects								
Figures	Channel 1	Channel 2	Colocalization	Total Objects	Rp	r	M1	M2
AA	36	36	36	36	1.00	1.00	1.00	1.00
AB	36	36	27	45	0.72	0.75	0.75	0.75
AC	36	36	18	54	0.44	0.50	0.50	0.50
AD	36	36	9	63	0.16	0.25	0.25	0.25
AE	36	36	0	72	-0.12	0.00	0.00	0.00
AF	36	27	9	54	0.22	0.29	0.25	0.33
AG	36	18	9	45	0.30	0.35	0.25	0.50
AH	36	9	9	36	0.48	0.50	0.25	1.00
AI	36	4	3	37	0.23	0.25	0.08	0.75

Table 10: Modified Equation Results. This table shows the results for the modified equations. All results except for Pearson's Correlation coefficient returned the same results as those from Manders' et al. Pearson's Correlation Coefficient (Rp), Overlap Coefficient (r), Manders' Colocalization Coefficient (Equation 4)(M1, M2, …, Mn).

Number of Objects								
Figures	Channel 1	Channel 2	Colocalization	Total Objects	Rp	r	M1	M2
AA	36	36	36	36	1.00	1.00	1.00	1.00
AB	36	36	27	45	0.735	0.75	0.75	0.75
AC	36	36	18	54	0.470	0.50	0.50	0.50
AD	36	36	9	63	0.206	0.25	0.25	0.25
AE	36	36	0	72	-0.060	0.00	0.00	0.00
AF	36	27	9	54	0.250	0.29	0.25	0.33
AG	36	18	9	45	0.328	0.35	0.25	0.50
AH	36	9	9	36	0.489	0.50	0.25	1.00
AI	36	4	3	37	0.239	0.25	0.08	0.75

4.3 Multi Channel Analysis Using the Spatial Colocalization Coefficient (L_s)

The same testing model that confirmed the validity of the modified equations was used on the new 3D spatial analysis technique. As described in the testing model, the results should not be the same if all the objects from the image are used in the calculations. The results from the tests are shown in Table 11.

In the second test, image A and image B are compared. Here, there is not full colocalization; the bottom-right nine blocks from image B are not aligned with those from image A. Although it would appear that there is 75% colocalization, this is not correct. Since there are 36 objects in image A and 36 objects in image B, but nine of those objects are in different positions, there are actually 45 distinct objects. Since only 27 of those 45 objects overlap, there is only 60% colocalization. Using the same logic that leads to the result of 60% instead of 75%, the other tests for the new equation are verified.

Table 11: Two Channel Results with the Colocalization Coefficient (L). These results compare the modified equation results (Table 10) to the results from the Colocalization Algorithm. Pearson's Correlation Coefficient (Rp)(Equation 5), Overlap Coefficient (r) (Equation 6), Manders' Colocalization Coefficient (Equation 7)(M1, M2,…,Mn).

Number of Objects									
Figures	Channel 1	Channel 2	Colocalization	Total Objects	Rp	r	M1	M2	L_s
AA	36	36	36	36	1.00	1.00	1.00	1.00	1.00
AB	36	36	27	45	0.735	0.75	0.75	0.75	.600
AC	36	36	18	54	0.470	0.50	0.50	0.50	.333
AD	36	36	9	63	0.206	0.25	0.25	0.25	.143
AE	36	36	0	72	-0.060	0.00	0.00	0.00	0.00
AF	36	27	9	54	0.250	0.29	0.25	0.33	.166
AG	36	18	9	45	0.328	0.35	0.25	0.50	.20
AH	36	9	9	36	0.489	0.50	0.25	1.00	.25
AI	36	4	3	37	0.239	0.25	0.08	0.75	.081

This logic can be applied to any of the following tests. In the case of images A and C, there are now 18 co-localizing objects, but with a total of 54 objects. This results in a total colocalization of one-third of the objects, not half. A strong example of this is test case AH, L_s returns 0.25, since there are 9 colocalizing objects and 36 distinct objects, there is 25% colocalization.

The test results for three channel analysis on all of the modified equations and on the Spatial Colocalization Coefficient value (L_s) are summarized in Table 12. Pearson's Correlation Coefficient (Equation 5), the Overlap Coefficient (Equation 6), Manders' Colocalization coefficient (Equation 4) (on M2 and M3), and the Spatial Colocalization Coefficient value (L_s) all return the same results. Since Manders' coefficient is calculated per channel there is now a third coefficient (M1), which should be and is identical to the M1 result from Table 11 (and M2 from Table 12) since it is on the same image.

Table 12: Three Channel Results. These results are from the modified equations and the Spatial Colocalization Coefficient (L_s) equation. The tests are from three channel analysis and attempt to show that by introducing an additional image that is identical to one of the other images, but no new additional objects the ratios remain unchanged. Pearson's Correlation Coefficient (Rp) (Equation 5), Overlap Coefficient (r) (Equation 6), Manders' Colocalization Coefficient (Equation 4) (M1, M2, … Mn) (Equation 4), Colocalization Algorithm (L_s) (Equation8).

Number of Objects											
Figures	Channel 1	Channel 2	Channel 3	Colocalization	Total Objects	Rp	r	M1	M2	M3	L_s
AAA	36	36	36	36	36	1.00	1.00	1.00	1.00	1.00	1.00
AAB	36	36	36	27	45	0.735	0.75	0.75	0.75	0.75	.600
AAC	36	36	36	18	54	0.470	0.50	0.50	0.50	0.50	.333
AAD	36	36	36	9	63	0.206	0.25	0.25	0.25	0.25	.143
AAE	36	36	36	0	72	-0.060	0.00	0.00	0.00	0.00	0.00
AAF	36	36	27	9	54	0.240	0.29	0.25	0.25	0.33	.166
AAG	36	36	18	9	45	0.288	0.35	0.25	0.25	0.50	.20
AAH	36	36	9	9	36	0.489	0.50	0.25	0.25	1.00	.25
AAI	36	36	4	3	37	0.239	0.25	0.08	0.08	0.75	.081

4. 4 3D Spatial Analysis of the Objects by the Region Growing Algorithm

The following examples show the results when analyzing spatial stacks:

The first 3D spatial analysis test stack is shown in Figure 9; channel 1 has three images and channel 2 has three images. All images are image A from Figure 6. The total colocalization on each slice should be 1 (complete colocalization). Spatially, the result should still be, and is, 1. Table 13 shows the results for each slice, as well as the spatial colocalization.

The 'Colocalized Objects' parameter includes only those objects that are colocalized within that slice. In slice 1, all objects from channel 1 and channel 2 are colocalized, and therefore all 36 objects are colocalized objects. The same is true for slices 2 and 3. This brings the Colocalized Objects count to 108. This yields a Spatial Colocalization Coefficient value (L_s) of 100.0% or 1.00.

Table 13: 3D Spatial Analysis Test on Stack AAA – AAA. The ‘Slice #’ column specifies the z-dimension in the image; Slice 1 is the top image, slice 2 is the middle image, and slice 3 is the bottom image. There is a column for each channel, in that column is the image for that channel and slice. The ‘L column specifies the colocalization coefficient for just that slice. ‘Total Objects’ is the count of all distinct objects in all the images. ‘Colocalized Objects’ are the number of objects that are colocalized. The 'Spatial Colocalization Coefficient (L_s)’ parameter is calculated from the Colocalized Objects divided by the Total Objects. This yields a percentage of the spatially colocalized objects. Colocalization Coefficient value (L), Spatial Colocalization Coefficient value (L_s).

Slice #	Channel 1	Channel 2	L
1	Image A	Image A	1
2	Image A	Image A	1
3	Image A	Image A	1
Spatial Colocalization		1.00	
Spatial Overlap Coefficient (Rn)		1.00	
Spatial Correlation Coefficient		1.00	
Spatial Manders’ Coefficient		1.00	
Spatial Manders’ Coefficient		1.00	
Total Objects		Colocalized Objects	
108		108	

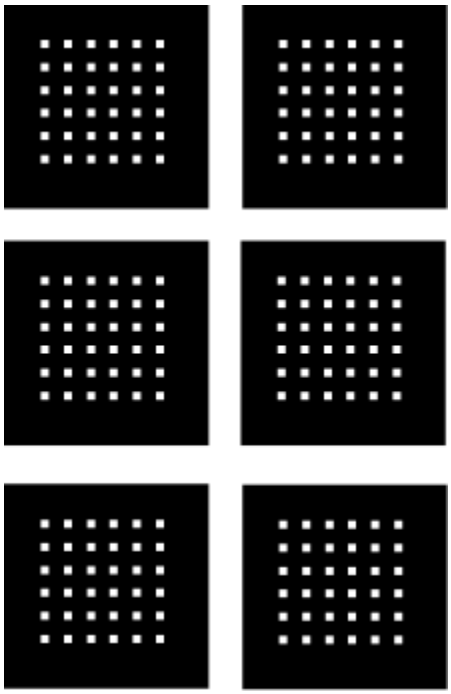

Figure 9: Stack AAA-AAA. This is a representation of the image stack. Each column represents a different channel, each row another slice or subsection of the experiment.

The second 3D spatial analysis test stack is shown in Figure 10; channel 1 has three images and channel 2 has three images. All images are image A from Figure 6, except for the Channel 2 slice 3 image, which is Image B from Figure 6. The total colocalization on slice 1 and slice 2 should be 1 (complete colocalization). The total colocalization on slice 3 is 0.6 which matches with the results from Table 11. Table 14 shows the results for each slice, as well as the spatial colocalization.

On slice 1, both channels are colocalized completely, so there are 36 Total Objects, and 36 Colocalized Objects. After slice 2, which is identical to slice 1, there are 72 Total Objects, and 72 Colocalized Objects. Since slice 3 has image A and image B, and there are 45 Total Objects for those images, and only 26 of those objects are Colocalized Objects, there are 117

Total Objects and 99 Colocalized Objects. This yields a Spatial Colocalization Coefficient value (L_s) of 84.6% or 0.846.

Table 14: 3D Spatial Analysis Test on Stack AAA – AAB Data. The 'Slice #' column specifies the z-dimension in the image; Slice 1 is the top image, slice 2 is the middle image, and slice 3 is the bottom image. There is a column for each channel, in that column is the image for that channel and slice. The 'L column specifies the colocalization ratio for just that slice. 'Total Objects' is the count of all distinct objects in all the images. 'Colocalized Objects' are the number of objects that are colocalized. The 'Spatial Colocalization Coefficient (L_s)' parameter is calculated from the Colocalized Objects divided by the Total Objects. This yields a percentage of the spatially colocalized objects. Colocalization Coefficient value (L), Spatial Colocalization Coefficient value (L_s).

Slice #	Channel 1	Channel 2	L
1	Image A	Image A	1
2	Image A	Image A	1
3	Image A	Image A	.6
Spatial Colocalization		0.846	
Spatial Overlap Coefficient (Rn)		0.9166	
Spatial Correlation Coefficient		0.9118	
Spatial Manders' Coefficient		0.9166	
Spatial Manders' Coefficient		0.9166	
Total Objects		Colocalized Objects	
117		99	

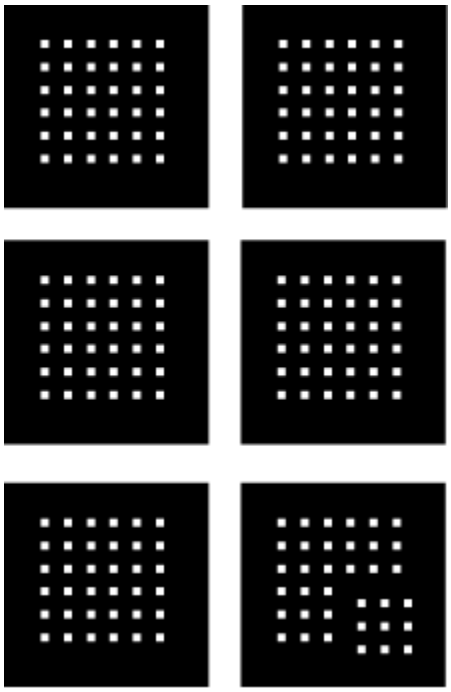

Figure 10: Stack AAA-AAB. This is a representation of the image stack. Each column represents a different channel, each row another slice or subsection of the experiment.

The third 3D spatial analysis test stack is shown in Figure 11; Channel 1 has three images and Channel 2 has three images. All images from Channel 1 are image A from Figure 6. In Channel 2 slice 1 and slice 3 are image B from Figure 6, while slice 2 is image A. The total colocalization on slice 2 is 1 (complete colocalization). The total colocalization on slice 1 and slice 3 is 0.6 which matches with the results from Table 11. Table 15 shows the results for each slice, as well as the spatial colocalization.

On slice 2, both channels colocalized completely, so there are 36 Total Objects, and 36 Colocalized Objects. Since slice 1 and 3 have image A and image B, and there are 45 Total Objects for those images, and only 26 of those objects are Colocalized Objects, then there are 126 Total Objects and 90 Localized Objects. This yields a Spatial Colocalization Coefficient value of 71.4% or 0.714.

Table 15: 3D Spatial Analysis Test on Stack AAA – BAB Data. The ‘Slice #’ column specifies the z-dimension in the image; Slice 1 is the top image, slice 2 is the middle image, and slice 3 is the bottom image. There is a column for each channel, in that column is the image for that channel and slice. The ‘L column specifies the colocalization ratio for just that slice. ‘Total Objects’ is the count of all distinct objects in all the images. ‘Colocalized Objects’ are the number of objects that are colocalized. The 'Spatial Colocalization Coefficient (L_s)’ parameter is calculated from the Colocalized Objects divided by the Total Objects. This yields a percentage of the spatially colocalized objects. Colocalization Coefficient value (L), Spatial Colocalization Coefficient value (L_s).

Slice #	Channel 1	Channel 2	L
1	Image A	Image A	0.6
2	Image A	Image A	1
3	Image A	Image A	0.6
Spatial Colocalization		0.714	
Spatial Overlap Coefficient (Rn)		0.8333	
Spatial Correlation Coefficient		0.8236	
Spatial Manders’ Coefficient		0.8333	
Spatial Manders’ Coefficient		0.8333	
Total Objects		Colocalized Objects	
126		90	

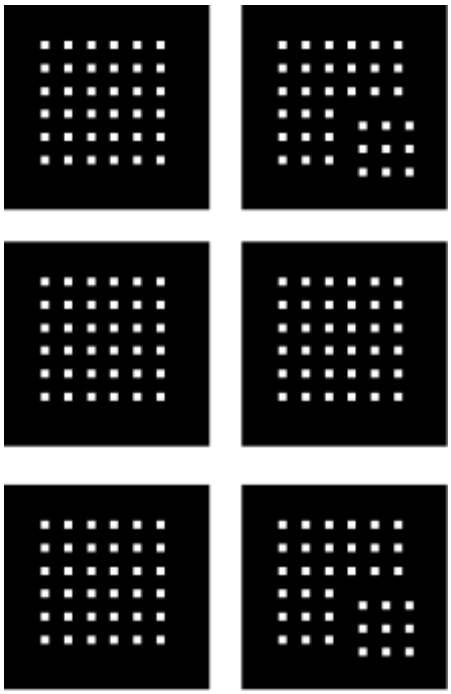

Figure 11: Stack AAA-BAB. This is a representation of the image stack, each column represents a different channel, each row another slice or subsection of the experiment.

4.5 Automatic Thresholding through Bimodal Histogram Analysis via Population-Based Hill Climbing

The first Automatic Thresholding test was performed on one of the test images from Figure 6 (image A). Since there are only two different pixel intensities throughout the image, the resulting pixel intensity thresholds are 0 (lower bound threshold) and 255 (upper bound threshold). Figure 13 is the histogram created from Figure 12. Table 16 shows the results from the population-based hill climbing algorithm. Although there are a total of 51 individuals in the population, only 6 were able to move to the global and second highest maxima. The other 45 individuals were unable to see any intensity values above zero in either direction. Three individuals made it to the

global maximum at 0, the other three individuals found the second global maxima at 255.

Table 17 shows the threshold selections based on the results of Table 16, as well as the limited exhaustive search algorithms results. Since there are only two intensity values the lowest pixel intensity becomes the lower bound threshold while the highest pixel intensity becomes the upper bound threshold.

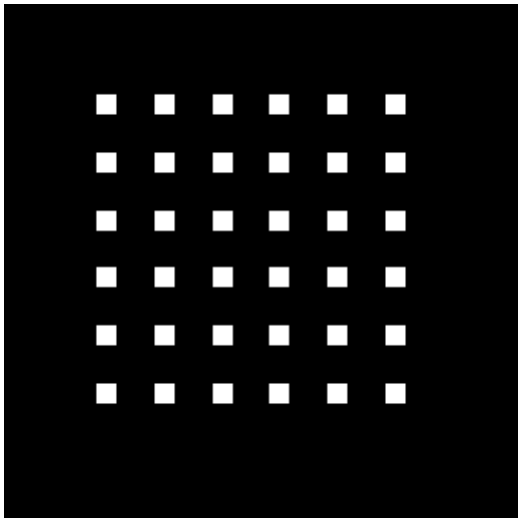

Figure 12: Image A. This is one of the benchmarking images from Figure 6. The histogram of this image is taken and used to select the thresholding inputs for the Region Growing Double Thresholding algorithm.

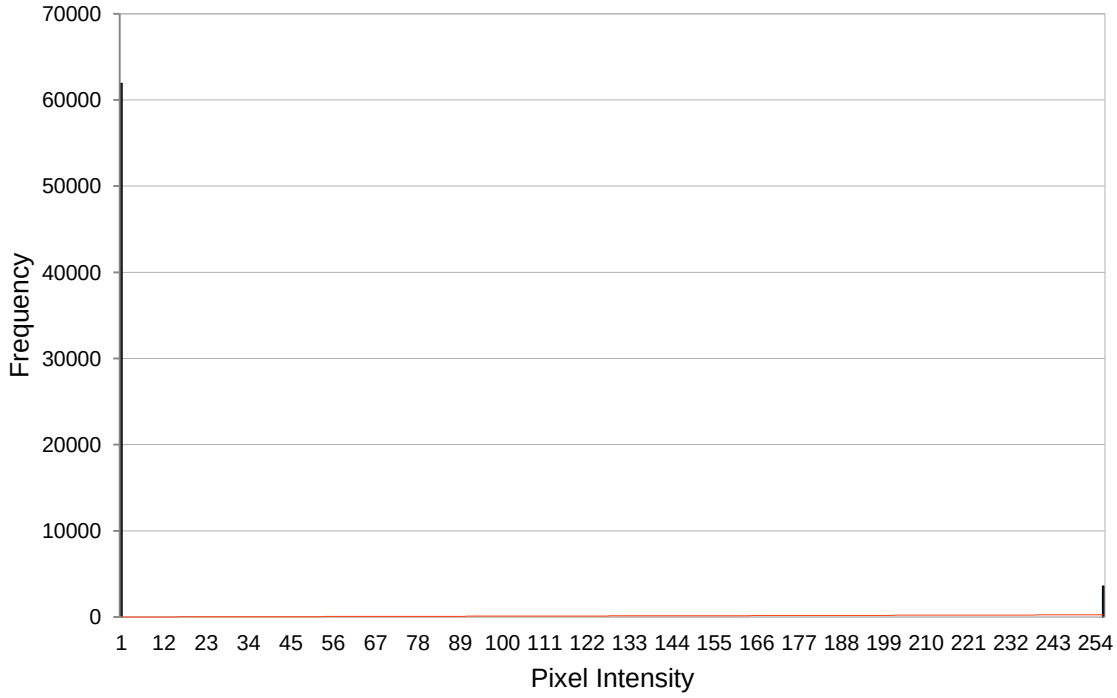

Figure 13: Histogram of Figure 12. This histogram only has two pixel intensities since Figure 12 is a black and white image; there are only two intensities 0 and 255.

Table 16: Population Occurrence of the Population-Based Hill Climbing Algorithm on Figure 12. The local search heuristic has a total population of 51, however some individuals were unable to move to any intensity values that have a frequency above zero. These occurrences are not shown in this table.

Population Occurrences	Intensity
3	0
3	255

Table 17: Selected Threshold from Table 16. These are the lower bound and upper bound selections from the Automatic Thresholding technique on Figure 12. HC refers to the population-based hill climbing algorithm and EX refers to the limited exhaustive search algorithm results.

Threshold	Intensity
HC- LB	0
HC - UB	255
EX – LB	0
EX – UB	255

The second Automatic Thresholding test, and all subsequent tests, were performed on an image produced by the confocal microscope. Using real images we show that, generally, images are bimodal. Unlike the pure black and white seen in the test image in Figure 12, the microscopic image seen in Figure 14 contains many different pixel intensities.

Figure 15 shows the histogram analysis of the pixel intensities for Figure 14. While the histogram does not appear to be bimodal, a closer examination of Table 18 proves otherwise. In Table 18 there are 7 local maxima that the individuals grouped around. 31 of these individuals found pixel intensity 0 to be the most frequent, and from the histogram we see that it is the global maximum.

The second most frequent pixel intensity is 184. 7 of the 51 individuals found this local maximum. Figure 16 shows a close up view of the histogram from Figure 15, displaying subtle peaks around all of the local maxima from Table 18.

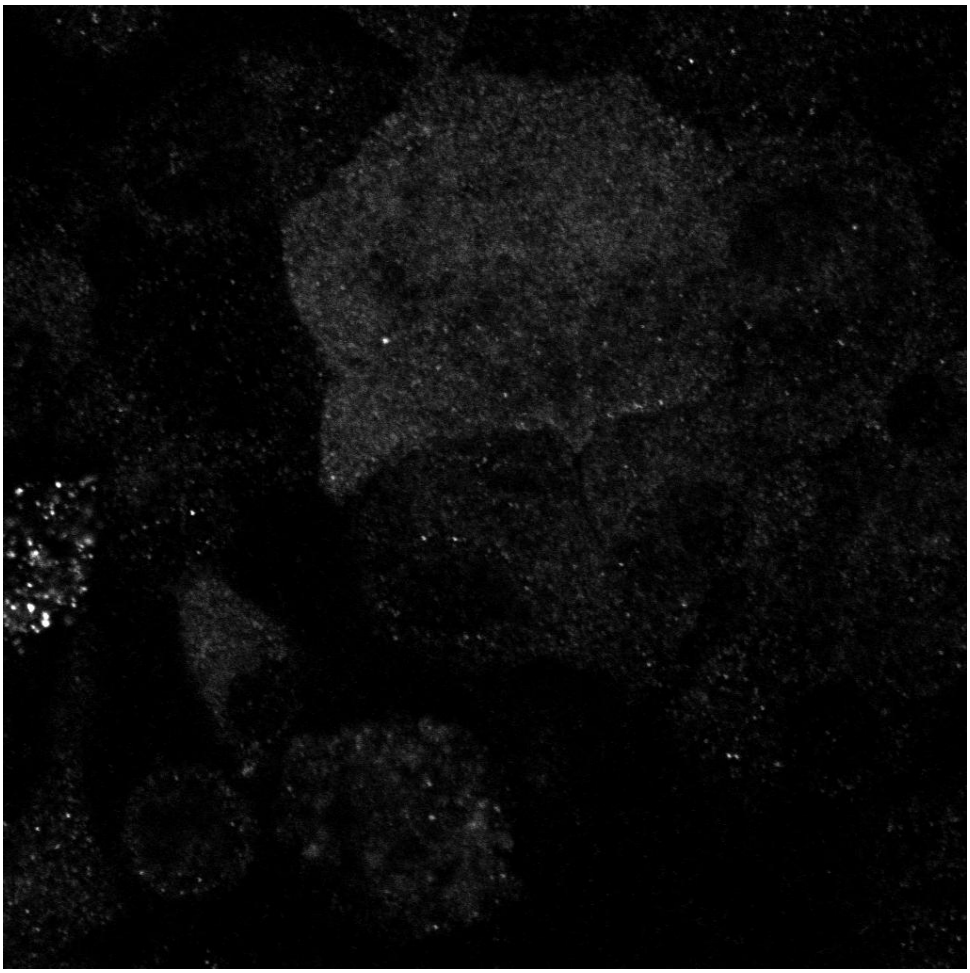

Figure 14: Real Image One. This image is an actual test case image produced by a confocal microscope.

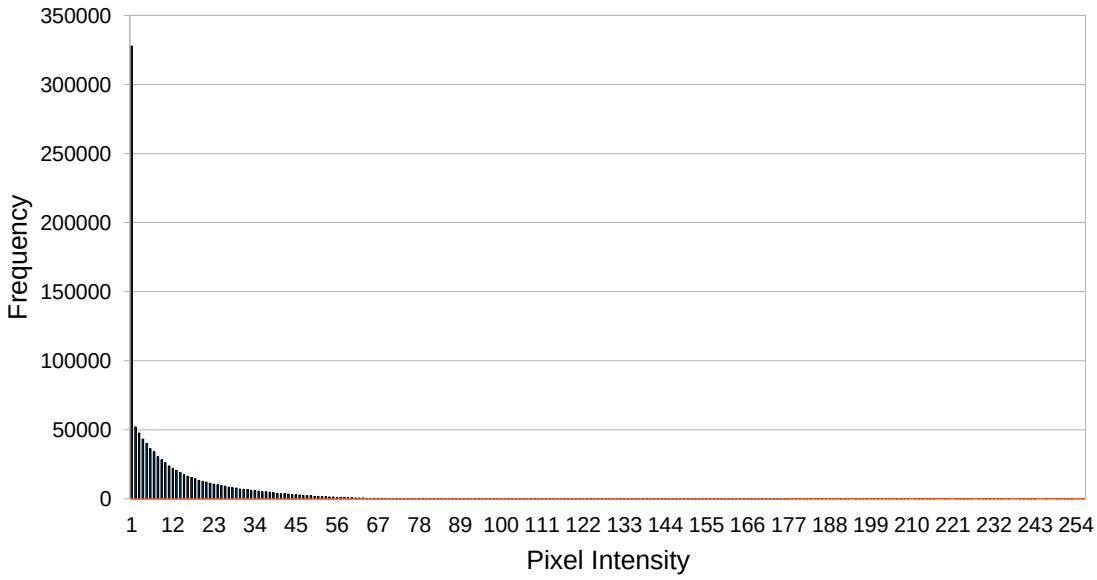

Figure 15: Histogram of Figure 14. This histogram shows a range of pixel intensities throughout the image. There are many pixel intensities that can't be seen due to the scale of the graph.

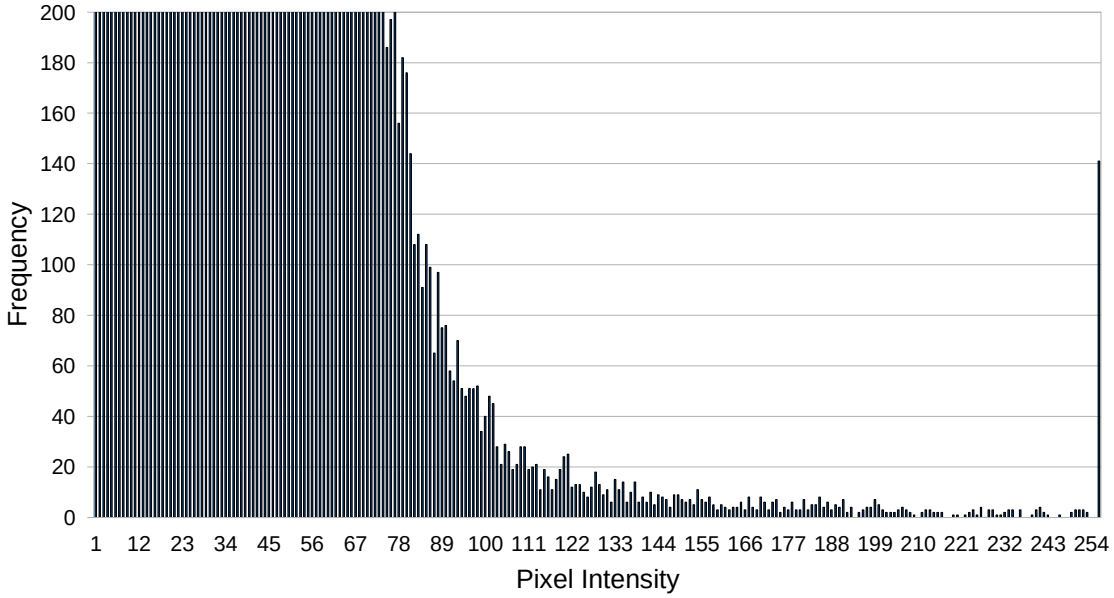

Figure 16: Histogram of Figure 14 Close-up. This histogram is zoomed in so that all the pixel intensity values can be seen. The local pixel intensity counts for most of the intensities are below 200. Since the lower pixel intensity counts reach 30,000 it is impossible to see the other local maxima in Figure 15.

Table 18: Population Occurrence of the Population-Based Hill Climbing Algorithm on Figure 14. The local search heuristic has a total population of 51, and all were able to find local maxima. The highest occurrence was at pixel intensity zero, while the second most occurring pixel intensity in the population was focused around pixel intensity 184.

Population Occurrences	Intensity
31	0
3	153
2	169
7	184
4	225
1	240
3	255

Table 19: Selected Threshold from Table 18. These are the lower bound and upper bound selections from the Automatic Thresholding technique on Figure 14. HC refers to the Population-Based Hill Climbing algorithm and EX refers to the limited exhaustive search algorithm results.

Threshold	Intensity
HC - LB	0
HC - UB	184
EX – LB	0
EX - UB	255

The third Automatic Thresholding test image is shown in Figure 19. This image is a lot brighter than the image from Figure 14; the images are from the same experiment, but from a different channel.

The histogram for the image in Figure 19 is in Figure 20. This histogram is much more clearly multimodal; there are actually three peaks 0, 90, and 255. However, the peak at 255 is an artifact; these pixels are saturated and this has caused them to pile up at 255. Pixel intensities 0 and 90 were found to be the most frequented by the individuals in the population as shown in Table 20. These are the results the algorithm needs to acurately sort out object and non-object pixels. The lower bound becomes 0 and the upper bound becomes 90 (see Table 21).

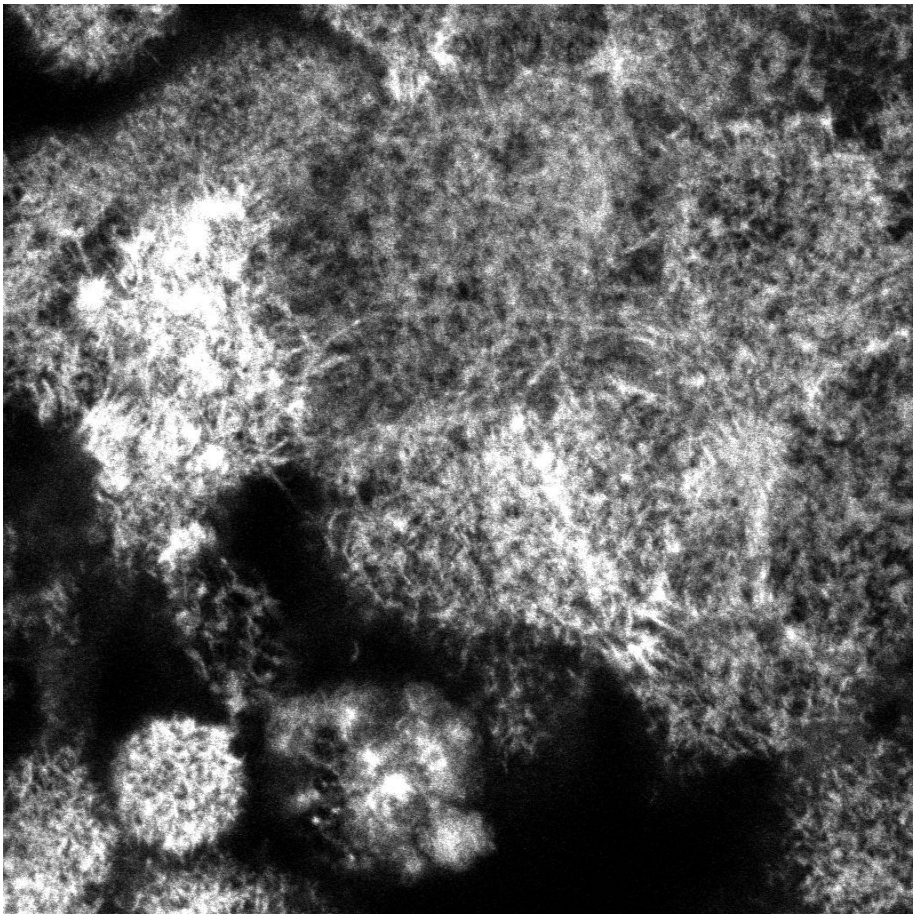

Figure 17: Real Image Two. This image is an actual test case image produced by a confocal microscope.

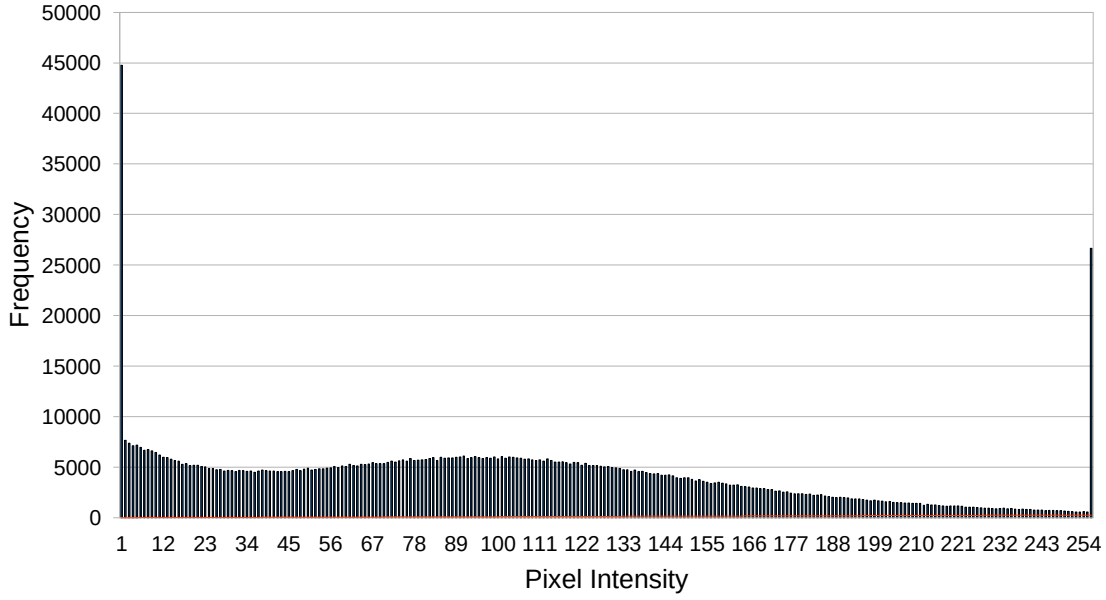

Figure 18: Histogram of Figure 17. This histogram is tri-modal, meaning it has three distinct peaks. However, most of the individuals from the population-based hill climbing algorithm have gathered about the peak at pixel intensity 90. Since the hill surrounding pixel intensity 90 is much larger than those surrounding 0 or 255, more individuals are encompassed by it.

Table 20: Population Occurrence of the Population-Based Hill Climbing Algorithm on Figure 17. This table shows the population occurrence from the population-based hill climbing algorithm on the histogram of Figure 18. Most of the individuals converged around pixel intensity 90.

Population Occurrences	Intensity
8	0
40	90
3	255

Table 21: Selected Thresholds from Table 20. These are the lower bound and upper bound selections from the Automatic Thresholding technique on Figure 17. HC refers to the population-based hill climbing algorithm and EX refers to the limited exhaustive search algorithm results.

Threshold	Intensity
HC - LB	0
HC - UB	90
EX – LB	0
EX - UB	255

The fourth Automatic Thresholding test is similar to Figure 17, where the image is very bright. However, the histogram for Figure 19 is skewed to the right (more white) as can be seen in Figure 20. Table 23 shows the local maxima the individuals clustered around, and Table 24 shows the lower bound (0) and upper bound (118).

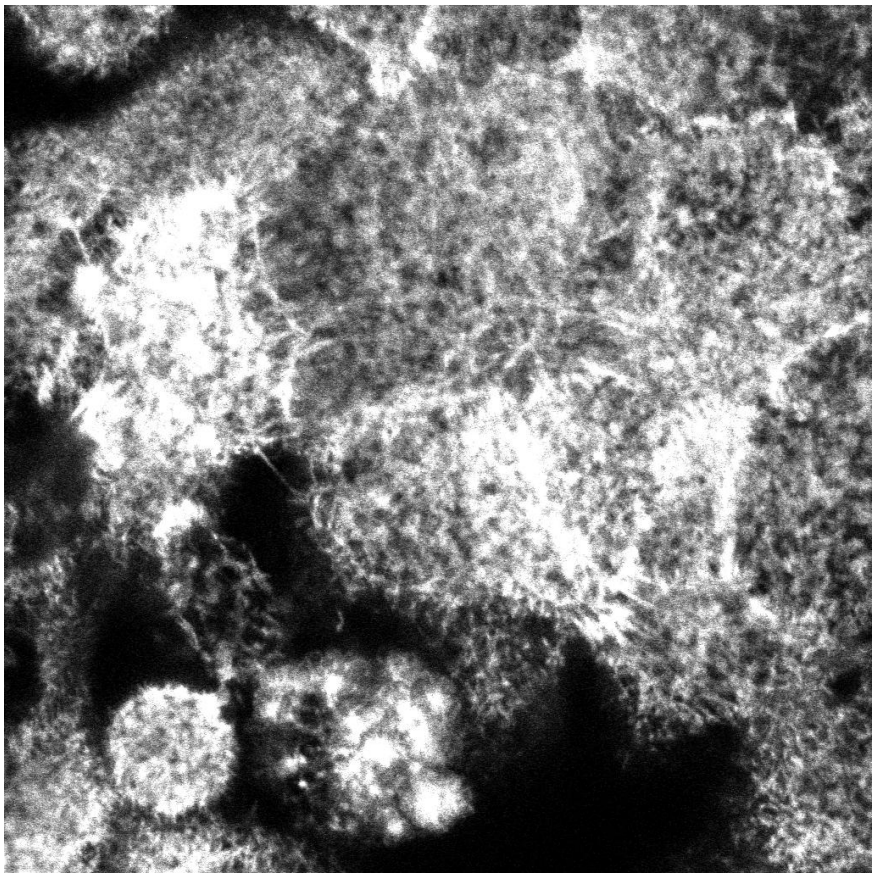

Figure 19: Real Image Three. This image is an actual test case image produced by a confocal microscope.

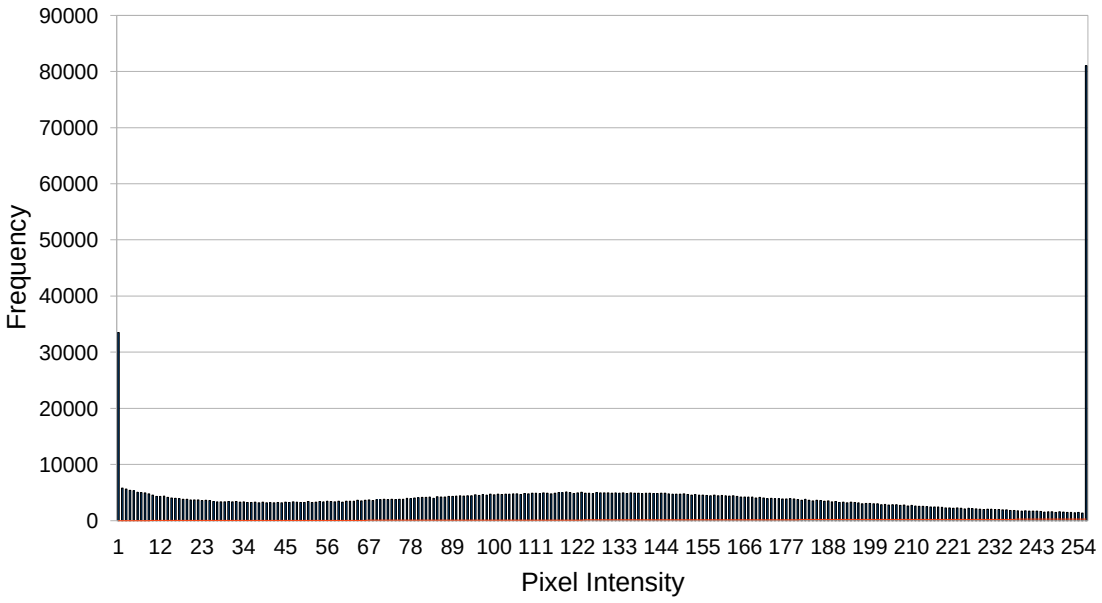

Figure 20: Histogram of Figure 19. This histogram is tri-modal; it has three distinct peaks at 0, 118, and 255. The peak at 255 is caused by pixel saturation and is an artificial peak.

Table 22: Population Occurrence of the Population-Based Hill Climbing Algorithm on Figure 19. This table shows the population occurrence from the population-based hill climbing algorithm on the histogram of Figure 20. Most of the individuals converged around pixel intensity 118.

Population Occurrences	Intensity
8	0
40	118
3	255

Table 23: Selected Threshold from Table 22. These are the lower bound and upper bound selections from the Automatic Thresholding technique on Figure 19. HC refers to the population-based hill climbing algorithm and EX refers to the limited exhaustive search algorithm results.

Threshold	Intensity
HC - LB	0
HC - UB	118
EX – LB	0
EX - UB	255

Figure 21 shows three channels from a test case. The image on the right and left have similar objects to the image in the middle, but they are much fainter. The results from the analysis on these images are in Table 24.

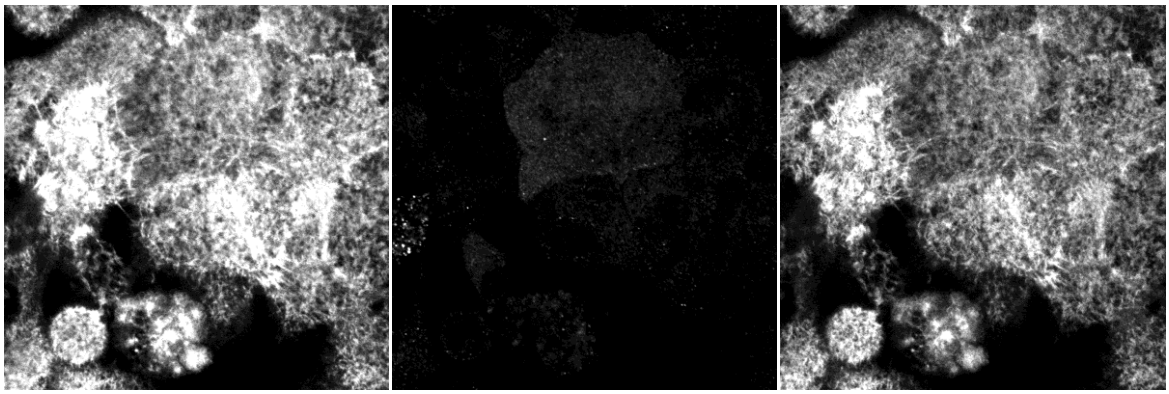

Figure 21: Confocal Test Case 1 Images. These three images are the results of a test case. They are from the same experiment but are three different channels. The image on the left is from Figure 19, the image in the center is from Figure 20 and the image on the right is from Figure 14.

Table 24: Confocal Test Case 1 Results. These are the results from Pearson's Correlation Coefficient (Rp) (Equation 5), the Overlap Coefficient (R) (Equation 6), Manders' Colocalization Coefficient (Equation 7) (Mn), and the Spatial Colocalization Coefficient (Ls) (Equation8) on the test case from Figure 21.To evenly compare the results the image segmentation used to remove background noise was used for all equations.

Pearson's Correlation Coefficient (Rp)	0.3618
Overlap Coefficient (r)	0.3618
Manders' Colocalization Coefficient (M0)	0.7862
Manders' Colocalization Coefficient (M1)	0.9962
Manders' Colocalization Coefficient (M2)	0.7899
Spatial Colocalization Coefficient (Ls)	0.6898

Figure 22 shows three channels from test case 2. The two images on the left have similar objects but the image on the left differs significantly. The results from the analysis on these images are in Table 25.

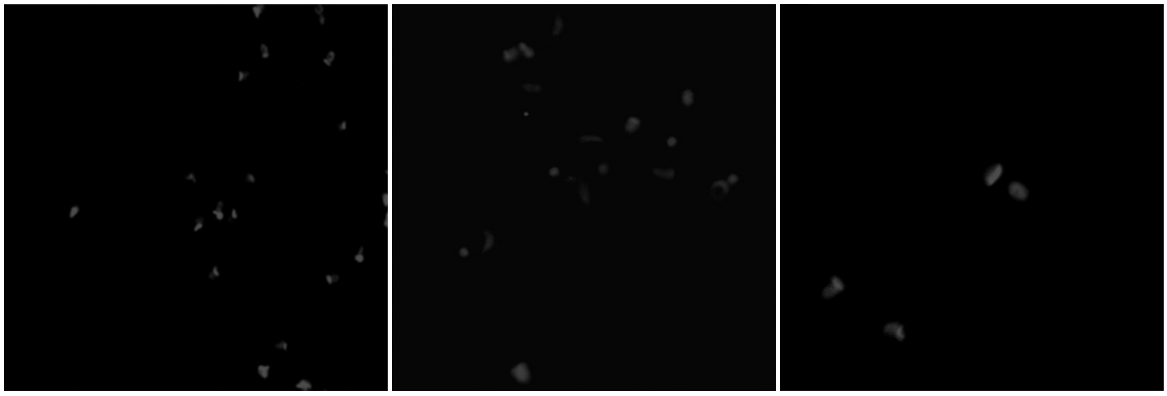

Figure 22: Confocal Test Case 2 Images. These three images are the results of a test case. They are from the same experiment but are three different channels.

Table 25: Confocal Test Case 2 Results. These are the results from Pearson's Correlation Coefficient (Rp) (Equation 5), the Overlap Coefficient (R) (Equation 6), Manders' Colocalization Coefficient (Equation 7) (Mn), and the Spatial Colocalization Coefficient (Ls) (Equation8) on the test case from Figure 22.To evenly compare the results the image segmentation used to remove background noise was used for all equations.

Pearson's Correlation Coefficient (Rp)	0.0870
Overlap Coefficient (r)	0.0870
Manders' Colocalization Coefficient (M0)	0.2817
Manders' Colocalization Coefficient (M1)	0.0773
Manders' Colocalization Coefficient (M2)	0.2305
Spatial Colocalization Coefficient (Ls)	0.0404

Figure 23 shows three channels from test case 3. The two images on the right have similar objects that appear to be colocalizing, the image on the left seems equally dispersed but with less cohesion. The results from the analysis on these images are in Table 26.

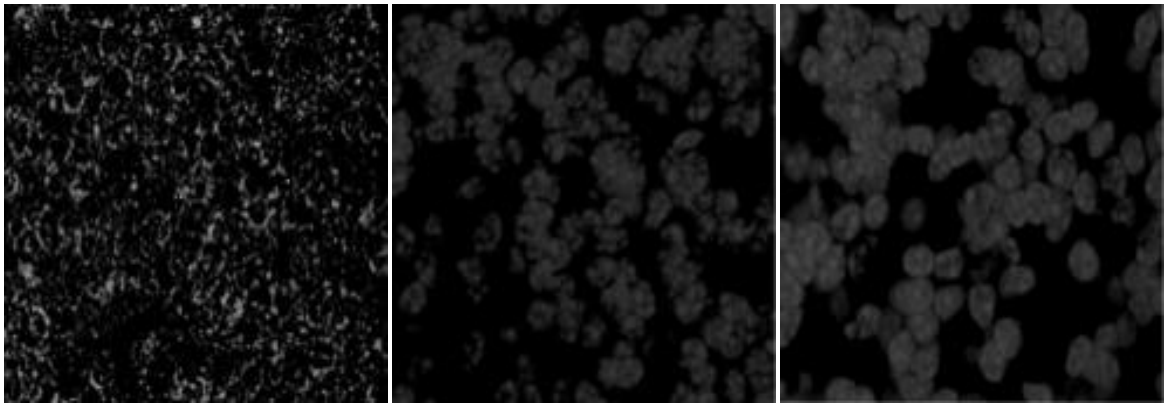

Figure 23: Confocal Test Case 3 Images. These three images are the results of a test case. They are from the same experiment but are three different channels.

Table 26: Confocal Test Case 3 Results. These are the results from Pearson's Correlation Coefficient (Rp) (Equation 5), the Overlap Coefficient (R)(Equation 6), Manders' Colocalization Coefficient Equation 7 (Mn), and the Spatial Colocalization Coefficient (Ls) (Equation8) on the test case from Figure 23.To evenly compare the results the image segmentation used to remove background noise was used for all equations.

Pearson's Correlation Coefficient (Rp)	0.1810
Overlap Coefficient (r)	0.1810
Manders' Colocalization Coefficient (M0)	0.6192
Manders' Colocalization Coefficient (M1)	0.6004
Manders' Colocalization Coefficient (M2)	0.4944
Spatial Colocalization Coefficient (Ls)	0.4270

4.6 Monte Carlo Simulation Results

Each combination of possible configurations is shown below. The chart shows the data points on a graph with the standard deviation for each point, the corresponding table shows the values for each data point, including the standard deviation. There is one chart and one table for each configuration based on the number of slices.

As more channels are added the average delta approaches zero. The data set is randomly generated therefore the colocalization between the channels is very low to begin with. The delta approaches zero as the colocalization ratio approaches zero.

4.6.1 Pearson's Correlation Coefficient

The results from the modified Pearson's Correlation Coefficient show the average change when adding a duplicate channel is a slightly positive. Since all of the images are randomly generated, the correlation between the images is very low to begin with, so the changes are also minor. The average change when adding an additional random image is slightly negative, which aligns with expectations.

Table 27: Monte Carlo Simulation PCC 5 Slices. This test case uses 5 image slices for the thickness of the image stack. Two channels are generated first (each with 5 image slices) and Pearson's Correlation Coefficient is ran on the data set. This process is repeated 50 times, using the results of each test case an average delta is taken and a standard deviation generated.

Monte Carlo trials: 50				
No. of Channels	Avgran(ΔCC)	ranSD	Avgdupe(ΔCC)	dupeSD
2	-0.0021	0.0027	0.0016	0.0047
3	-0.0016	0.0019	0.0045	0.0007
4	-0.0002	0.0010	0.0003	0.0012
5	-0.0005	0.0006	0.0006	0.0010
6	-0.0003	0.0003	0.0002	0.0005
7	0.0000	0.0002	0.0002	0.0004
8	-0.0001	0.0001	0.0000	0.0001
9	0.0000	0.0001	0.0000	0.0001

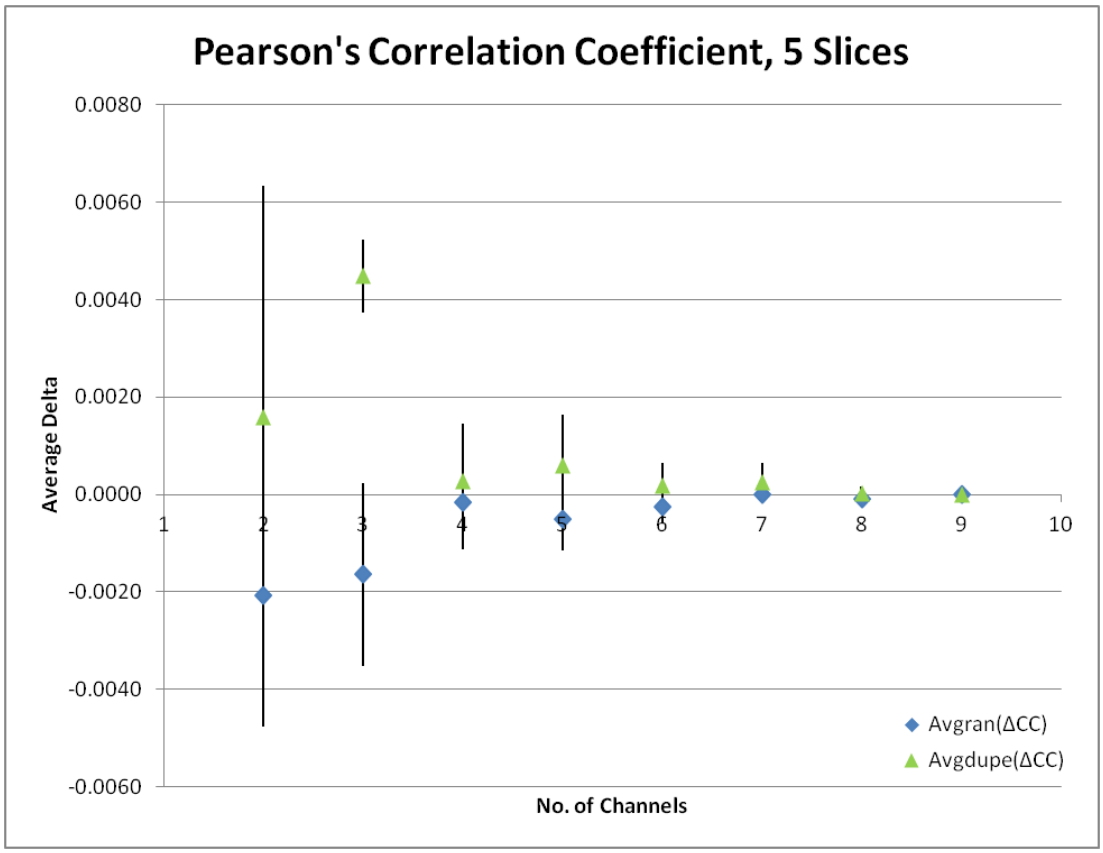

Figure 24: Monte Carlo Simulation PCC 5 Slices. Each data point represents the average delta from adding a random or duplicate channel. The graph shows that the average delta is less when a duplicate channel is added to the data.

Table 28: Monte Carlo Simulation PCC 10 Slices. This test case uses 10 image slices for the thickness of the image stack. Two channels are generated first (each with 10 image slices) and Pearson's Correlation Coefficient is run on the data set. This process is repeated 50 times, using the results of each test case an average delta is taken and a standard deviation generated.

Monte Carlo trials: 50				
No. of Channels	Avgran(ΔCC)	ranSD	Avgdupe(ΔCC)	dupeSD
2	-0.0011	0.0014	0.0011	0.0050
3	-0.0006	0.0013	0.0013	0.0008
4	-0.0007	0.0008	0.0004	0.0004
5	-0.0006	0.0004	0.0013	0.0005
6	0.0000	0.0002	0.0001	0.0002
7	-0.0001	0.0001	0.0002	0.0001
8	0.0000	0.0001	0.0000	0.0002
9	-0.0002	0.0000	0.0002	0.0000

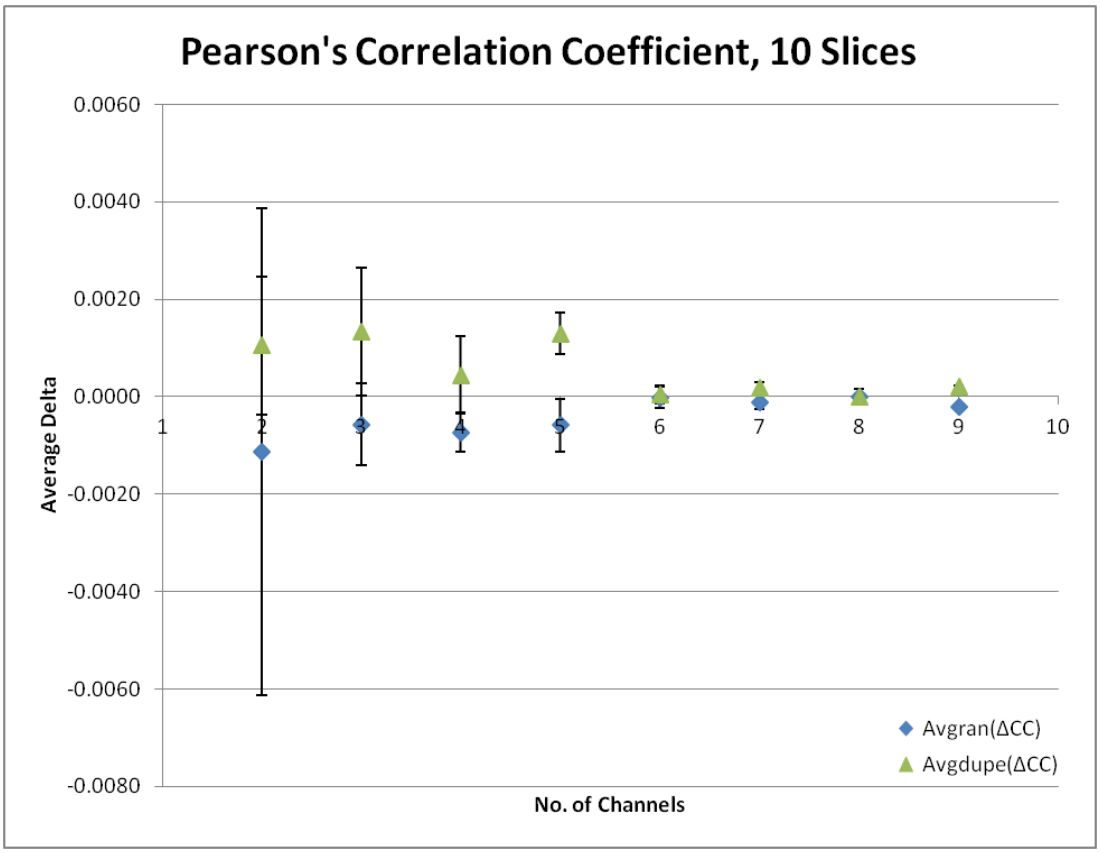

Figure 25: Monte Carlo Simulation PCC 10 Slices. Each data point represents the average delta from adding a random or duplicate channel. The graph shows that the average delta is less when a duplicate channel is added to the data.

Table 29: Monte Carlo Simulation PCC 15 Slices. This test case uses 15 image slices for the thickness of the image stack. Two channels are generated first (each with 15 image slices) and Pearson's Correlation Coefficient is run on the data set. This process is repeated 50 times, using the results of each test case an average delta is taken and a standard deviation generated.

Monte Carlo trials: 50				
No. of Channels	Avgran(ΔCC)	ranSD	Avgdupe(ΔCC)	dupeSD
2	-0.0025	0.0015	0.0033	0.0024
3	-0.0004	0.0007	0.0020	0.0037
4	-0.0018	0.0006	0.0015	0.0005
5	-0.0005	0.0003	0.0007	0.0006
6	-0.0003	0.0002	-0.0001	0.0002
7	-0.0002	0.0001	-0.0002	0.0002
8	-0.0002	0.0000	0.0002	0.0001
9	0.0000	0.0000	0.0000	0.0000

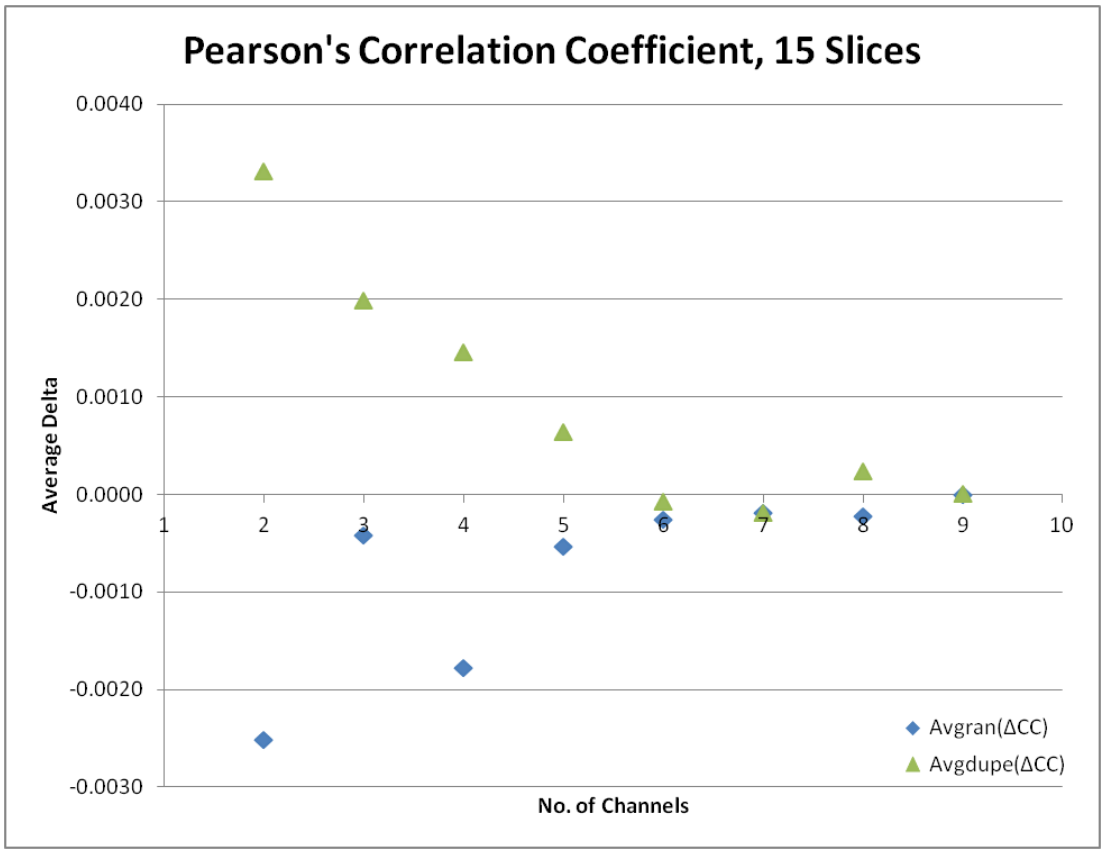

Figure 26: Monte Carlo Simulation PCC 15 Slices. Each data point represents the average delta from adding a random or duplicate channel. The graph shows that the average delta is less when a duplicate channel is added to the data.

4.6.2 Overlap Coefficient

The results from the Modified Overlap Coefficient show that when adding additional images the average delta is negative. When adding a duplicate channel from the data set, the delta is less than when adding a random channel to the data set.

Table 30: Monte Carlo Simulation OC 5 Slices. This test case uses 5 image slices for the thickness of the image stack. Two channels are generated first (each with 5 image slices) and the Overlap Coefficient is ran on the data set. This process is repeated 50 times, using the results of each test case an average delta is taken and a standard deviation generated.

Monte Carlo trials: 50				
No. of Channels	$Avg_{ran}(\Delta OC)$	ranSD	$Avg_{dupe}(\Delta OC)$	dupeSD
2	-0.2502	0.0021	-0.0835	0.0013
3	-0.1851	0.0021	-0.0838	0.0012
4	-0.1244	0.0016	-0.0623	0.0006
5	-0.0786	0.0012	-0.0416	0.0009
6	-0.0465	0.0006	-0.0258	0.0004
7	-0.0271	0.0004	-0.0155	0.0005
8	-0.0163	0.0002	-0.0092	0.0004
9	-0.0089	0.0001	-0.0053	0.0001

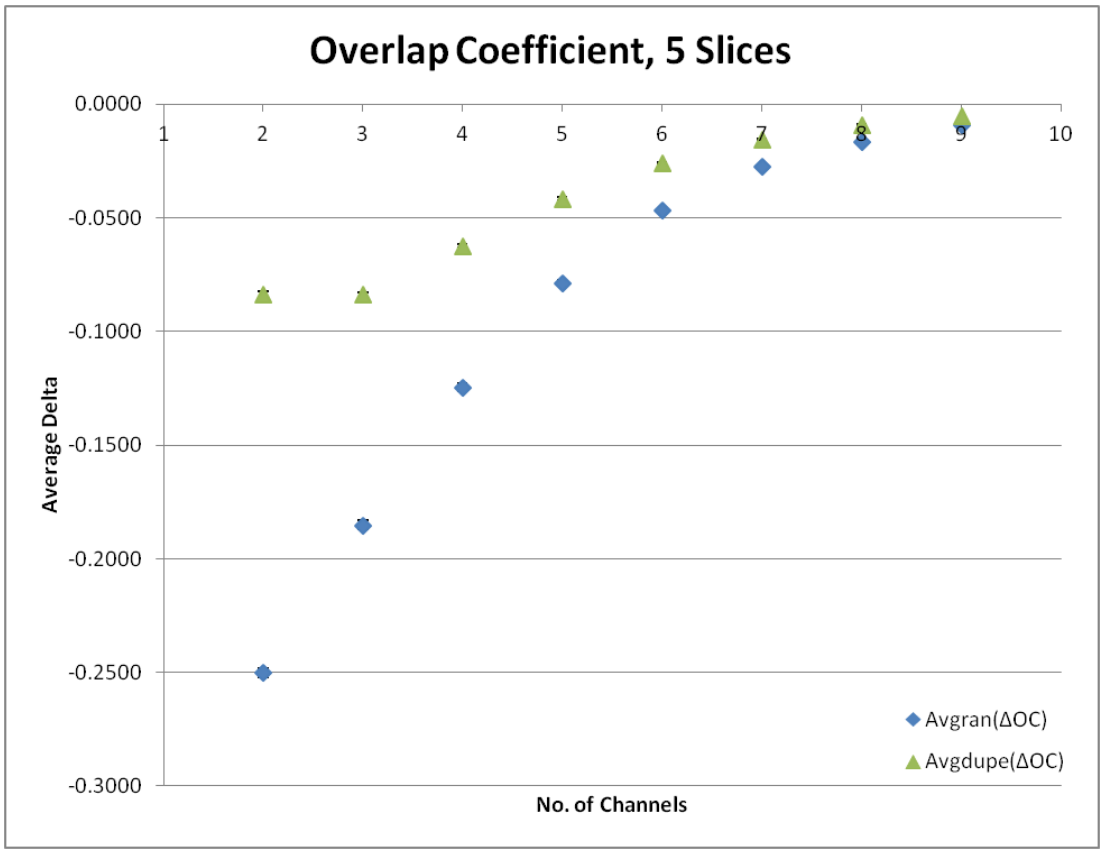

Figure 27: Monte Carlo Simulation OC 5 Slices. Each data point represents the average delta from adding a random or duplicate channel. The graph shows that the average delta is less when a duplicate channel is added to the data.

Table 31: Monte Carlo Simulation OC 10 Slices. This test case uses 10 image slices for the thickness of the image stack. Two channels are generated first (each with 10 image slices) and the Overlap Coefficient is run on the data set. This process is repeated 50 times, using the results of each test case an average delta is taken and a standard deviation generated.

Monte Carlo trials: 50				
No. of Channels	$Avg_{ran}(\Delta OC)$	ranSD	$Avg_{dupe}(\Delta OC)$	dupeSD
2	-0.2502	0.0011	-0.0832	0.0005
3	-0.1865	0.0013	-0.0832	0.0005
4	-0.1250	0.0011	-0.0620	0.0007
5	-0.0767	0.0008	-0.0414	0.0008
6	-0.0466	0.0003	-0.0257	0.0006
7	-0.0277	0.0002	-0.0156	0.0001
8	-0.0154	0.0002	-0.0089	0.0001
9	-0.0087	0.0001	-0.0052	0.0001

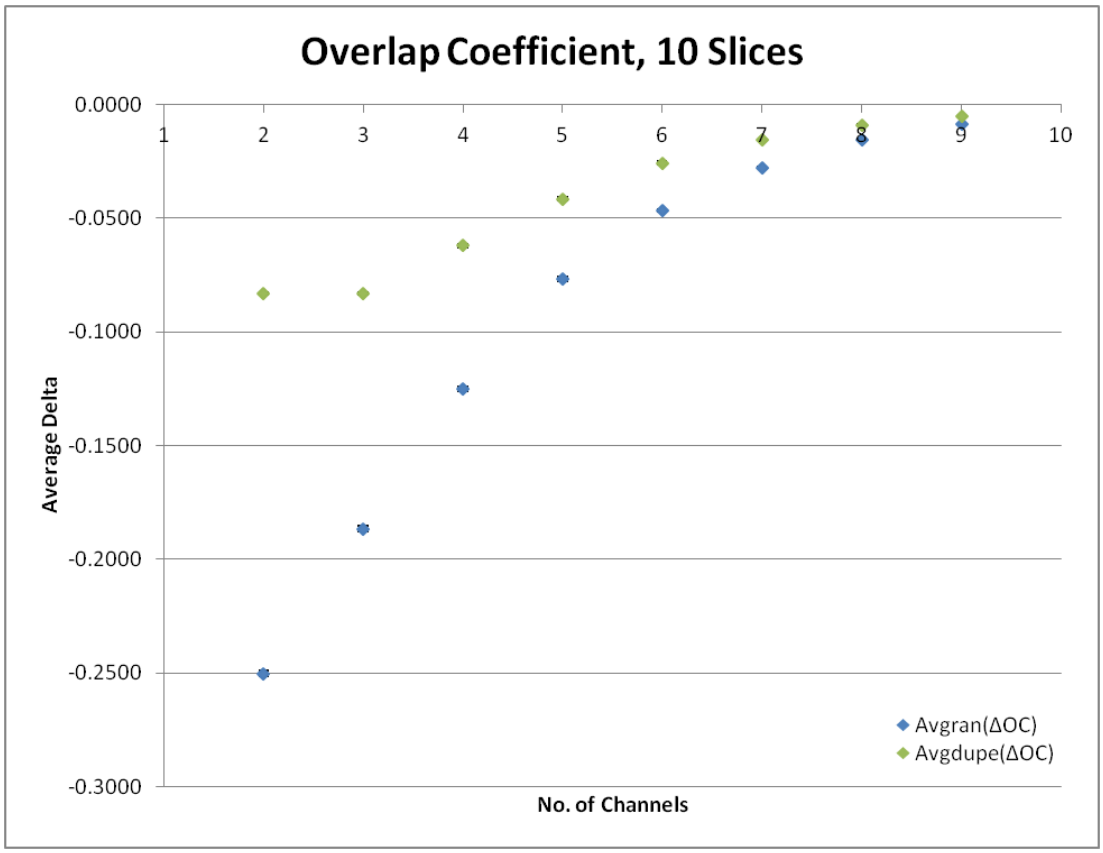

Figure 28: Monte Carlo Simulation OC 10 Slices. Each data point represents the average delta from adding a random or duplicate channel. The graph shows that the average delta is less when a duplicate channel is added to the data.

Table 32: Monte Carlo Simulation OC 15 Slices. This test case uses 15 image slices for the thickness of the image stack. Two channels are generated first (each with 15 image slices) and the Overlap Coefficient is run on the data set. This process is repeated 50 times, using the results of each test case an average delta is taken and a standard deviation generated.

Monte Carlo trials: 50				
No. of Channels	$Avg_{ran}(\Delta OC)$	ranSD	$Avg_{dupe}(\Delta OC)$	dupeSD
2	-0.2498	0.0018	-0.0840	0.0001
3	-0.1857	0.0015	-0.0835	0.0013
4	-0.1253	0.0012	-0.0622	0.0006
5	-0.0784	0.0007	-0.0414	0.0005
6	-0.0465	0.0004	-0.0258	0.0004
7	-0.0273	0.0003	-0.0155	0.0001
8	-0.0151	0.0002	-0.0088	0.0001
9	-0.0087	0.0001	-0.0051	0.0001

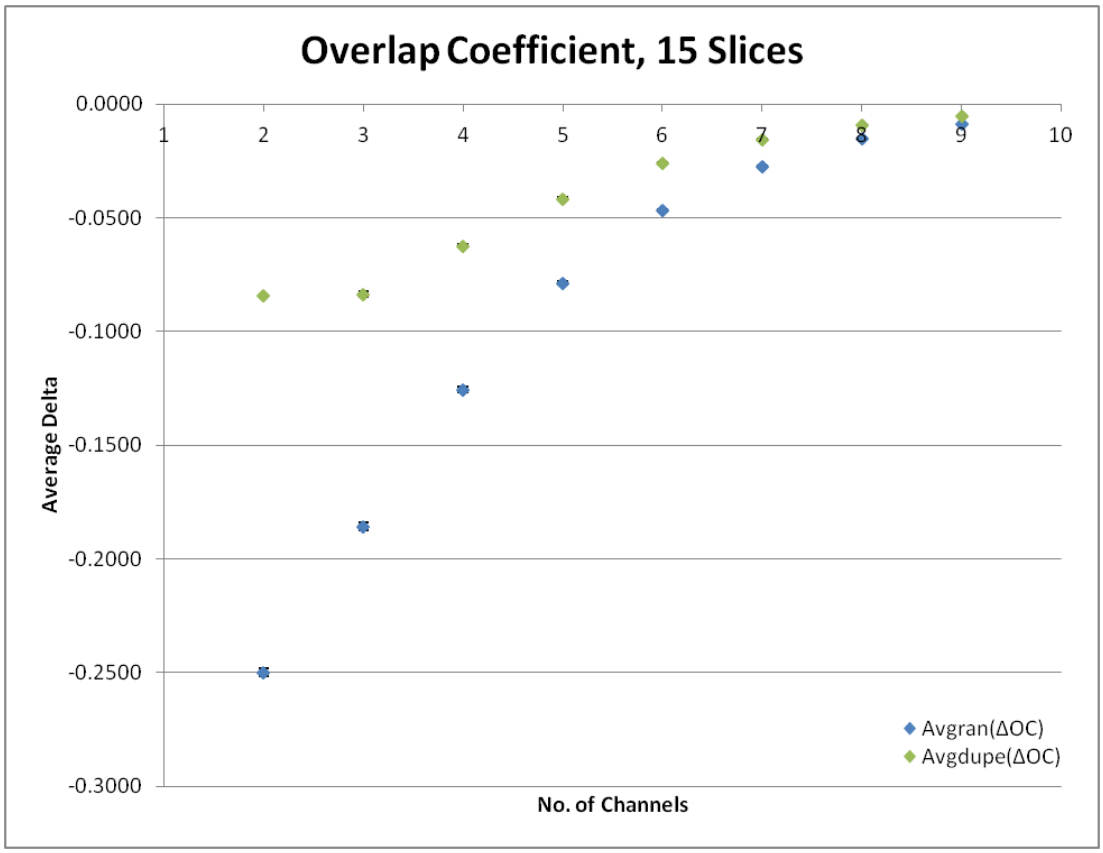

Figure 29: Monte Carlo Simulation OC 15 Slices. Each data point represents the average delta from adding a random or duplicate channel. The graph shows that the average delta is less when a duplicate channel is added to the data.

4.6.3 Manders' Colocalization Coefficient

The results from the Modified Manders' Colocalization Coefficient show that adding an additional random channel to the data set produce a small negative delta. Adding a duplicate channel to the data set does not cause any change on average.

The Manders' Colocalization Coefficient typically produces a pair-wise comparison for each channel. In order to product a more meaningful representation of the data, the pair-wise comparisons were averaged for each test configuration. This produced an average delta of zero

when adding a duplicate channel to the data set, while the values average to very near zero there may be slight deltas if the pair-wise comparison were to be examined.

Table 33: Monte Carlo Simulation MCC 5 Slices. This test case uses 5 image slices for the thickness of the image stack. Two channels are generated first (each with 5 image slices) and Manders' Colocalization Coefficient is run on the data set. This process is repeated 50 times, using the results of each test case an average delta is taken and a standard deviation generated.

Monte Carlo trials: 50				
No. of Channels	$Avg_{ran}(\Delta MCC)$	ranSD	$Avg_{dupe}(\Delta MCC)$	dupeSD
2	-0.0039	0.0002	0.0000	0.0000
3	-0.0039	0.0002	0.0000	0.0000
4	-0.0039	0.0002	0.0000	0.0000
5	-0.0039	0.0002	0.0000	0.0000
6	-0.0038	0.0002	0.0000	0.0000
7	-0.0038	0.0002	0.0000	0.0000
8	-0.0038	0.0002	0.0000	0.0000
9	-0.0038	0.0002	0.0000	0.0000

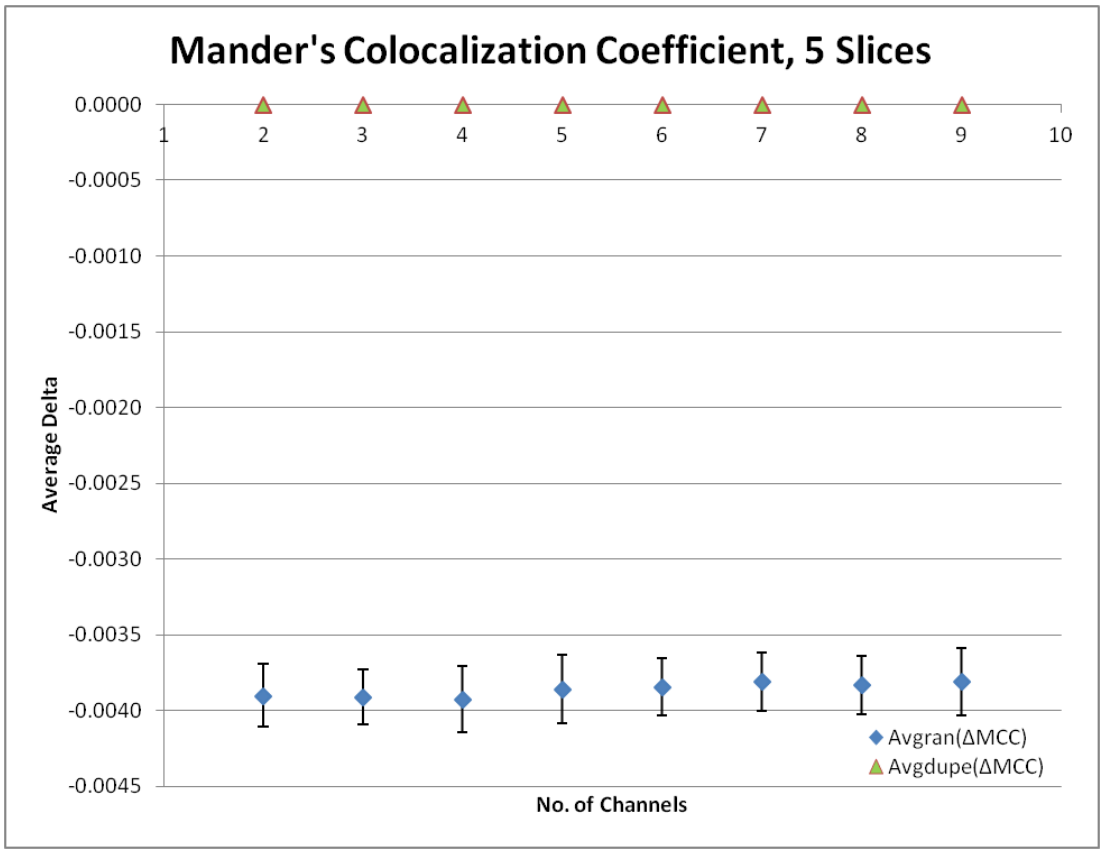

Figure 30: Monte Carlo Simulation MCC 5 Slices. Each data point represents the average delta from adding a random or duplicate channel. The graph shows that the average delta is less when a duplicate channel is added to the data.

Table 34: Monte Carlo Simulation MCC 10 Slices. This test case uses 10 image slices for the thickness of the image stack. Two channels are generated first (each with 10 image slices) and Manders' Colocalization Coefficient is ran on the data set. This process is repeated 50 times, using the results of each test case an average delta is taken and a standard deviation generated.

Monte Carlo trials: 50				
No. of Channels	$Avg_{ran}(\Delta MCC)$	ranSD	$Avg_{dupe}(\Delta MCC)$	dupeSD
2	-0.0039	0.0001	0.0000	0.0000
3	-0.0039	0.0001	0.0000	0.0000
4	-0.0039	0.0002	0.0000	0.0000
5	-0.0039	0.0002	0.0000	0.0000
6	-0.0038	0.0002	0.0000	0.0000
7	-0.0039	0.0001	0.0000	0.0000
8	-0.0038	0.0001	0.0000	0.0000
9	-0.0038	0.0001	0.0000	0.0000

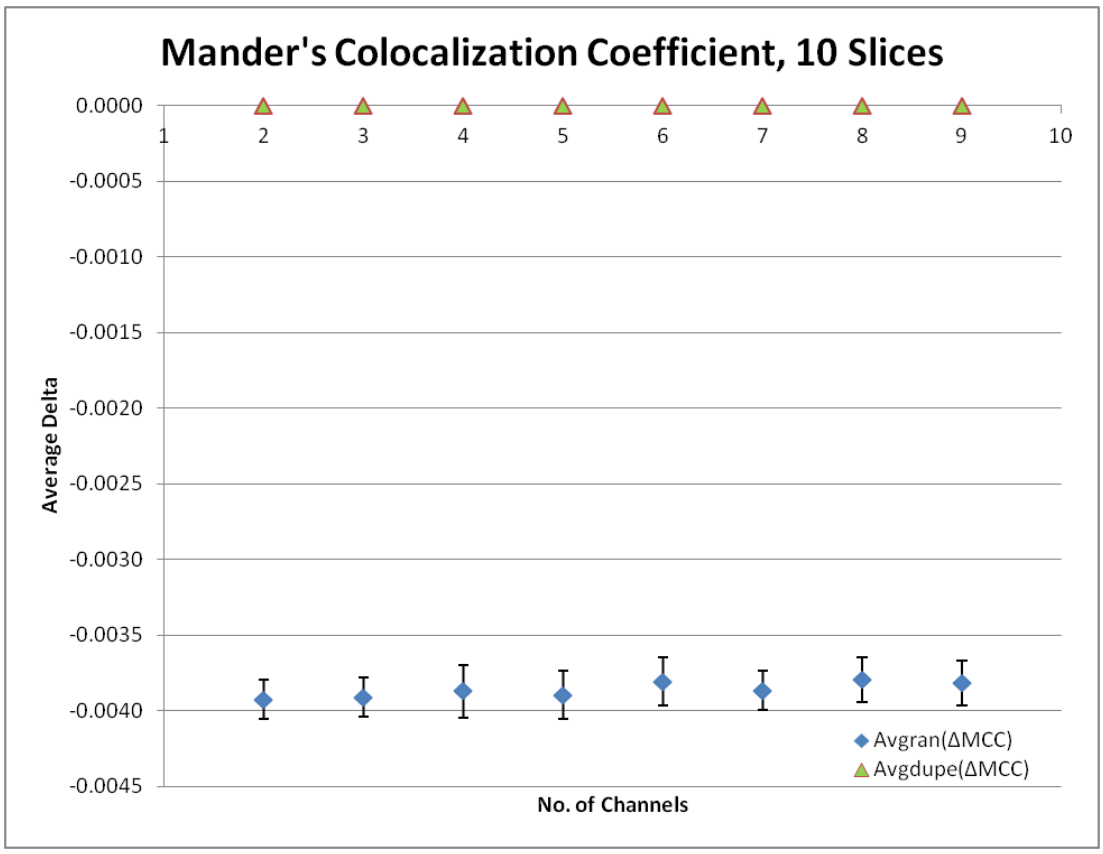

Figure 31: Monte Carlo Simulation MCC 10 Slices. Each data point represents the average delta from adding a random or duplicate channel. The graph shows that the average delta is less when a duplicate channel is added to the data.

Table 35:Monte Carlo Simulation MCC 15 Slices. This test case uses 15 image slices for the thickness of the image stack. Two channels are generated first (each with 15 image slices) and Manders' Colocalization Coefficient is run on the data set. This process is repeated 50 times, using the results of each test case an average delta is taken and a standard deviation generated.

Monte Carlo trials: 50				
No. of Channels	$Avg_{ran}(\Delta MCC)$	ranSD	$Avg_{dupe}(\Delta MCC)$	dupeSD
2	-0.0039	0.0001	0.0000	0.0000
3	-0.0039	0.0001	0.0000	0.0000
4	-0.0039	0.0001	0.0000	0.0000
5	-0.0039	0.0001	0.0000	0.0000
6	-0.0038	0.0001	0.0000	0.0000
7	-0.0039	0.0001	0.0000	0.0000
8	-0.0038	0.0001	0.0000	0.0000
9	-0.0038	0.0001	0.0000	0.0000

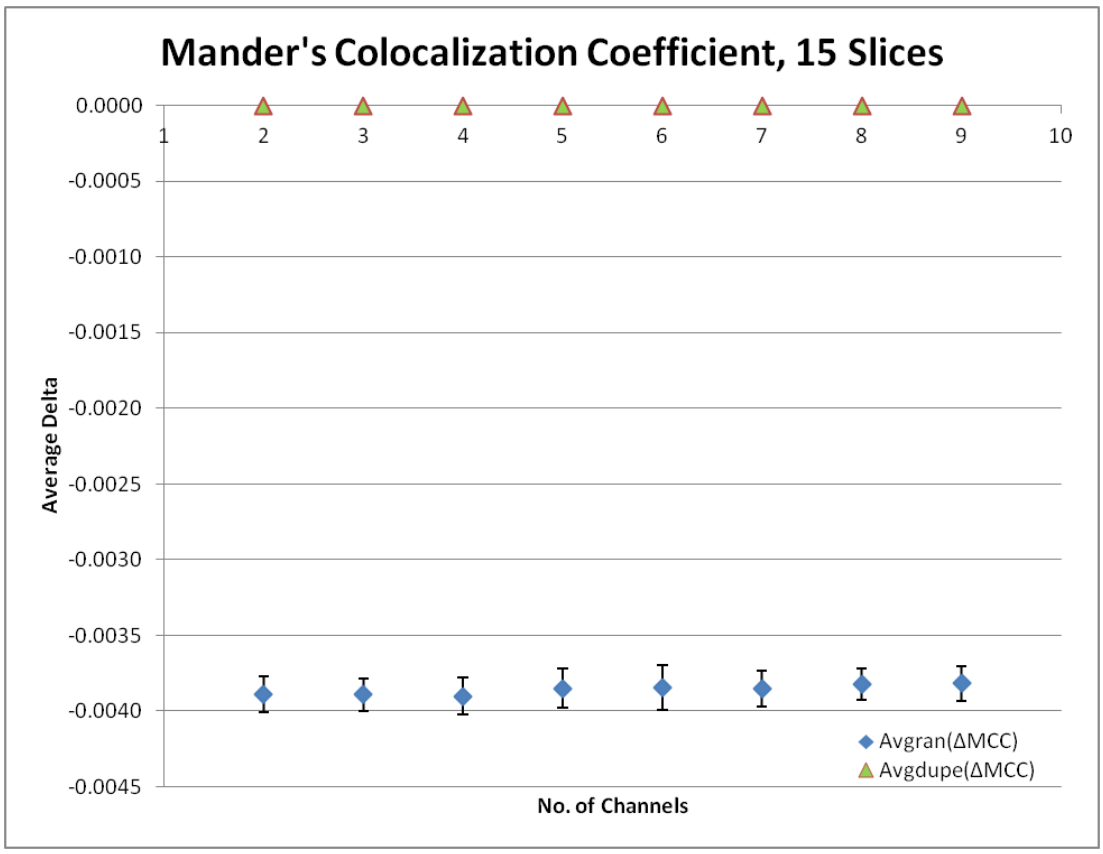

Figure 32: Monte Carlo Simulation MCC 15 Slices. Each data point represents the average delta from adding a random or duplicate channel. The graph shows that the average delta is less when a duplicate channel is added to the data.

4.6.4 Spatial Correlation Coefficient

The results from the Spatial Overlap Coefficient show that adding an additional random channel to the data set result in a negative delta. Adding a duplicate channel produces a zero delta.

The standard deviations that result from adding a random channel to the data set are larger than in other test cases. This is due to the algorithm used to classify the regions of the image that are considered part of the object. When a random image is added, the object regions are recalculated and any reclassification of background and object pixels will affect the outcome.

The variations only arise from adding images to the data set, running the Spatial Overlap

Coefficient on the same data set will consistently produce the same results.

Table 36: Monte Carlo Simulation L_s 5 Slices. This test case uses 5 image slices for the thickness of the image stack. Two channels are generated first (each with 5 image slices) Spatial Correlation Coefficient is run on the data set. This process is repeated 50 times, using the results of each test case an average delta is taken and a standard deviation generated.

Monte Carlo trials: 50				
No. of Channels	$Avg_{ran}(\Delta Ls)$	ranSD	$Avg_{dupe}(\Delta Ls)$	dupeSD
2	-0.0404	0.0320	0.0000	0.0000
3	-0.0362	0.0295	0.0000	0.0000
4	-0.0370	0.0257	0.0000	0.0000
5	-0.0280	0.0212	0.0000	0.0000
6	-0.0318	0.0251	0.0000	0.0000
7	-0.0368	0.0300	0.0000	0.0000
8	-0.0232	0.0126	0.0000	0.0000
9	-0.0314	0.0210	0.0000	0.0000

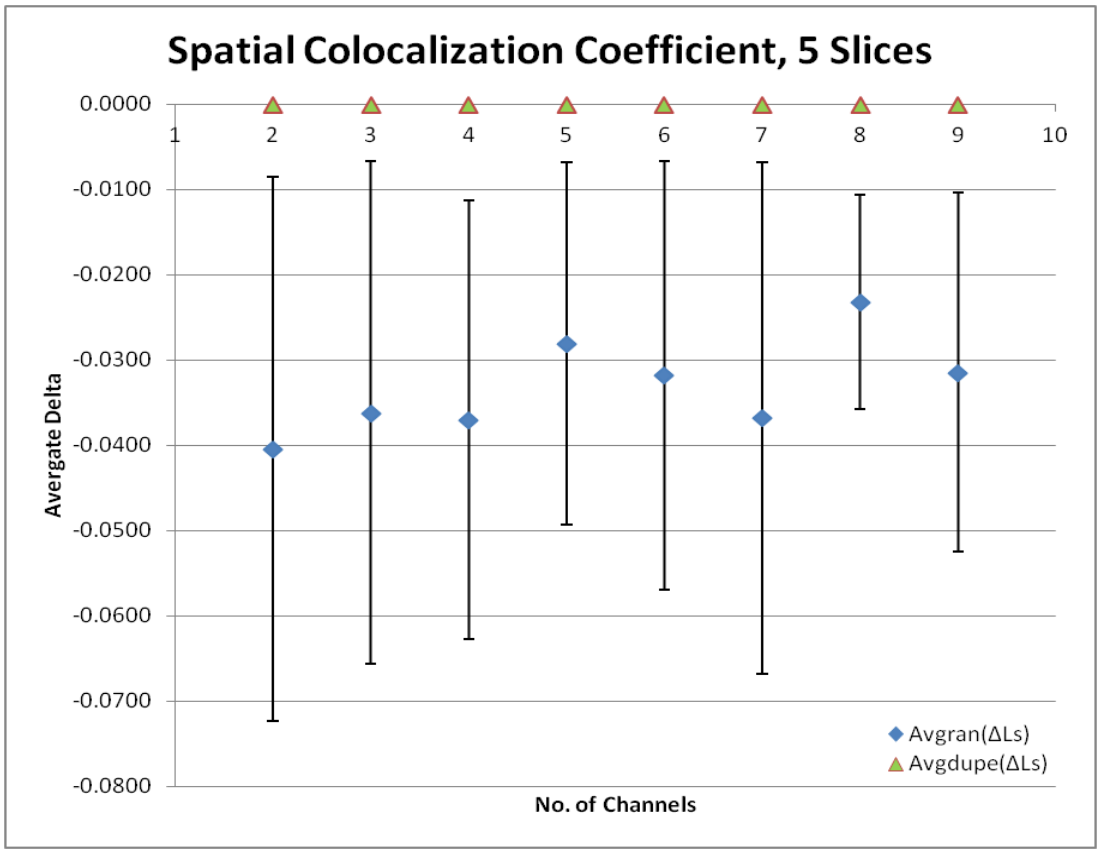

Figure 33: Monte Carlo Simulation L_s 5 Slices. Each data point represents the average delta from adding a random or duplicate channel. The graph shows that the average delta is less when a duplicate channel is added to the data.

Table 37: Monte Carlo Simulation L_s 10 Slices. This test case uses 10 image slices for the thickness of the image stack. Two channels are generated first (each with 10 image slices) Spatial Overlap Coefficient is run on the data set. This process is repeated 50 times, using the results of each test case an average delta is taken and a standard deviation generated.

Monte Carlo trials: 50				
No. of Channels	$Avg_{ran}(\Delta Ls)$	ranSD	$Avg_{dupe}(\Delta Ls)$	dupeSD
2	-0.0404	0.0253	0.0000	0.0000
3	-0.0412	0.0316	0.0000	0.0000
4	-0.0439	0.0300	0.0000	0.0000
5	-0.0376	0.0262	0.0000	0.0000
6	-0.0363	0.0284	0.0000	0.0000
7	-0.0255	0.0214	0.0000	0.0000
8	-0.0430	0.0265	0.0000	0.0000
9	-0.0318	0.0250	0.0000	0.0000

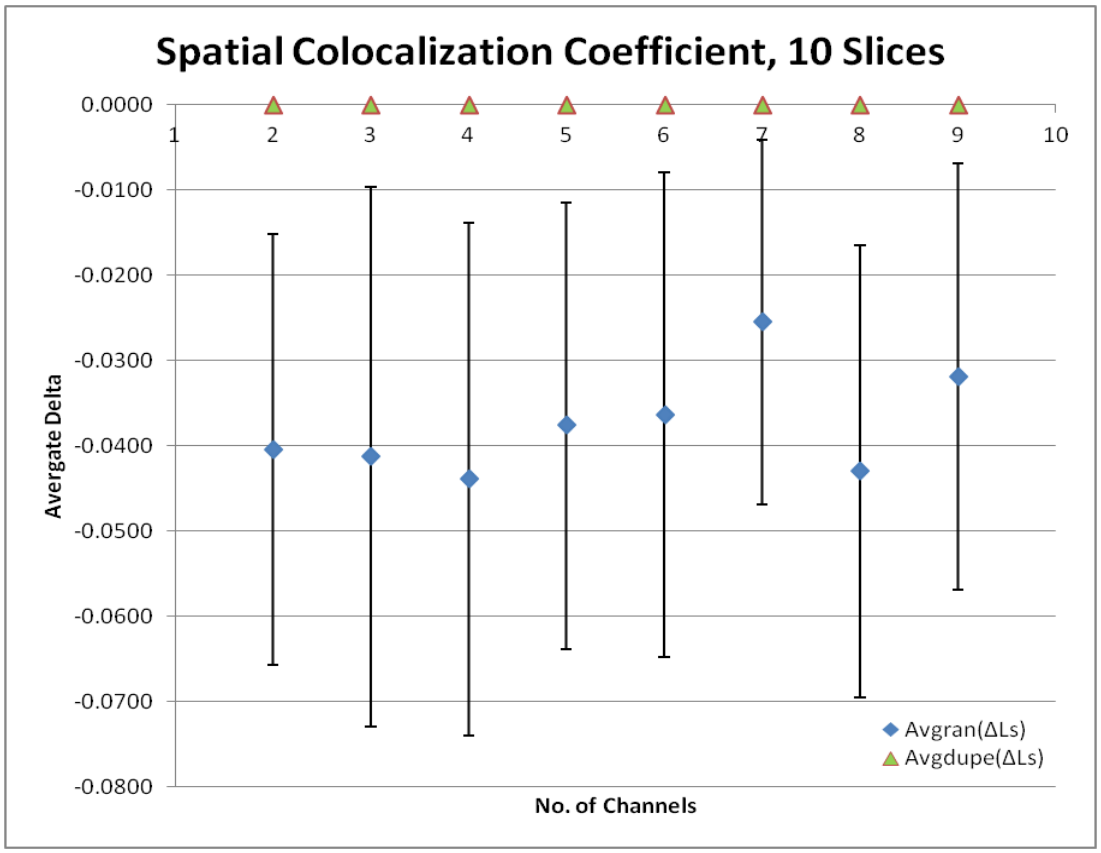

Figure 34: Monte Carlo Simulation L_s 10 Slices. Each data point represents the average delta from adding a random or duplicate channel. The graph shows that the average delta is less when a duplicate channel is added to the data.

Table 38: Monte Carlo Simulation L_s 15 Slices. This test case uses 15 image slices for the thickness of the image stack. Two channels are generated first (each with 15 image slices) Spatial Overlap Coefficient is run on the data set. This process is repeated 50 times, using the results of each test case an average delta is taken and a standard deviation generated.

Monte Carlo trials: 50				
No. of Channels	$Avg_{ran}(\Delta Ls)$	ranSD	$Avg_{dupe}(\Delta Ls)$	dupeSD
2	-0.0397	0.0294	0.0000	0.0000
3	-0.0349	0.0217	0.0000	0.0000
4	-0.0458	0.0321	0.0000	0.0000
5	-0.0327	0.0270	0.0000	0.0000
6	-0.0340	0.0270	0.0000	0.0000
7	-0.0365	0.0242	0.0000	0.0000
8	-0.0254	0.0160	0.0000	0.0000
9	-0.0370	0.0290	0.0000	0.0000

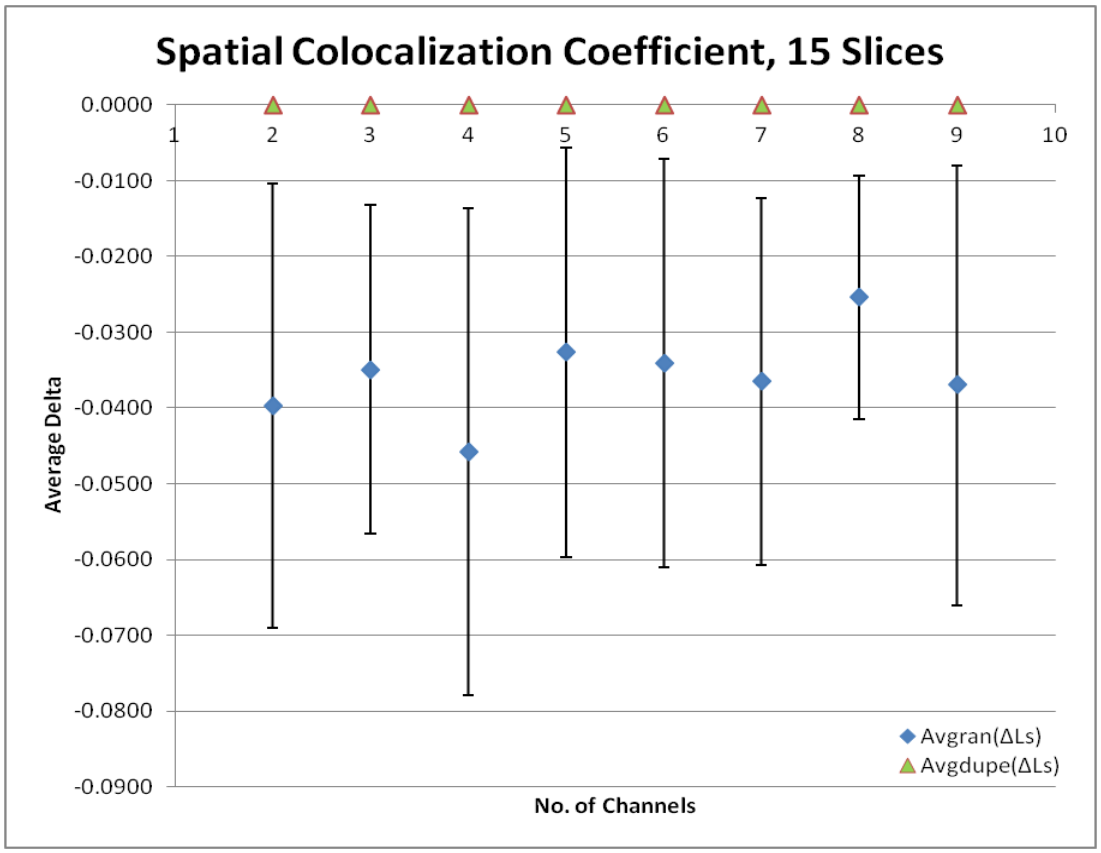

Figure 35: Monte Carlo Simulation L_s 15 Slices. Each data point represents the average delta from adding a random or duplicate channel. The graph shows that the average delta is less when a duplicate channel is added to the data.

CHAPTER 5

DISCUSSION

5.1 Pearson's Correlation Coefficient (Rp)

The modifications made to Pearson's Correlation Coefficient (Equation 5) produce accurate results on any number of channels. After modifying the equations to work on n-channels and creating a test case for two and three channels that produce identical results, it has been shown that the modified equation is consistent across two or more channels, as shown with the Monte Carlo simulation results. The results from the three channel test were expected to be the same as the results from the two channel test because no additional objects were introduced into the experiment. The results from the 3D spatial analysis show that the modified equation also works on 3D image stacks. While the results of this implementation of the equation are different from the results reported by Manders et al. (1993), it should be noted that the implementation used here has been tested on a sample that can be worked on by hand. The results of these tests are in Table 4, Table 6, and Table 8.

There are some limitations to the generalized Pearson's Correlation Coefficient (Equation 5) when comparing an image and an inverse image. Using the original Pearson's Correlation Coefficient (Equation 1) on two images, image A and its inverse ~A, should and does result in anti-correlation (-1). However, using the generalized equation with four images, it is not possible to obtain anti-correlation as comparing AA~A~A would show correlation between A and A as

well as correlation between ~A and ~A resulting in perfect correlation (1.0). Scenarios such as this result in the sub-optimal performance of the generalized Pearson's Correlation Coefficient (Equation 5). Through the testing that has been performed on the generalized Pearson's Correlation Coefficient (Equation 5), standardized, randomized, and real test cases, the equation performs well. To fully encompass all of the special cases this equation may run into, and the corresponding impacts to the resulting coefficient, will require further analysis.

Table 39: Anti-Correlation Analysis. Results for all equations for case A,A,~A,~A.

Pearson's Correlation Coefficient (Rp)	1.0
Overlap Coefficient (r)	0.0
Manders' Colocalization Coefficient (M0)	0.0
Manders' Colocalization Coefficient (M1)	0.0
Manders' Colocalization Coefficient (M2)	0.0
Spatial Colocalization Coefficient (Ls)	0.0

Pearson's Correlation Coefficient (Equation 1) is used to denote linear dependence between two variables or in Confocal Microscopy between two channels. The range of values for Pearson's Correlation Coefficient (Equation 1) is inclusive between -1 and 1. A coefficient value of -1 shows a strong inverse correlation, where all values of one variable (X) increases while the second variable (Y) decreases. When the coefficient value equals 1, all the data points align exactly and X increases as Y increases. The Modified Pearson's Correlation Coefficient (Equation 5) compares multiple channels in Confocal Microscopy, comparing the pixel intensity value on each channel and resulting in a strong correlation when all channels are on the same side of their respective means. Pearson's Correlation Coefficient (Equation 5) is able to show covariance of the two or more channels indicating colocalization between the channels.

5.2 Overlap Coefficient (r)

The Overlap Coefficient modifications (Equation 6) now allow for multi channel analysis. Results are shown comparing test cases on two and three channels. The two channel results exactly match the three channel results as expected. Since no new objects are introduced, and all the objects from the additional image are colocalized with an existing image, the ratio remains unchanged. Since this equation is shown to work on two and three channels, as shown with the Monte Carlo simulation results, it will work on more than three channels. The results from the 3D spatial analysis show that the modified equation also works on 3D image stacks. Similar to Pearson's Correlation Coefficient (Equation 5), the Overlap Coefficient (Equation 6) does not take into account the total number of distinct objects. If there are more objects present the total colocalization should decrease because it represents a percentage of colocalization.

The Modified Overlap Coefficient (Equation 6) is used to measure the covariance of multiple channels in Confocal Microscopy returning a value between 0 and 1. The Modified Overlap Coefficient (Equation 6) is very similar to the Modified Pearson's Correlation Coefficient (Equation 5) as the average channel pixel intensity value approaches the average object pixel intensity value. Instead of using the mean of the channel to determine covariance and if the pixel values are on the respective sides of the mean, the Modified Overlap Coefficient (Equation 6) only uses pixel intensity information when pixels from each channel are colocalizing. The measurement of the Modified Overlap Coefficient (Equation 6) measures how similar the pixel intensity values from each channel are compared to each channel measured individually.

5.3 Manders' Colocalization Coefficient (M)

The results from Manders Colocalization Coefficient (Equation 7) depend on which channel has focus. There is one result for the Manders' equation for each channel being examined. If there are four channels there will be M1, M2, M3, and M4. M1 would compare all the objects from channel one to all other channels, the result would signify the ratio of colocalization for that channel's fluorescence label. The results from the 3D spatial analysis show that the modified equation also works on 3D image stacks.

The results from Manders' equation are important because it can show how one fluorescence label, or variable, interacts with every other. This metric is important as it can show if a particular variable is or is not colocalizing with all other variables. If one particular variable is not colocalizing with the remaining variables it could be causing issues and needs to be removed. This equation is very similar to the Modified Overlap Coefficient (Equation 6) as it takes only colocalizing pixel information and compares it to all pixel information for that channel, resulting in an overlap colocalization for each channel. However, Manders Colocalization Coefficient (Equation 7) is not a good metric to show colocalization across all fluorescence labels, which is what Pearson's (Equation 5) and the Overlap Coefficient (Equation 6) attempt to show. Manders' Colocalization Coefficient (Equation 7) does not show total, overall colocalization by taking all objects into account – it checks if every object in that specific channel appears in all other channels.

5.4 Testing Model on Benchmark Images

The differences between the results from Pearson's Correlation Coefficient (Equation 5), the Overlap Coefficient (Equation 6), and Manders' Colocalization Coefficient (Equation 7) and the results from the Colocalization Algorithm can be explained by the nature of the equations. Since there are more objects that do not align, more of the numerator gets zeroed out. As the number of co-localizing objects decreases, the resulting ratio will likewise decrease. Since the Colocalization Algorithm takes into account every object from every channel, and calculates the total colocalized objects compared to the total objects, the resulting ratio is lower.

5.5 Region Growing Versus Edge Detection

Region growing and edge detection algorithms both have the same purpose when used for colocalization analysis preprocessing, to distinguish object from background pixels. The images produced by the confocal microscope often have a lot of background, noise, and pixels that may or may not be part of the objects. Therefore it was necessary to grow the object regions and classify those regions as objects.

Most edge detection techniques blur parts of the images to lessen the impact of noise. While this may be beneficial for edge detection, it might also blur object pixels into background pixels. Therefore, a region growing technique was preferred over an edge detection algorithm.

5.6 Spatial Colocalization Coefficient (L_s)

When comparing stack AAA to stack AAA, the results are clearly correct. Every pixel from every object is exactly the same. All objects are colocalized between the two channels.

When comparing stack AAA to stack AAB, the results are similar to the previous non-spatial results. Since there are more objects, and less of these objects colocalized, the colocalization is not complete. There are now more total objects and less objects co-localizing.

The Spatial Colocalization Coefficient value (L_s) (Equation 8) technique performs the analysis on all of the data. This algorithm isn't meant to replace the other equations, but meant as a measurement that addresses other concerns such as proportion of infection throughout the experiment. The proportion of infection is the ratio of cells or organism having been infected with a virus or bacteria. For instance, if human blood cells were placed in a Petri dish with the AIDS virus, one cell having been infected, an analysis could be done overtime to see what percentage of the cells were infected after that period of time. By measuring the spatial colocalization information – including image slices above and below – the Spatial Colocalization Coefficient value (L_s) (Equation 8) is able to determine a ratio of colocalizing pixels. This differs from the other equations as they use the pixel intensity value to determine the colocalization between objects, and while these are good for showing degree of colocalization between variables, the Spatial Colocalization Coefficient value (L_s) (Equation 8) equation shows the ratio between colocalizing objects and ignores the pixel intensity information as the pixels have already been determined to be part of the object.

5.7 Comparing Results from a Confocal Test Image Case

Interestingly, Pearson's Correlation Coefficient (Equation 5) and the Overlap Coefficient (Equation 6) return the same colocalization ratio within each test for all three test cases (Table 24, Table 25 and Table 26). The equations return the same value since the non-object pixels have been removed and the only difference between the two equations is subtracting the average channel pixel intensity. As the average channel pixel intensity value approaches the average object pixel intensity value the results from Pearson's Correlation Coefficient (Equation 5) and the Overlap Coefficient (Equation 6) converge. Generally the results for Pearson's Correlation Coefficient (Equation 5) and the Overlap Coefficient (Equation 6) were low with test case 1 (Figure 21 and Table 24) and test case 3 (Figure 23 and Table 26), and the results were aligned with the other equations on test case 2 (Figure 22 and Table 25).

Manders' Colocalization Coefficient (Equation 7) returns a higher colocalization ratio than the other equations on average. Since the Manders' Colocalization Coefficient (Equation 7) compares the pixels intensity values from one channel to each other channel, checking that the other channels have a pixel intensity value above a threshold, the resulting colocalization ratios are generally higher than the other equations. In each of the three test cases there was one channel for Manders' Colocalization Coefficient (Equation 7) that returned well below the other two channels. This shows that there is not colocalization across all channels and examining them individually shows which channels are not colocalizing well. This is very important from a research perspective as each channel typically has a different impact on the entire sample. Manders' Colocalization Coefficient (Equation 7) allows the researcher to easily see which channel is not having a strong impact.

The Spatial Colocalization Coefficient value (L_s) (Equation 8) returned values between those for the Pearson's Correlation Coefficient (Equation 5), the Overlap Coefficient (Equation 6) and the Manders' Colocalization Coefficient (Equation 7) for each test case (Figure 21, Table 24; Figure 22, Table 25; Figure 23, Table 26). The Spatial Colocalization Coefficient value (L_s) (Equation 8) examines the object pixels for all channels similar to the Pearson's Correlation Coefficient (Equation 5) and the Overlap Coefficient (Equation 6), and only taking into account whether the pixels are colocalized similar to Manders' Colocalization Coefficient (Equation 7). Spatial Colocalization Coefficient (L_s) (Equation 8) takes the strong features of each equation, coupled with foreground image segmentation to produce a colocalization ratio that focuses on object pixel colocalization across all channels. Each equation has it's specific uses and is just another data point a research can use to validate each experiment. The ratio returned by the Spatial Colocalization Coefficient (L_s) (Equation 8) was observed to be the median of the four coefficients tested.

5.8 Automatic Thresholding through Bimodal Histogram Analysis via Population-Based Hill Climbing

While not every confocal image is bimodal, every image should have two categories of pixels: background pixels and object pixels. By automatically finding the threshold at which those categories begin/end we are able to select a threshold without bias. Using an automatic thresholding technique removes any bias that could be generated by the researcher. For instance, by classifying a threshold at a non-object pixel value, it would artificially increase the results of the algorithm by showing more colocalization of objects that aren't actually objects.

Each histogram example was able to be analyzed by the Population-Based Hill Climbing algorithm. The individuals of the population were able to find distinct peaks which were local maxima. These local maxima serve as possible thresholds. By counting the number of individuals at each local maxima two thresholds are able to be selected.

When reading published papers that use colocalization analysis to describe the results, it is not always known how or why the authors chose the used thresholds. While the details explaining the reasoning behind the threshold selection process and providing images showing the scatter plots of the overlapping channels can be shown, it would be cumbersome with more than two channels.

Using this algorithm to automatically select the threshold values from each image adds standardization to the threshold selection process. Standardizing the threshold selection process is important because inaccurate threshold selection can impact the significance of the results heavily. A poorly selected threshold could make great results look terrible, and terrible results look great.

Standardizing the threshold selection process using this algorithm makes replicating the results very easy. There are only two inputs to this algorithm that can be changed, distance the individuals can see (Vision) and the number of rounds the individuals attempt to move to a better hill (Iterations). These results are easily reproducible as long as the parameters (Iterations and Vision) are known.

5.9 Automatic Thresholding through Bimodal Histogram Analysis via Limited Exhaustive Search

The limited exhaustive search algorithm searches for the highest frequency of pixel intensity value in the range of pixel intensity values. In most confocal images there are a lot of background pixels and a lot of object pixels, the number of pixels that need to be categorized are a lot fewer. The image can be skewed light or dark, if it is skewed light there are more object pixels, dark and there are more background pixels.

The limited exhaustive search algorithm is only examining pixel intensity frequency, which usually dominate the pixel intensity histogram. In Tables 19, 21, 23, this is very evident from the returned values of the limited exhaustive search algorithm. The upper bound threshold is always 255, and the lower bound is always 0. The pixel intensities 0 and 255 are the most frequent pixels found in the pixel intensity range. This recurring issue was the motivation for implementing a population-based hill climbing algorithm to more accurately assess the upper and lower bound thresholds of the image.

5.10 Monte Carlo Simulation

The Monte Carlo Simulations provide a view into how the algorithms will perform on increasingly large data sets. The tests were used to show two things: the algorithms were modified successfully to produce results on n-channels, and the produced values are expected.

The tests ranged from two channels to nine channels, with each channel having 5,10, or 15 image slices for depth. For each modified equation 24 different configurations were run, and

the results averaged from 50 tests on each configuration. These tests then added either a duplicate channel, or a random channel. This is a total of 9600 tests completed on the modified equations.

The tests were designed to show that adding an image we know to be identical should not decrease the returned values more than those obtained by adding a random image. Depending on the equation, the addition of a duplicate channel may cause an increase in the value of the colocalization coefficient, however, it is very unlikely that adding a random channel will result in an increase in the value of the colocalization coefficient.

Pearson's Correlation Coefficient (Equation 5) is the only equation that shows an increase when adding a duplicate channel to the data set. This shows that as the data set is more similar the coefficient increases. Although there is no new correlation between the images in the data set, the equation shows that a stronger correlation exists. As expected, adding random images has a negative impact on the correlation of the data set.

The Overlap Coefficient (Equation 6) decreases as random or duplicate channels are added to the data set. This is the only equation that decreases when a duplicate channel is added. The equation analyzes the data set for objects that overlap, if there are already objects that don't overlap adding the duplicate channel will not affect the results. The total objects in the data set will still increase when a duplicate image is added, which is evident in the results of the test decreasing slightly. As is consistent with all of the equations, adding a random channel to the data set will decrease the colocalization value to a greater extent than when a duplicate channel is added.

Manders' Colocalization Coefficient (Equation 7) produces a change in the colocalization metric value only when a random channel is added to the data set. This equation returns a pair-

wise comparison of all channels in the data set, which is then averaged. When adding a new channel (duplicate or random) every other channel compares itself to that new channel. Adding a duplicate channel would result in the same coefficient being produced as from the duplicated channel, which would only minimally affect the average. Adding a random channel would produce new data and would impact the average of the pair-wise comparisons.

The Spatial Colocalization Coefficient (L_s) performs similarly to Manders' Colocalization Coefficient in that the results produced by adding a duplicate channel have a change in the colocalization metric value of zero. The Spatial Colocalization Coefficient (L_s) counts the number of objects in the data set. When adding a duplicate channel, there are no new objects. Since there are no new objects the total objects in the data set remains the same. The non-colocalizing objects in the duplicate channel will become colocalized objects only if they are adjacent to the objects in the same region, most likely this would be the duplicated channel. This scenario has a 1 in 8 chance of arising, with 50 tests performed it statistically occurred several times but was averaged out.

Adding random channels to the data set will result in new objects, increasing the total number of objects in the data set. The colocalization of the data set is likely to decrease as random channels are added. There is a large standard deviation for the random channels added to the Spatial Colocalization Coefficient (L_s) tests. The larger standard deviation is likely due to the re-categorization of the data set objects, which is performed whenever the data set is changed. Since the new channel affects the classification of the data set objects it is likely to be the cause of the larger standard deviation. The tests on this equation were run with several hundred tests, up from 50; there was no significant change in the standard deviation.

The results from the Monte Carlo Simulation show the equations perform properly when the number of channels continuously increases, when there are large numbers of image slices, and when duplicate or random images are added to the data set. The equations are consistent in the returned results on all of the tests performed.

5.11 Problems and Limitations

There are several limitations to this software package. Mainly, the images need to be exported to an acceptable image format (PNG, TIFF, GIF, BMP, XMP, PSD, ICO, and most JPEG; most bit depths for these image formats are also supported) before they are imported and examined. This allows the ability for this software package to work with any confocal microscope as it is not written for a specific data format, but for images. The types of image formats that the software is capable of analyzing are currently limited. Some confocal microscope software packages may not natively produce images that are compatible with this software. Therefore, the image format would need to be changed beforehand.

5.12 Future Development

This work has made several important advancements to colocalization analysis. However, there are still several improvements that could be made to this project.

This software package could be adapted into an ImageJ (ImageJ) plug-in to allow broad access across the scientific community.

This program does not read the raw data directly from the confocal microscope. Future expansions to this project could analyze the raw data output and have no need for intermediate software.

The software could be modified to periodically take colocalization measurements throughout a time-elapsed experiment. This would measure the progression of the colocalization which would be useful for live cell imaging. Implementing the capability to read the raw data directly from the confocal microscope would be a requirement for time-elapsed analysis.

5.13 Summary

This software will now allow researchers to provide a full 3D spatial analysis of their experiments. By analyzing the spatial colocalization of an experiment, it is possible to determine whether the entire specimen that was fluorescently labeled completely colocalized or whether only some sections of the experiment colocalized.

The Region Growing algorithm and the Automatic Thresholding algorithm have produced spatial results based off of regions of interest that were not present in previous analysis software. The Region Growing algorithm is able to intelligently grow regions of interest while eliminating background data and noise. Growing regions-of-interest, and examining those regions, ensures that background and noise pixels are not factored into the results. The bimodal model finder provides the Region Growing algorithm the inputs it needs to accurately partition the image into background and object regions.

The largest problem with existing software was the lack of analysis of more than two interacting fluorescence labels. All of the previously used equations that were considered in this

study were modified and tested to work on any number of channels. These modified equations now work in more scenarios and with the same results on two channels that they previously produced. The newly implemented 3D spatial analysis technique is able to provide a different perspective on the experiment that was not available before. The results from this new technique provide reasoned results: total number of colocalized object pixels divided by the total number of object pixels.

REFERENCES

Adler, J., Parmryd, I. (2010). *Quantifying Colocalization by Correlation: The Pearson Correlation Coefficient is Superior to the Mander's Overlap Coefficient.* Cytometry. Part A 77A p.733-742.

Barlow, A., MacLeod, A., Noppen, S., Sanderson, J., Guerin, C. (2010) *Colocalization Analysis in Fluorescence Micrographs: Verification of a More Accurate Calculation of Pearson's Correlation Coefficient.* Microsc. Microanal. 16, 710–724, 2010 doi:10.1017/S143192761009389X

Bolte, S., Cordelieres, F. P. (2006). *A guided tour into subcellular colocalization analysis in light microscopy*. Journal of Microscopy. Vol 224. Pt 3 December 2006. Pp. 213-232.

Dunn, K., Kamocka, M., and McDonald, J. (2011) *A practical guide to evaluating colocalization in biological microscopy.* Am J Physiol Cell Physiol April 1, 2011 vol. 300 no. 4 C723-C742

1*Department of Medicine, Division of Nephrology, Indiana University Medical Center, Indianapolis,*

ImageJ. http://rsbweb.nih.gov/ij. NIH

Jain, R., Kasturi, R., Schunck, B. *Machine Vision*. Published by McGraw-Hill, Inc., ISBN 0-07-032018-7, 1995.

Jaskolski, F., Normand, E., Mulle‡, C., and Coussen F. *Differential Trafficking of GluR7 Kainate Receptor Subunit Splice Variants*. The Journal of Biological Chemistry Vol. 280, No. 24, Issue of June 17, pp. 22968–22976, 2005.

Kreft, M., Milisav, I., Potokar, M., Zorec, R. (2004). *Automated high through-put colocalization analysis of multichannel confocal images*. Computer Methods and Programs in Biomedicine. 1 April 2004 (volume 74 issue 1 Pages 63-67 DOI: 10.1016/S0169-2607(03)00071-3)

Kuchcinski, K., and Szymanek, R.. JaCoP Library. User's Guide. http: //www.jacop.eu, 2011

Manders, E.M.M., Stap, J., Brakenhoff, GJ, Driel, R van, and Aten, J.A.(1992). *Dynamics of three-dimensional replication patterns during the S-phase, analysed by double labelling of DNA and confocal microscopy*. Journal of Cell Science 103, 857-862 (1992) 857 Printed in Great Britain © The Company of Biologists Limited 1992.

Manders. E.M.M., Verbeek, F.J., Aten, J.A. (1993). *Measurement of co-localization of objects in dual-colour confocal images*. Journal of Microscopy, Vol 169, pt3, March 1993, pp. 275-382.

MetaMorph® Analysis. http://www.diaginc.com/software/metamorph.html.

Patwardhan, A and Manders, E. M. M. (1996). *Three-colour confocal microscopy with improved colocalization capability and cross-talk suppression*. Bioimaging 4(1996) 17–24.

Vitriol, E., Uetrecht, A., Shen, F., Jacobson, K., and Bear, J. *Enhanced EGFP-chromophore-assisted laser inactivation using deficient cells rescued with functional EGFP-fusion proteins.* PNAS April 17, 2007 vol. 104 no. 16 6702-6707.

Xu, A., Kaelin, C., Takeda, K., Akira, S., Schwartz, M., Barsh, G. *PI3K integrates the action of insulin and leptin on hypothalamic neurons*. *J Clin Invest.* 2005;115(4):951–958. doi:10.1172/JCI24301.

Zinchuk, V., Zinchuk, O., Okada, T. (2007). *Quantitative Colocalization Analysis of Multicolor Confocal Immunofluorescence Microscopy Images: Pushing Pixels to Explore Biological Phenomena*. Acta Histochem. Cytochem. 40 (4): 101–111, 2007. doi:10.1267/ahc.07002